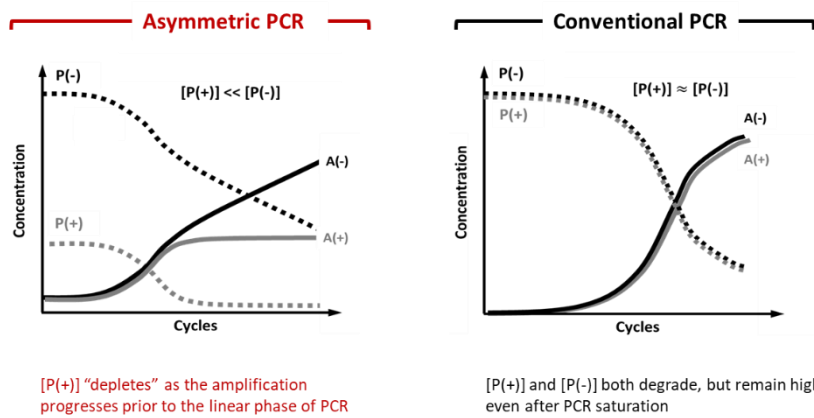
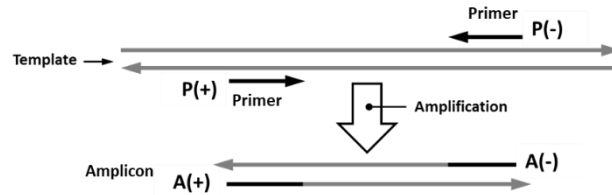
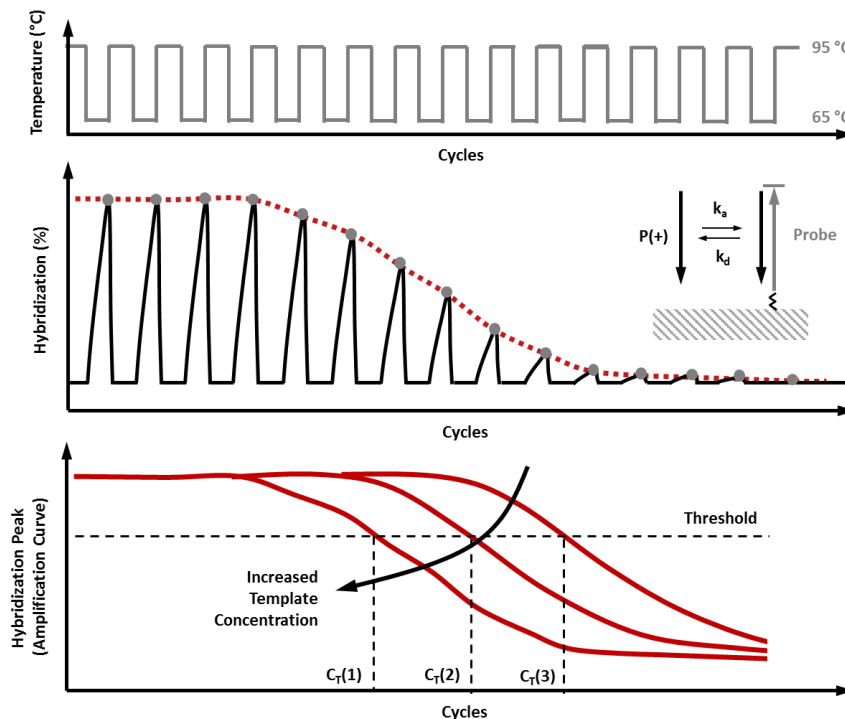


Supplementary Note 1

Description: Depiction of amplicon generation for both conventional PCR and asymmetric PCR and real-time solid-phase capturing to quantify the initial template concentration



Quantifying PCR products by solid-phase capturing of $[P(+)]$, monitoring its depletion, creating an amplification curve, and designating a "threshold cycle (C_T)" to quantify the initial template concentration



Supplementary Note 2

Description: Materials and methods for generating the example inverse fluorescence transduction data.

The melt curves in **Fig. 2** (cf. manuscript) were generated by first PCR asymmetrically amplifying a region of the *rpoB* of *M. tuberculosis* (H37Rv), removing the reaction into a flow-through chamber with a probe-printed 1"x3" slide, hybridizing it such that enough ssDNA amplicons bind to the probes and finally imaging the slide (and the probes) when subject to a 55°C to 95°C melt process. The details of each experiment are below.

Primers for amplifying the targeted *rpoB* region

FIGURE	PRIMER	RATIO	SEQUENCE (5'-3')
2A	Forward (Excess)	2.5:1	5'-CY5-TGGTCGCCGCGATCAAGGAG-3'
	Reverse (Limiting)		5'-CTCCAGCCCGGCACGCTC-3'
2B	Forward (Excess)	3:1	5'-BHQ3-TGGTCGCCGCGATCAAGGAG-3'
	Reverse (Limiting)		5'-CTCCAGCCCGGCACGCTC-3'
2C	Forward (Excess)	3:1	5'-TGGTCGCCGCGATCAAGGAG-3'
	Reverse (Limiting)		5'-CTCCAGCCCGGCACGCTC-3'

Probes pairs

FIGURE	PRIMER	SEQUENCE (5'-3')
2A	Wild Type (WT)	5'-GAATTGGCTC <u>A</u> GCTGGCTAAAAAA-C ₆ -NH ₂ -3'
	Mutant (MT)	5'-GAATTGGCTC <u>G</u> GCTGGCTAAAAAA-C ₆ -NH ₂ -3'
2B	Wild Type (WT)	5'-NH ₂ -C ₆ -AAAAATGAATTGGCTC <u>A</u> GCTGGCTATCGCGCG-TYE665-3'
	Mutant (MT)	5'-NH ₂ -C ₆ -AAAAATGAATTGGCTC <u>G</u> GCTGGCTATCGCGCG-TYE665-3'
2C	Wild Type (WT)	5'-Cy3-GAATTGGCTC <u>A</u> GCTGGCTAAAAAA-C ₆ -NH ₂ -3'
	Mutant (MT)	5'-Cy3-GAATTGGCTC <u>G</u> GCTGGCTAAAAAA-C ₆ -NH ₂ -3'

PCR amplification chemistry

FIGURE	Master Mix	dNTP	TEMPLATE
2A	Multiplex PCR Master Mix (NEB)	200 μM each	66 fM genomic H37Rv
2B	Advantage 2 Master Mix (Clontech)	200 μM each	135 fM genomic H37Rv
2C	Q5® Master Mix (NEB)	200μM dATP, dTTP, and dGTP, 100μM dCTP, and 100μM Q-dCTP*	660 fM genomic H37Rv

* Black Hole Quencher 10 (BHQ10)-dCTP (BioSearch Laboratories)

PCR instrument/conditions. C1000 Touch (BioRad Laboratories, Inc.) 95°C for 3 min, followed by 45 cycles of amplification at 95°C for 20 s, 64°C for 40 s, and 68°C for 20 s, and 3) a final extension step for 3 min extension at 68°C.

Hybridization and melt. Reaction was removed from PCR instrument and inserted into the probe-printed slide, hybridized for 1 hour at 55°C followed by a melt from 55°C to 95°C over 20 min. In case of **Fig. 2a** (cf. manuscript), after the hybridization and prior to melt, the slide was washed with 1 mL of 1x hybridization buffer (5x Denhardt's reagent, 5 mM KH₂PO₄, 0.1% SDS, and 5x SSC).

Supplementary Note 3

Description: Materials and methods for characterization and study of the labeling of PCR amplicons using quencher-labeled dNTPs (Q-dNTPs).

Measuring and Optimizing Q-dNTP Incorporation Rate

We developed simplified analytical methods to characterize the ability of a polymerase to suitably incorporate various quencher-labeled dCTP conjugates. This methodology allowed for the initial empirical optimization of product extension yield and also Q-dCTP incorporation frequency. To help ensure effective energy transfer (quenching) during the IFT melt curve phase of the assays, we have targeted approximately one Q-dCTP every fifteen nucleotides. This spacing represents a balance between signal transduction and amplicon yield.

Thermostable DNA polymerase was used to extend a self-priming hairpin oligonucleotide sequence in the presence and absence of Q-dCTP (BHQ-10 dCTP conjugate, MW 1051.78, LGC BioSearch) in addition to the four natural dNTPs at 1:1:1:1 mole ratio. The resulting nucleic acid components were then evaluated for the proportion of starting material converted into dsDNA (via gel electrophoresis, **Fig. Supp. 1**) and the probability of Q-dCTP incorporation (via UV-Vis spectrophotometry), by virtue of the unique Q-dCTP absorbance at 516 nm (**Fig. Supp. 2**).

Representative reactions employing SuperScript III (Thermo-Fisher pn 11732-020) included 1 μ L enzyme, 12.5 μ L 2x reaction mix, 1 μ L 50 mM MgSO₄, 2.5 μ L 50 μ M self-priming oligonucleotide, 0-200 μ M Q-dCTP conjugate and sufficient water for 25 μ L total volume. Extension conditions were 5 min at 95°C, 20 min at 68°C and hold at 15°C. 1 μ L of the reaction mixture was analyzed with an Agilent RNA 6000 Nano Chip (Agilent pn 5067-1511), according to the Nano Kit Guide. 20 μ L of the reaction mixture was treated with a QIAquick PCR Purification Kit (Qiagen pn 28106) according to the manufacturer's protocol and eluted in 20 μ L EB buffer. 12.5 μ L of the purified sample (free of unincorporated dNTPs) was diluted into DNA Suspension Buffer (10 mM Tris, 0.1 mM EDTA, pH 8.0) and its UV-Vis spectrum was collected on a Beckman DU-800 spectrophotometer with a 1 cm path-length cuvette.

The self-priming 100mer oligonucleotide sequence Oligo1 was as follows:

5'-TGC CTC AGC GTA AGG TTC CAG ATA AAT AGG TCA GGC CTG ATT CAA GTG TTC TTT GCA AAC TCC TCT TGG CTA ATC GCG GCT CGC GTG TCG CGA GCC GCG A-3'

This construct possesses 16 potential sites for the polymerase to incorporate either natural dCTP or the corresponding Q-dCTP. The extended sequence has a calculated extinction coefficient of 133,9511 at 260 nm. The Q-dCTP conjugate has a measured extinction coefficient of ~30,000 at 516nm. The probability of Q-dCTP incorporation was calculated with the following formula: $P = (\text{moles Q-dCTP} / \text{moles DNA})/16$. Typically, polymerase extension reactions containing up to 200 μ M Q-dCTP (in addition to the four standard dNTPs) afforded P values of ~0.21, which for Oligo1 corresponds to, on average, 3.36 Q-dCTP incorporations per strand.

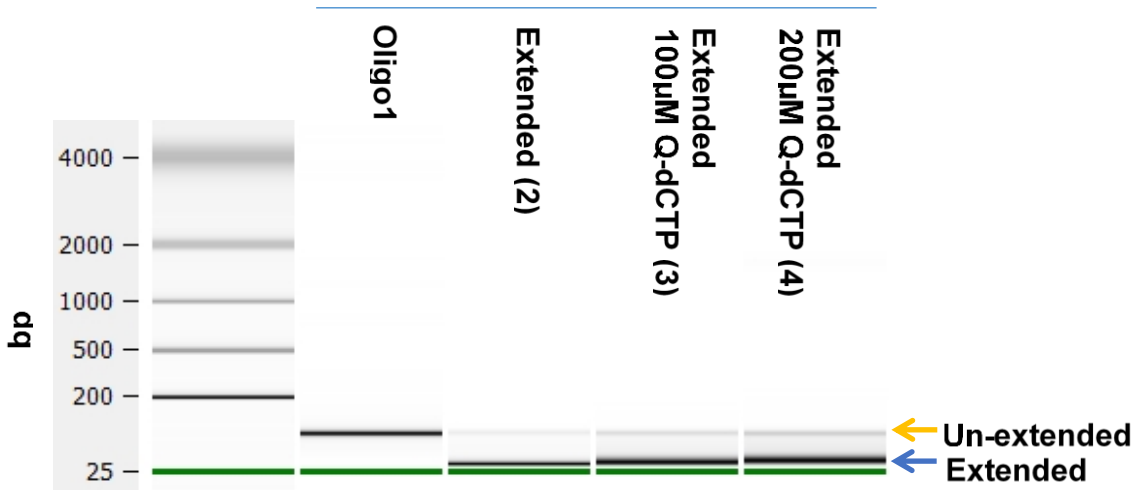


Figure Supp. 1: Gel view of Bioanalyzer data from RNA 6000 Nano Chip for Oligo1 alone (1), Oligo1 extended using SSIII without Q-dCTP (2) or in the presence of 100 μ M (3) or 200 μ M Q-dCTP (4). This experiment was conducted once.

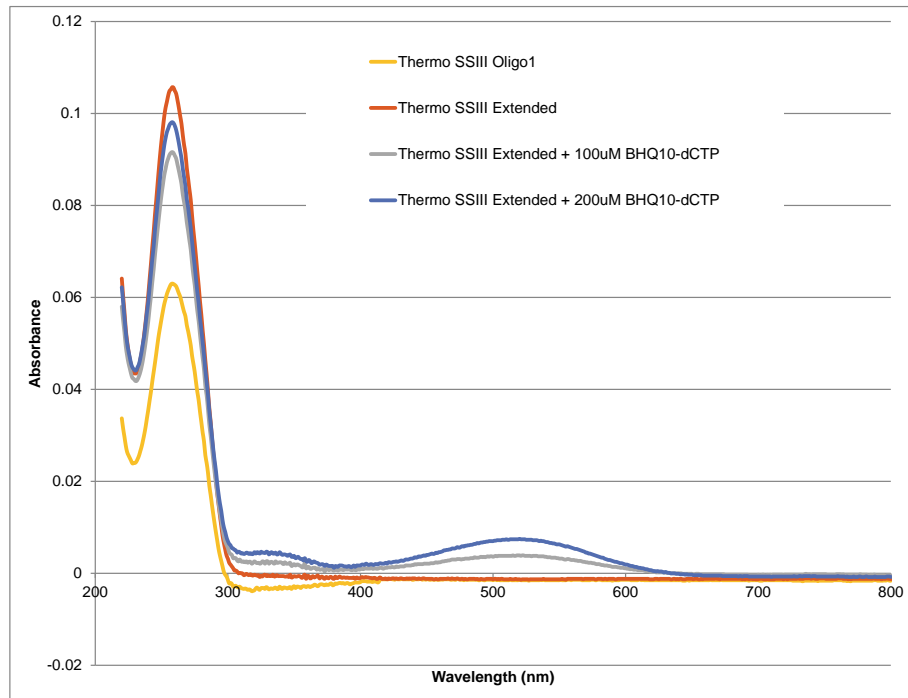


Figure Supp. 2: UV-Vis scan of purified products from extensions performed in the absence/presence of Q-dCTP. Each measurement (spectral scan) was conducted once.

Supplementary Note 4

Description: Materials and methods for characterization and evaluation of FAM-TAM construct.

A. Absorption Spectra

A DU800 UV/Vis spectrophotometer (Beckman Coulter) was utilized to obtain the absorption spectrum and the molar extinction coefficient of the FAM-TAM construct and BHQ10 and BHQ2 quenchers. Lyophilized FAM-TAM oligo (5'-6-TAMN/TTT TTT /iFluorT/TT CCC TGA GCT GAA CGG GAA GC -3') was obtained from Integrated DNA Technologies. The oligo was diluted in distilled water to obtain a 100 μM stock solution. From the stock solution, a final 1 μM analyte concentration with a total volume of 1000 μL was created in aqueous buffer (Tris-HCl, pH 8.7 @ 25°C, $[\text{K}^+] = 55 \text{ mM}$, $[\text{Mg}^{2+}] = 3.5 \text{ mM}$).

The normalized absorption spectrum of the 1 μM analyte measured at room temperature is shown in normalized units in **Fig. Supp. 3**. Peak absorbance measured close to the donor (FAM) absorption peak, is 0.1184 at 495 nm. For a concentration of 1 μM and an optical path length of 1 cm, the molar extinction coefficient is calculated to be $118,400 \text{ M}^{-1} \text{ cm}^{-1}$, using Beer Lambert's law. The absorption spectra of BHQ10 and BHQ2 quenchers were also obtained and are shown in **Fig. Supp. 4**.

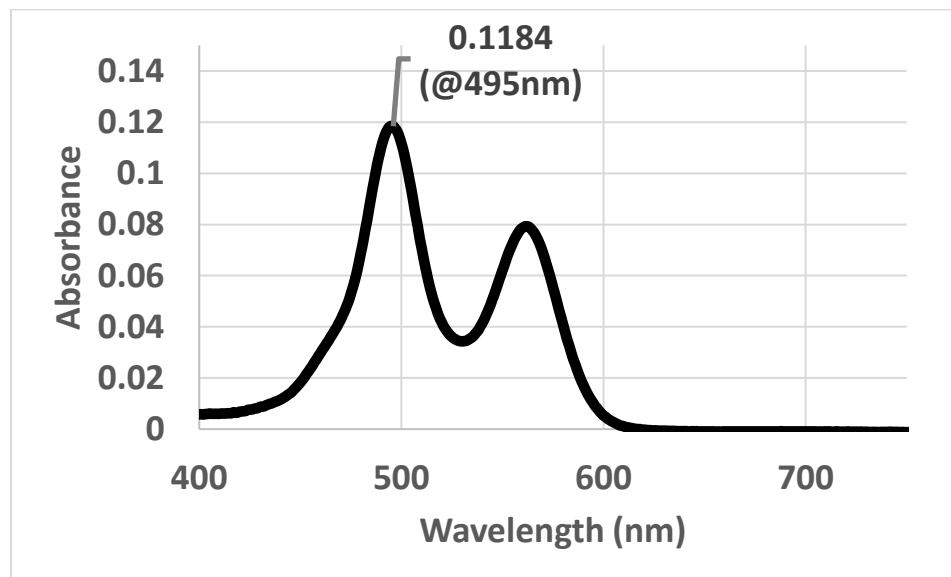


Figure Supp. 3: Measured absorbance spectrum of the FAM-TAM construct. This measurement was conducted once.

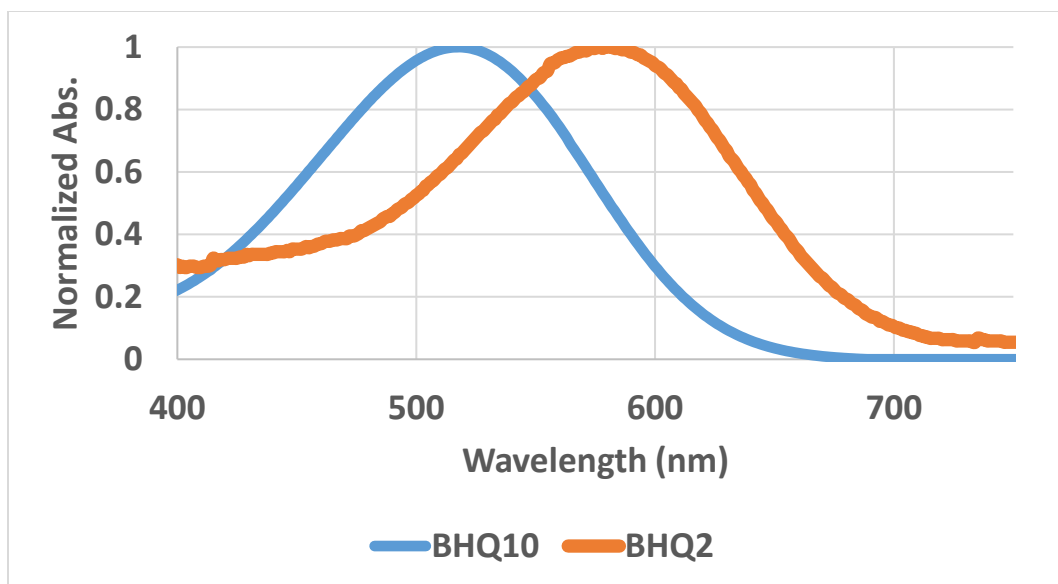


Figure Supp. 4: Normalized measured absorbance spectrum of BHQ10 and BHQ2 quenchers. The measurement for each quencher was conducted once.

B. Emission Spectra:

A QuantaMaster QM-400 spectrofluorometer (PTI-Horiba) was utilized to obtain the emission spectrum of the FAM-TAM construct (5'-6-TAMN/TTT TTT /iFluorT/TT CCC TGA GCT GAA CGG GAA GC -3'). The oligo was diluted in distilled water to obtain a 100 μ M stock solution. From the stock solution, a final 10 nM analyte concentration with a total volume of 1000 μ L was created in aqueous buffer (Tris-HCl, pH 8.7 @ 25°C, [K⁺] = 55 mM, [Mg²⁺] = 3.5 mM).

The emission spectrum of the 10 nM analyte measured at room temperature is shown in normalized units in **Fig. 3** (cf., manuscript). The excitation wavelength is 495 nm.

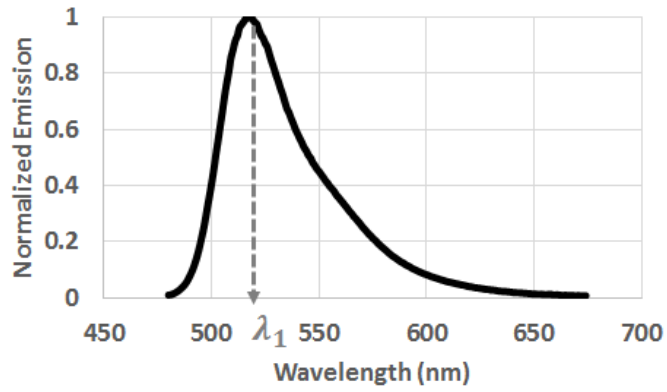
C. FRET Efficiency Calculation:

A linear superposition concept was employed to estimate the FRET efficiency of FAM-TAM construct, denoted here by η_{FRET} . If we assume $f_{FAM}(\lambda)$, $f_{TAM}(\lambda)$ and $f_{FAM-TAM}(\lambda)$ are the emission spectra of FAM, TAM, and FAM-TAM, respectively, then we have

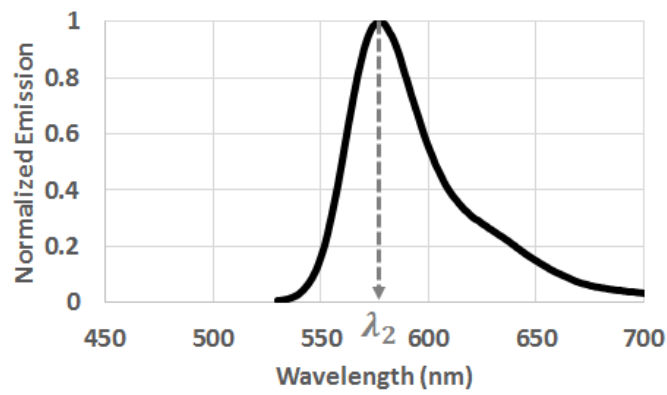
$$f_{FAM-TAM}(\lambda) = (1 - \eta_{FRET})\phi_{FAM}f_{FAM}(\lambda) + \eta_{FRET}\phi_{FAM}f_{TAM}(\lambda), \quad (1)$$

where $\phi_{FAM} \cong 0.9$ and $\phi_{TAM} \cong 0.41^{1,2}$ are the quantum yields of FAM and TAM, respectively.

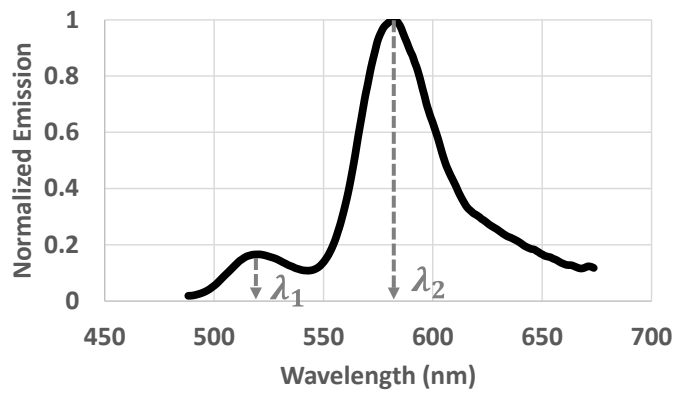
In **Fig. Supp. 5**, we show the measured emission spectra of the fluorophores. Using this data and applying (1), we estimated η_{FRET} to be ~ 0.92 .



(a)



(b)



(c)

Figure Supp. 5: Measured emission spectrum of (a) FAM; (b) TAM; and (c) FAM-TAM. $\lambda_1 = 518$ nm and $\lambda_2 = 583$ nm. Each measurement was conducted once.

D. Estimating Fluorophore-Quencher FRET Distance:

The efficiency of FRET, E has an inverse relationship with the sixth power of r , the donor-to-acceptor distance³, such that

$$E = \frac{1}{1 + \left(\frac{r}{R_0}\right)^6}, \quad (2)$$

where R_0 is the Förster distance, defined as the distance where the $E = 50\%$ efficient. Now, R_0 can be computed by the following⁴

$$R_0 = 0.211 \left(\frac{k^2 \phi_D J}{\eta^4} \right)^{\frac{1}{6}}, \quad (3)$$

where ϕ_D is donor quantum yield, J is the spectral overlap between donor emission and acceptor absorption spectra, η is the refractive index of the medium, and k^2 is the dipole orientation factor between the FRET moieties.

In FAM-TAM construct, we have two fluorophores that can be quenched, hence R_0 should be calculated individually for each one. Below, we show the values of R_0 for both pairs separately; FAM-BHQ10 and TAM-BHQ10. The simulated FRET efficiency vs. distance is shown in **Fig. Supp. 6**.

	FAM-BHQ10	TAM-BHQ10
η	1.33	1.33
ϕ_D	0.9 ¹	0.41 ²
k^2	2/3 ⁵	2/3 ⁵
J	1.927x10 ¹⁵ (nm) ⁴ M ⁻¹ cm ⁻¹	1.291x10 ¹⁵ (nm) ⁴ M ⁻¹ cm ⁻¹
R_0	5.27 nm	4.62 nm

Table Supp. I: FRET Distance between donors and quenchers.

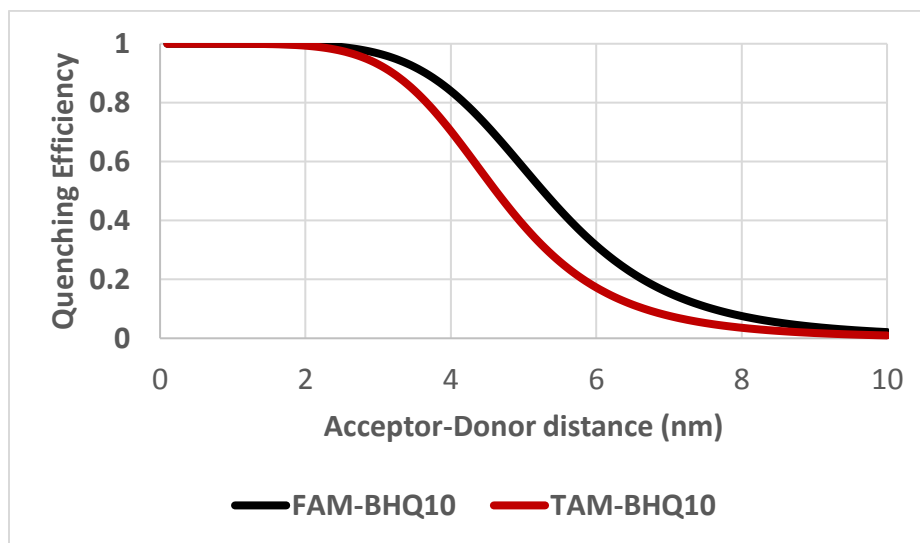


Figure Supp. 6: Simulated FRET efficiency vs. intermolecular distance for FAM-BHQ10 and TAM-BHQ10 FRET pairs.

Supplementary Note 5

Description: Architecture, photo-sensor topology, pixel circuitry, and the measured results of the CMOS integrated circuit.

A. Array Architecture

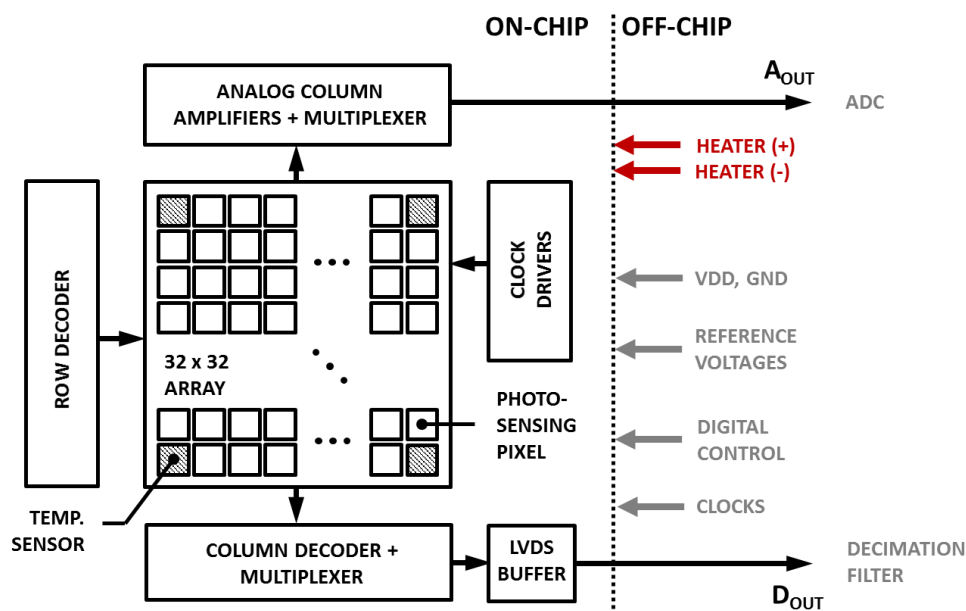


Figure Supp. 7: Architecture of the CMOS biochip and its main functional blocks.

The implemented biochip (Fig. Supp. 7) includes a 32×32 element biosensor array with 13 temperature sensor pixels. These pixels have an identical architecture to photo-sensing pixels (Fig. Supp. 8-13), except their photodiode is covered by metal layers. This blocks the photon flux and enables us to continually measure the temperature-dependent dark current of the pixels as a surrogate for the temperature on that coordinate.

For readout, each element can be individually addressed through row and column decoders. D_{OUT} is the digital output of the column multiplexer which is sent off chip (to the FPGA) through a low voltage differential signaling (LVDS) buffer. All the necessary clocks, row and column select signals, the analog reference voltages and power supply (3.3V) are applied externally as shown above.

The analog column reader is implemented for testing, debugging, and calibration.

The on-chip heating element is a 2.5Ω passive multi-finger metal resistor, implemented using the top metal layer (M4) of the CMOS process to deliver up to 10W of power from a 5V source. This heater is distributed uniformly within the chip both in the biosensor array area and its periphery.

The measured performance summary is listed in Fig. Supp. 14-17 and Supplementary Note 5.1.

B. In-pixel $\Sigma\Delta$ photo-sensor topology

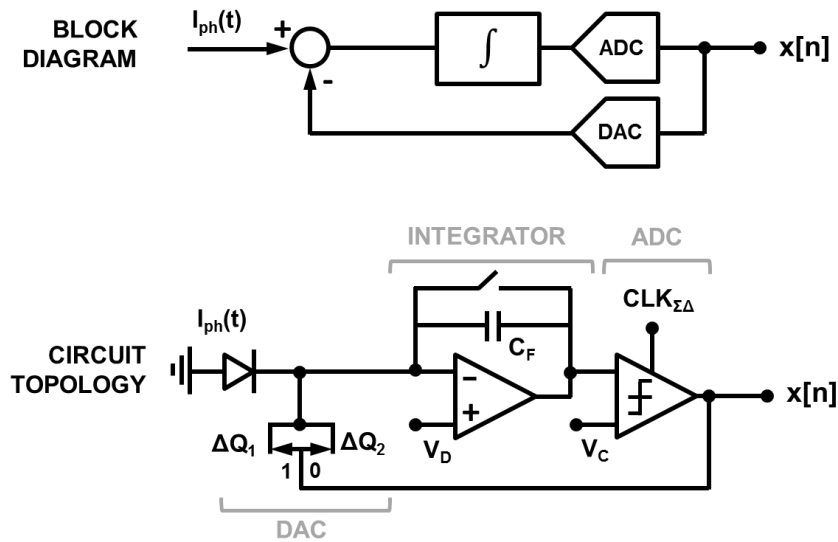


Figure Supp. 8: Circuit topology of the in-pixel $\Sigma\Delta$ photo sensor connected to the CMOS-compatible photodiode to detect I_{ph} .

C. Pixel Circuitry

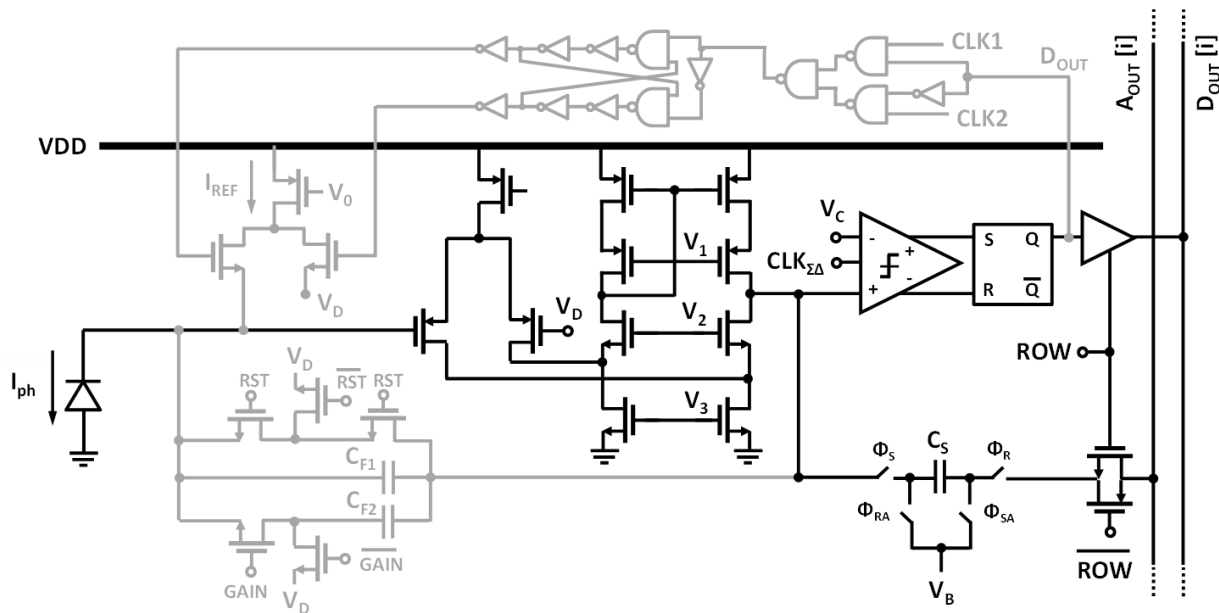


Figure Supp. 9: Detailed circuit implementation of the biosensor pixel.

C.1. Current Integrator (Transistor-Level)

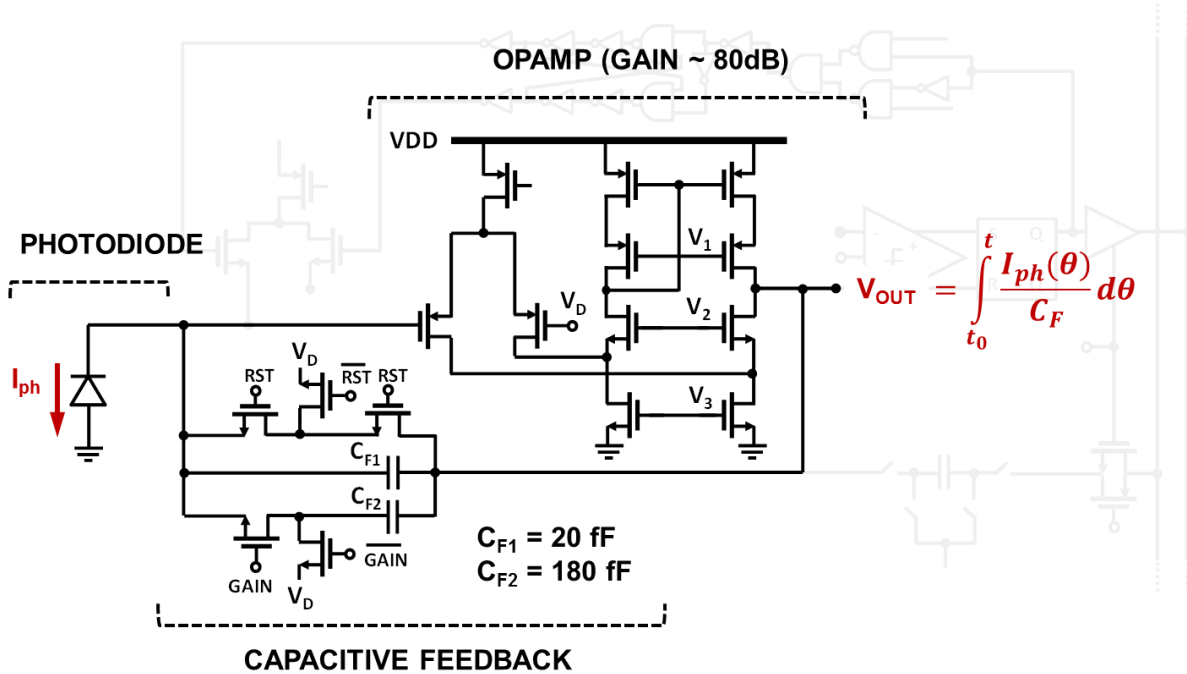


Figure Supp. 10: Transistor level implementation of the in-pixel current integrator with capacitive feedback.

C.2. Quantizer and S&H

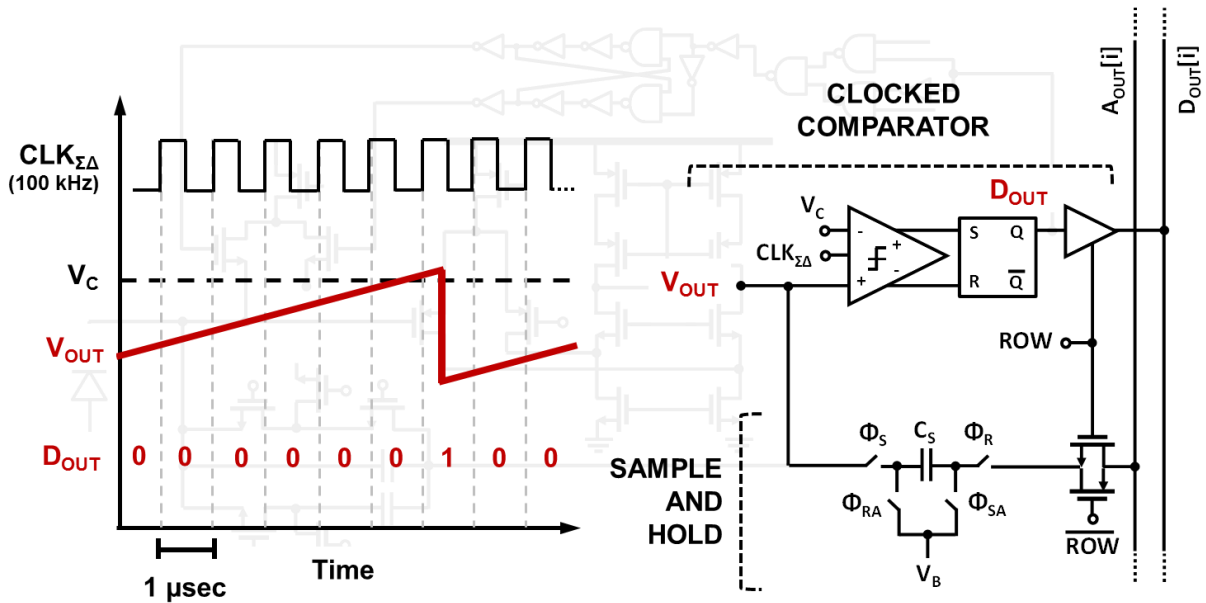


Figure Supp. 11: Timing diagram and transistor level implementation of the in-pixel quantizer and the sample and hold circuitry.

C.3. Digital-to-Analog (DAC) Converter and Timing Diagram

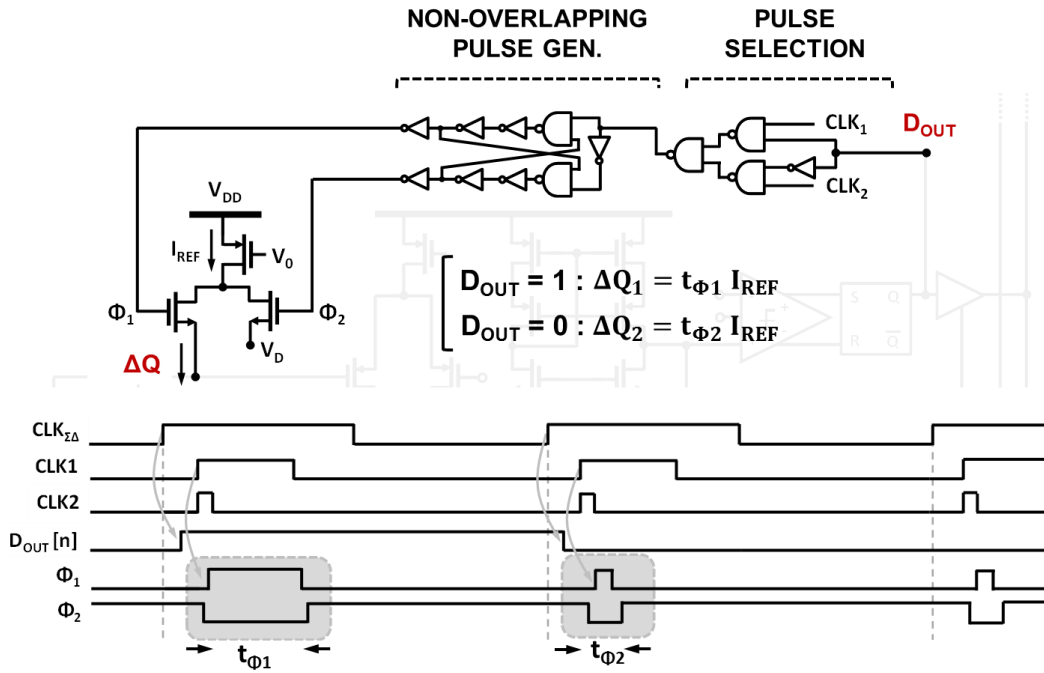


Figure Supp. 12: Timing diagram and transistor level implementation of the in-pixel digital-to-analog converter (DAC).

D. Pixel Layout and Individual Circuit Blocks

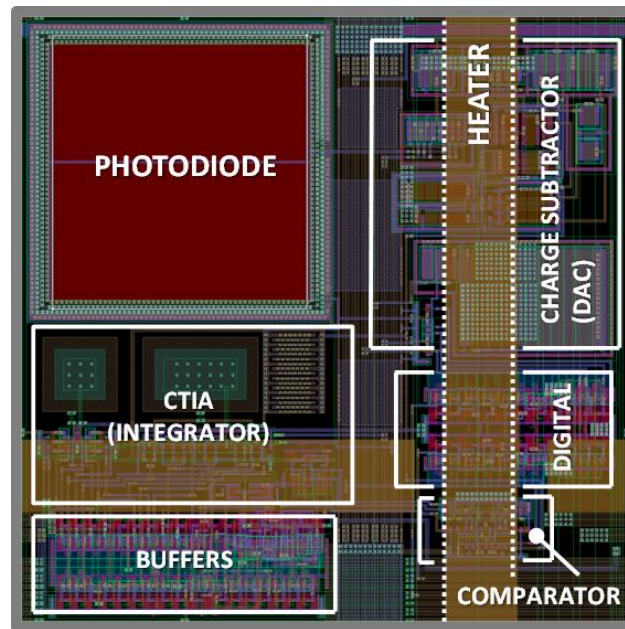


Figure Supp. 13: Layout of the biosensor pixel with the individual circuit blocks.

E. Measured External Quantum Efficiency (Q.E.) of the CMOS Photodiode (No Filter)

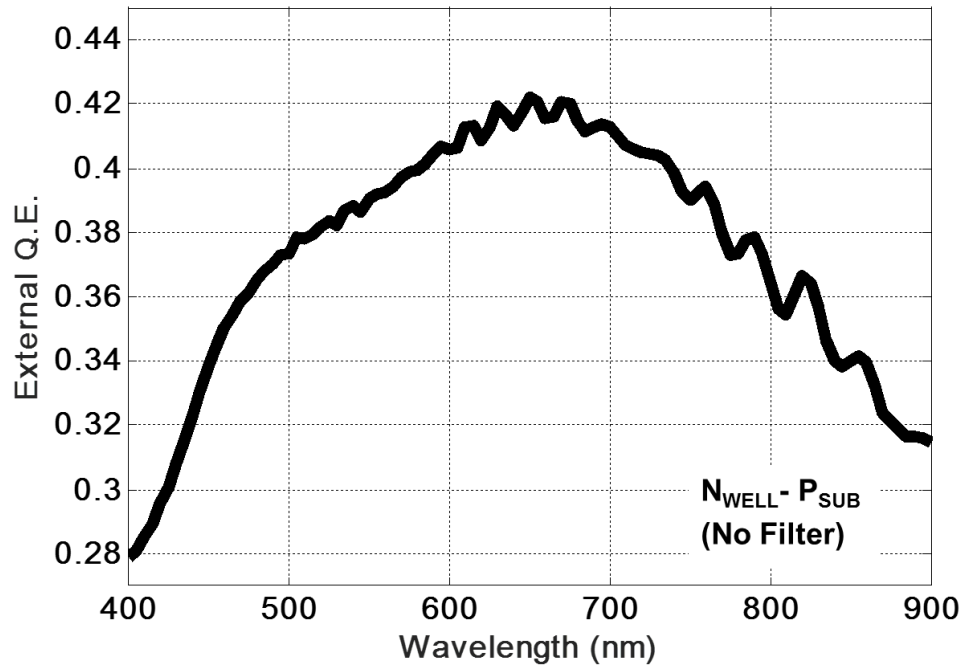


Figure Supp. 14: Measured external quantum efficiency (Q.E) of the embedded photodiode. The data is the average of 1011 pixels on a single CMOS chip. The measurement was conducted once.

F. Measured Dark Current across the Array vs. temperature

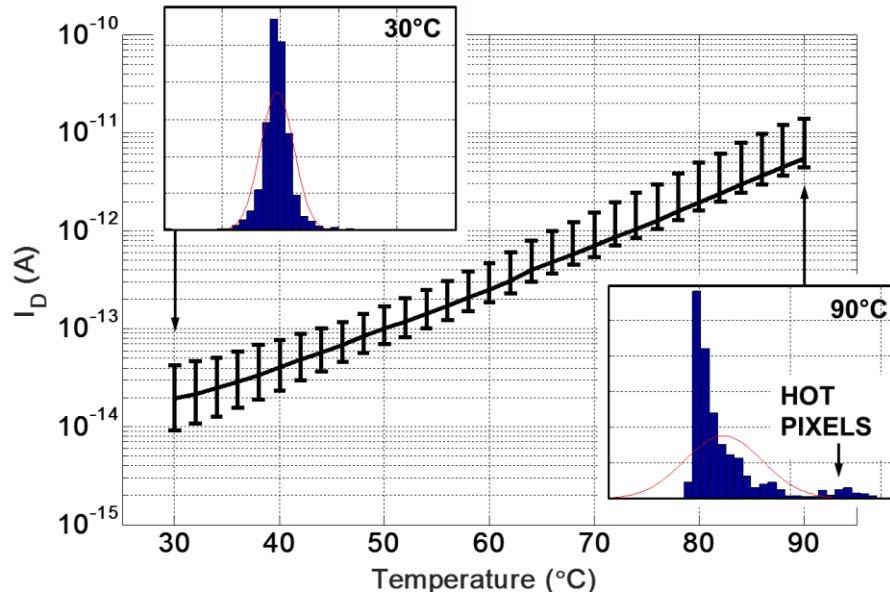


Figure Supp. 15: Measured dark current (I_D) as a function of temperature. The average from 1024 pixels from one experiment is plotted with error bars showing the minimum and maximum range. The histogram shows the pixel count vs. I_D at 30°C and 90°C.

G. Measured Photo Sensor Linearity ($\lambda_x = 495$ nm)

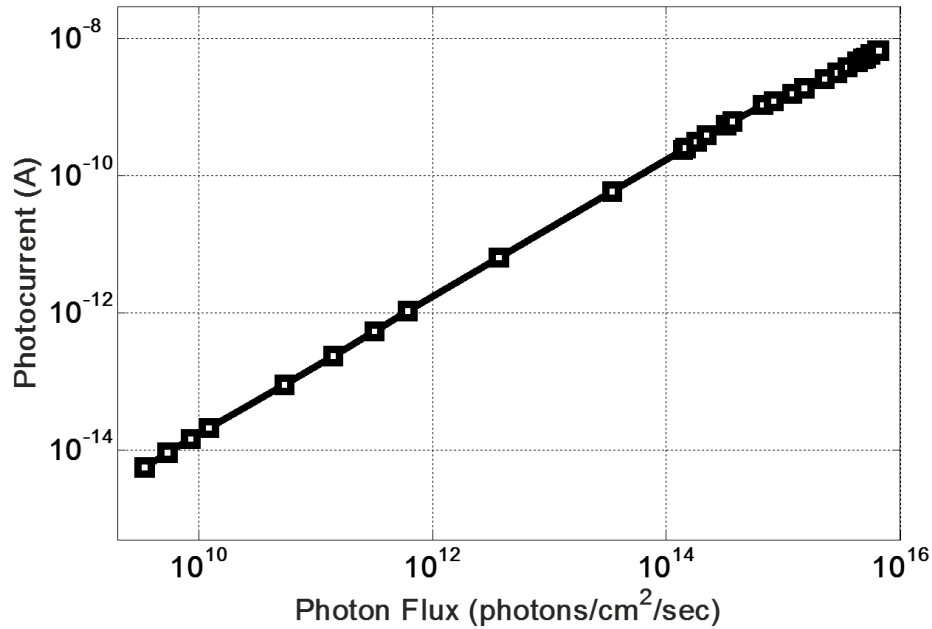


Figure Supp. 16: Measured photo-sensor linearity vs. incident photon flux (495nm excitation wavelength). The plot shows the average of 1011 pixels from one experiment.

H. Signal-to-Noise (SNR) vs. Shot-Noise Limit

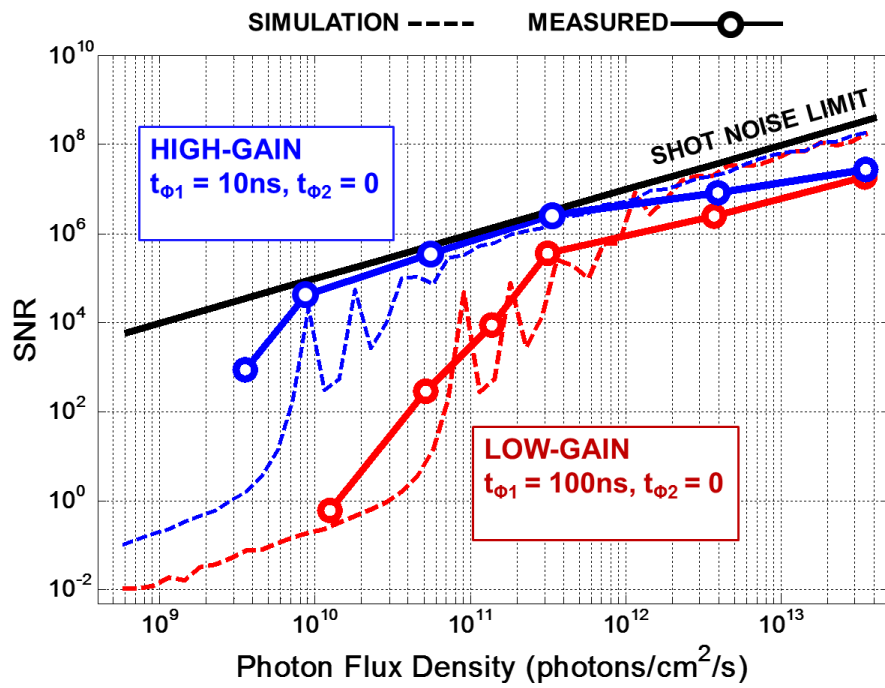


Figure Supp. 17: The measured vs. theoretical signal-to-noise (SNR) ratio for high and low gain modes. Each measurement was conducted once.

I. Chip Performance Summary

Technology	0.25 μm CMOS
Supply voltage	2.5V
Die dimensions	7.0mm x 9.0mm
Array dimensions	32 x 32
Biosensor size	100 μm x 100 μm
Photodiode	50 μm x 50 μm ($N_{\text{well}}\text{-}P_{\text{sub}}$)
Photodetector dark current (I_{dc})	20 fA (30°C) – 5.5 pA (90°C)
Photodetector $Q_E(\lambda)$	>0.38 (500nm – 775nm)
Frame rate (BW)	1Hz to 50Hz
Well capacity (Q_{well})	6.25 $\times 10^{10}$ e ⁻ (Low Gain) 6.25 $\times 10^9$ e ⁻ (High Gain)
Maximum photocurrent ($I_{D_{\text{max}}}$)	10nA (Low Gain) at $f_{\Delta} = 100$ kHz 1nA (High Gain) at $f_{\Delta} = 100$ kHz
CLK₁, CLK₂ pulse width ($t_{\Phi 1,2}$)	10ns – 100ns
Detection linearity	> 10 ⁵
Detection dynamic range (DDR)	116 dB
Chip Output	102.4 Mbps LVDS serialized
Heating/cooling rate	4°C/sec
Operating temperature range	25°C – 100°C
Temperature sensor resolution	0.3°C (for chip temperature 45°C - 100°C)
Total power consumption	62mW (array) + 50mW (LVDS) + 6mW (analog column amplifiers) = 118mW

Supplementary Note 6

Description: Emission filter structure and measured response.

To measure fluorescence emission, the biochip utilizes an emission filter to selectively block the excitation light of the LED source while passing the emitted photons that originate from FAM-TAM constructs. The cross section of the filter and its structure is shown in **Fig. Supp. 18**, and is made of two thin-film coatings, patterned and deposited on top of the CMOS chip.

The first coating in our design is a traditional multi-layer dielectric long-pass optical filter, which consists of alternating layer of dielectric materials with different refractive index n_1 and n_2 . Such a structure offers excellent rejection; yet its transmittance is highly angle-sensitive (defined by θ in the **Fig. Supp. 18**).

To mitigate this problem, a coating is used which is made of alternating layers of metal and dielectric materials. This metal-dielectric interference filter offers less rejection when compared to the full dielectric long-pass filter but it is less angle-sensitive. Combining the two filters permits us to build a filter with excellent rejection of the excitation light and minimum sensitivity to non-normal angles of incidence (AOI).

Both coatings are carefully designed using Essential McLeod Software (Thin Film Center, Tuscon, AZ). The simulated filter responses are shown in **Fig. Supp. 19**. As explained in **Fig. 3** (cf. manuscript), the filter has to block the excitation light in the 440-480 nm wavelength range while permitting the emitted light in the 600-700nm range. The optical density (OD) of the complete stack is > 6 for AOI of 0° and 30° . Even at high AOI of 60° , the effective OD for excitation wavelength of 470nm is 4.12. Also, the top layer thickness is adjusted to maximize the E-field at the filter-solution interface to ensure proper excitation of the fluorophores at the interface. The measured transmittance of the filter in presence of the PCR reagents and the fluidic cap is shown in **Fig. Supp. 20**.

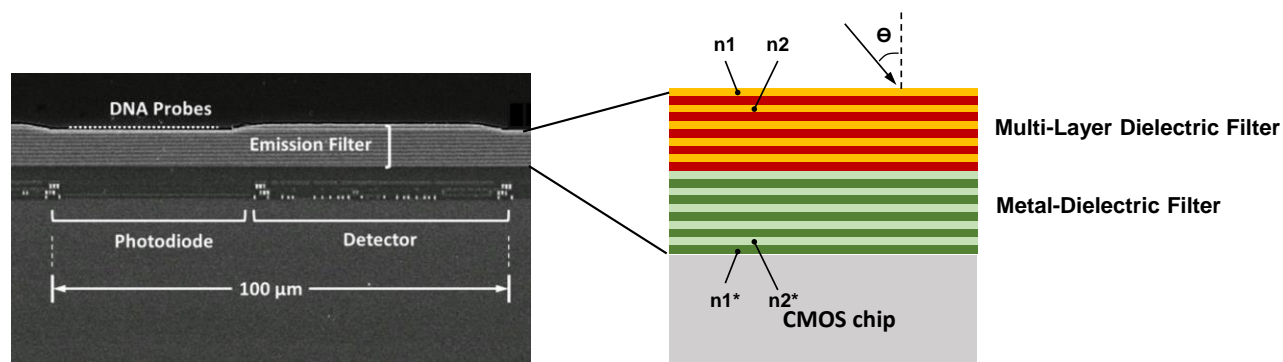


Figure Supp. 18: CMOS biochip cross-section with the excitation filter structure.

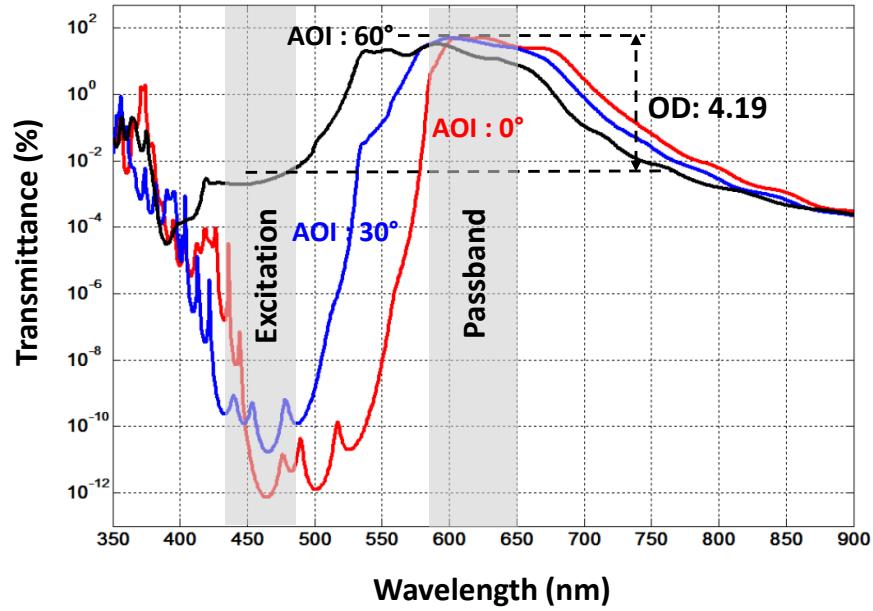


Figure Supp. 19: Simulated filter response for the filter structure shown in Fig. Supp. 18.

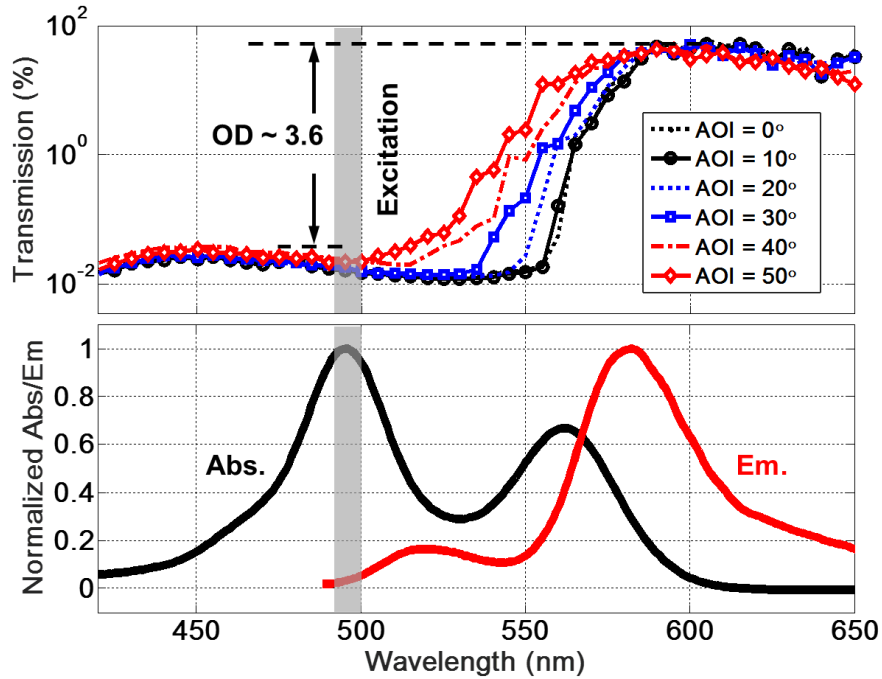


Figure Supp. 20: Measured transmittance of the filter in presence of the PCR reagents and the fluidic cap. All the experiments, including spectral scans and transmittance measurements, were conducted once.

Supplementary Note 7

Description: Variations, failure rates, and prototype manufacturing/assembly yields.

Component	Parameter	Observed Variations/Error	Mitigation/Calibration Process
CMOS IC	Electronic functionality (analog/digital)	~2/250 non-functional	Functionality test prior to biochip assembly
	Photo-sensing quantum efficiency (Q.E.)	< 10% variation	Correct using the normalization probes
	Dark Current (Id)	< 40% variation	Correct using CDS
Emission Filter	Transmittance	None	Verify each wafer coating run prior to biochip assembly
Probe Printing	Surface Functionalization	< 10% water contact angle variation	Verify expected witness coupon water contact angle and recorded instrument process parameters
	Probe Printing	< 5% devices scrapped due to spot diameter or spot placement accuracy or probe signal out of range	Real-time instrument optical droplet confirmation and fiducial alignment score, batch sampling and fluorescence imaging of assay and control probes.
Fluidic Cap*	Mechanical	~20% have defects	Inspect and discard imperfect components prior to biochip assembly
	Optical	~10% have small scratches	Inspect before assembly
Setup/Instrument	Temperature Control	0.3°C	Calibrate after each 10 experiments
CMOS Biochip Experiments	Sample Quality	Varied	Quantify using qRT-PCR process every week or 10 experiments
	Reaction Mix	Varied	Verify using assay CNTRL(+)
	RT-PCR	15% formed bubbles*	Disqualify experiment

* The fluidic cap used in this research was a prototype and had the lowest yield among all components.

Supplementary Note 8

Description: Reader instrument of the CMOS biochip platform.

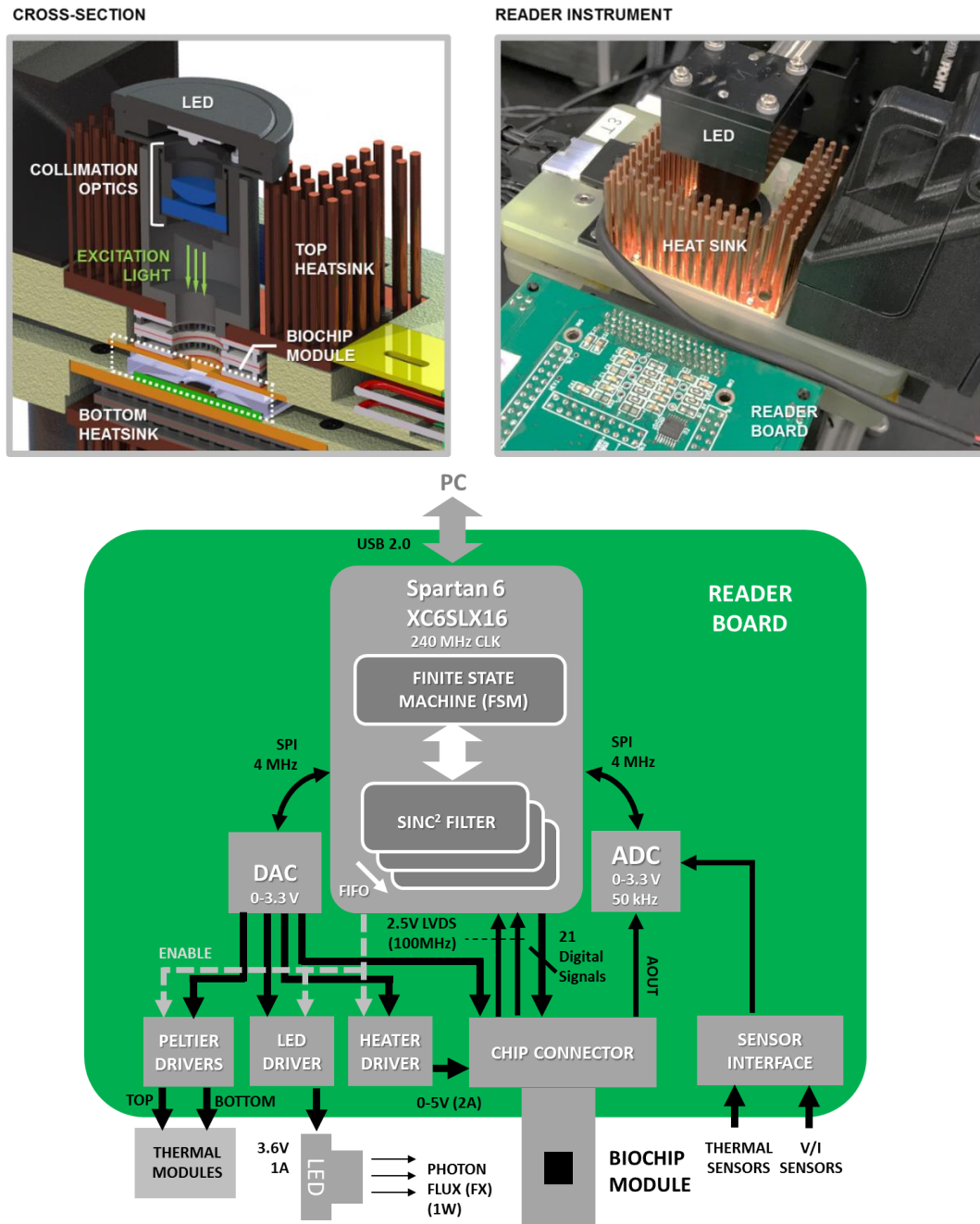


Figure Supp. 21: Reader instrument block diagram and its interface with the CMOS biochip module.

Supplementary Note 9

Description: Methods for CMOS biochip data acquisition and analysis.

In this supplementary, we discuss how we dealt with non-idealities of the measurements such as sensor additive noise, excitation light non-uniformity and etc.

A. Dark Current Subtraction

Dark current subtraction is the first step in data processing for the photo-sensor pixels. Dark current, denoted here by I_d , is a temperature-dependent additive value that is added to photocurrent signal. Its value is not constant during the experiments and can change by 2 orders of magnitude over the course of the melt phase. A correlated double sampling (CDS) technique is used to eliminate the undesired effect of I_d from the photocurrent reading (see **Fig. Supp. 22**). The output of the photo-sensor is measured twice, once without excitation light (LED-OFF), and once with excitation light (LED-ON).

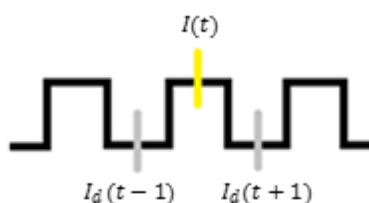


Figure Supp. 22: Concept of correlated double (CDS) sampling to remove dark current, I_d .

For a given LED-ON cycle, n chip reading frames are down-sampled to one by using the mean frame value. For that specific frame, I_d is defined to be the average of the measurements during two adjacent LED-OFF cycles. Therefore, the photocurrent, $I_{ph}(i)$, is computed by

$$I_{ph}(i) = \frac{1}{n} \sum_{k=1}^n I(i+k) - \frac{1}{2} \left[\frac{1}{n} \sum_{k=1}^n I_d(i+k-n) + \frac{1}{n} \sum_{k=1}^n I_d(i+k+n) \right], \quad (1)$$

where $I(t)$ is the measurement during LED-ON cycle and $I_d(t)$ is the measurement during LED-OFF cycle.

B. Background Subtraction

Background subtraction corrects for any excitation light that passes through the filter and reaches the photodiode. To do that, specific pixels are left “blank” and without FAM-TAM probes and hence their corresponding readings are used to estimate background signal across the array.

C. Calibration

In the array, we take advantage of calibration probes with unique sequences that do not hybridize to any of the amplicons or primers. The purpose of using these probes is to: (1) Measure the temperature-

dependent quantum yield, bleaching, probe detachment or any other amplitude-affecting characteristic of fluorophore emission in the pixels; and (2) use the information to calibrate (correct) the signals of the other probes. The two assays (URP and MTB) described in this manuscript use 15 calibration probe replicates. The calibration signal, \bar{I}_c , is calculated after the removal of outliers from the set of calibration probe replicates, $I_c(i)$, where

$$\bar{I}_c = \frac{1}{n} \sum_{i=1}^n I_c(i). \quad (2)$$

In **Fig. Supp. 23a** and **Fig. Supp. 23b**, as an example, we show signal of probe D516V from the MTB assay, before and after calibration, respectively. As evident, prior to calibration, the signal decreases as a function of temperature after the melt has occurred. This is because of the quantum yield of the fluorophore decreases with increasing temperature, producing the temperature dependence. After calibration, the temperature dependence is corrected and the signal does reach the expected plateau.

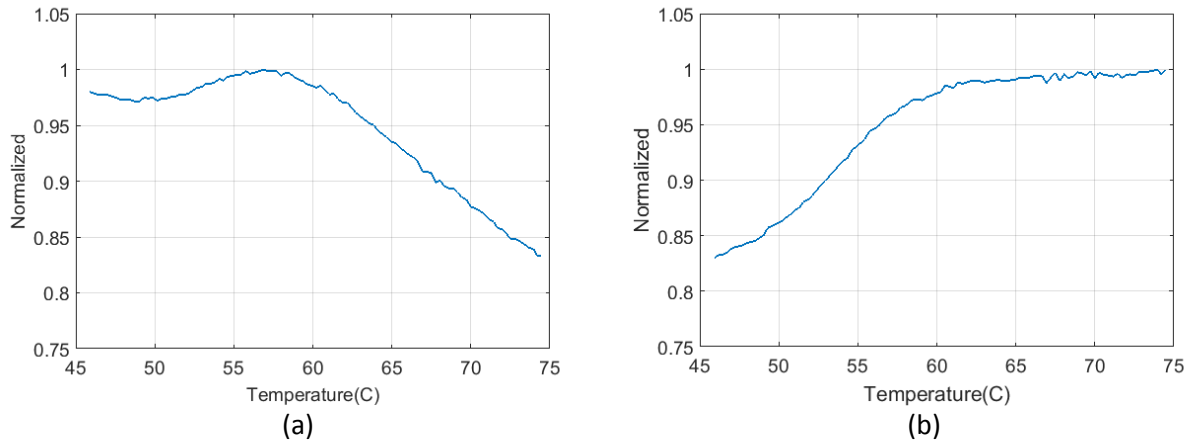


Figure Supp. 23: Signal from D516V WT probe from MTB Assay (a) before and (b) after calibration. The curves are the mean of 5 replicate probes from one experiment.

D. De-noising

The goal of de-noising is to compensate for errors in the data due to random fluctuations (e.g., thermal noise, shot noise, LED fluctuation and spontaneous drifts). To accomplish this, we find the closest smooth signal x to the measurements y by penalizing the changes of the output signal x by the penalty factor λ . In the specific case of solid-phase melting curve analysis all signals should monotonically increase; therefore a non-decreasing constraint has been considered.

The de-noising algorithm begins with a set of T noisy measurements that form the melting curve. Let x be the de-noised signal. The following formulation gives the convex optimization equation with the applied constrained to calculate x .

$$\begin{aligned} \min \quad & \|y - x\|^2 + \lambda \sum_{i=0}^{T-1} (x_{i+1} - x_i)^2 \\ \text{s.t.} \quad & x_{i+1} - x_i \geq 0. \text{ for } i = 0, \dots, T-1 \end{aligned} \quad (3)$$

To solve (3), we reformulate it to

$$x = \begin{pmatrix} x_0 \\ x_1 \\ \vdots \\ x_{T-1} \end{pmatrix} = \begin{pmatrix} x_0 \\ x_0 + \delta_1 \\ \vdots \\ x_0 + \delta_1 + \dots + \delta_{T-1} \end{pmatrix} = \mathbf{1}x_0 + \begin{pmatrix} 0 & 0 & \dots & 0 \\ 1 & 0 & \dots & 0 \\ \vdots & \vdots & \ddots & \vdots \\ 1 & 1 & \dots & 1 \end{pmatrix} \begin{pmatrix} \delta_1 \\ \delta_2 \\ \vdots \\ \delta_{T-1} \end{pmatrix} = \mathbf{1}x_0 + \mathbf{L}\boldsymbol{\delta}. \quad (4)$$

Therefore, the optimization problem can be re-written in terms of $\boldsymbol{\delta}$ as follows:

$$\begin{aligned} \min \quad & \|y - \mathbf{1}x_0 - \mathbf{L}\boldsymbol{\delta}\|^2 + \lambda\|\boldsymbol{\delta}\|^2 \\ \text{s.t.} \quad & \boldsymbol{\delta} \geq \mathbf{0} \end{aligned} \quad (5)$$

Now, to remove the dependency on the decision variable x_0 , we find its optimal value by minimizing the objective with respect to it

$$x_0 = \frac{\mathbf{1}'(y - \mathbf{L}\boldsymbol{\delta})}{T} \quad (6)$$

By substituting x_0 into (5), this equation can be expressed as the maximization of its dual function:

$$\begin{aligned} \max \quad & \min(y - \mathbf{L}\boldsymbol{\delta})' \left(\mathbf{I} - \frac{\mathbf{1}\mathbf{1}'}{T} \right) (y - \mathbf{L}\boldsymbol{\delta}) + \lambda\|\boldsymbol{\delta}\|^2 - 2\boldsymbol{\mu}'\boldsymbol{\delta} \\ \text{s.t.} \quad & \boldsymbol{\mu} > \mathbf{0} \ \& \ \boldsymbol{\delta} \geq \mathbf{0} \end{aligned} \quad (7)$$

By applying KKT conditions to (7), we can use Algorithm 1, defined below, in order to compute x in an iterative manner.

$$\boldsymbol{\delta} = [\mathbf{S}(I_\delta, I_\delta)]^{-1} \mathbf{L}(I_\delta, :)' \left(\mathbf{I} - \frac{\mathbf{1}\mathbf{1}'}{T} \right) y, \text{ and} \quad (8)$$

$$\boldsymbol{\mu} = \mathbf{S}(I_\mu, I_\delta) \boldsymbol{\delta} - \mathbf{L}(I_\mu, :)' \left(\mathbf{I} - \frac{\mathbf{1}\mathbf{1}'}{T} \right) y, \quad (9)$$

where $\mathbf{S} = \lambda \mathbf{I} + \mathbf{L}' \left(\mathbf{I} - \frac{\mathbf{1}\mathbf{1}'}{T} \right) \mathbf{L}$

Algorithm 1: De-noise by applying increasing constraint

Input: Noisy observations $y \in \mathbb{R}^T$, smoothing coefficient λ and maximum number of iterations n

1: Initialization: $I_\delta \leftarrow [1 \ 2 \ \dots \ T]$, $I_\mu \leftarrow \emptyset$, $l \leftarrow 1$

2: do

3: Find $\delta^{[l]}$ from equation 10, given $I_\delta^{[l-1]}$

4: if $\delta^{[l]} \geq 0$ then

5: break

6: end if

7: Find $\mu^{[l]}$ from equation 11, given $I_\mu^{[l-1]}$

8: $I_\delta^{[l]} \leftarrow (\delta^{[l]} \geq 0) + (\mu^{[l]} < 0)$

9: $I_\mu^{[l]} \leftarrow (\delta^{[l]} < 0) + (\mu^{[l]} \geq 0)$

10: $l \leftarrow l + 1$

11: while $l < n$

Output $x \leftarrow x_0 \mathbf{1} + \mathbf{L}(I_\delta^{[l]})' \delta^{[l]}$

E. Calculate Mutation “Score”

The MTB assay requires not only the detection of the amplicon, but also a decision as to whether the WT or MT strain is present at each mutation site. To do this, we compute the integral of the area between the WT and MT probes.

If N is the number of measurements during the melt reaction, I_W is the de-noised WT signal and I_M is the de-noised MT signal, then we can define S , the score by

$$S = \frac{1}{N} \sum_{i=0}^{N-1} I_W(i) - I_M(i) \quad (10)$$

Now if $S \geq 0$ for a specific probe pair, we conclude the WT target is present, and if $S < 0$, the MT is present. **Fig. Supp. 24** shows the averaged raw data for a probe pair before and after de-noising and applying the increasing constraint.

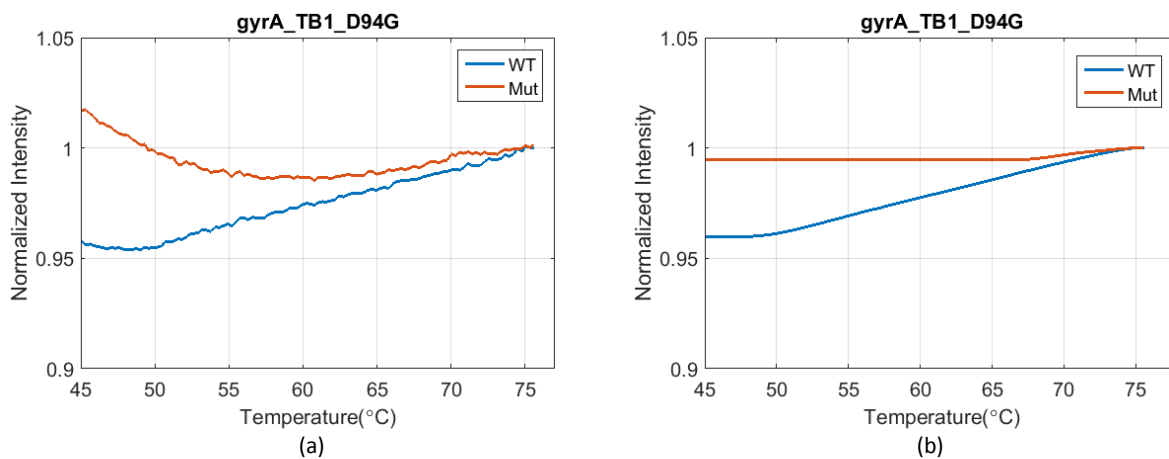


Figure Supp. 24: Average MT-WT results (a) before and (b) after de-noising ($n = 5$ replicate probes in one experiment).

Supplementary Note 10

Description: Materials and methods for *in-silico* design of real-time probes and multiplex PCR primers used in the CMOS biochip platform.

A. Thermodynamic Simulation Software Tools

Optimal design of both primers and probes requires examination of the structure of the amplicon in the assay physiochemical condition. In this project, we have used Oligonucleotide Modeling Platform (OMP) software package (DNA Software, MI) to simulate the interactions of one or more oligonucleotides under user-specified solution conditions. This software computes a multi-state equilibrium model of competing interactions that considers the random coil state and a user-specified number of possible conformations⁶. Parameters that can be defined as input include, but not limited to the initial concentrations of each species, the temperature, monovalent and divalent ion concentrations, the concentrations of various additives, and the maximum number of suboptimal conformations of each species to consider.

OMP is also capable of constructing a simulated melt curve for an oligonucleotide's hybridization to an amplicon by running simulations at a variety of temperatures. OMP also calculates the energy required to unfold each region of the amplicon structure (target unfolding ΔG°); this output is particularly useful for selecting optimal regions for primer design in cases of highly structured amplicons.

We have created a suite of in house tools in Perl and MATLAB to perform various functions relating to OMP simulations, including:

1. Generation of probe candidates around mutation sites;
2. Creation and evaluation of sticky-end probe candidates; and
3. Automation of OMP simulations and extraction of relevant metrics.

B. Primer Design for Multiplex PCR

Our approach to primer design and qualification using OMP includes the following steps:

1. Selection of regions for primer design: For highly structured amplicons, we use local unfolding energies calculated by OMP to focus primer design on regions that are most likely to be accessible for binding.
2. Ensure that OMP predicts that the binding of the primer to the template is thermodynamically favorable.
3. Ensure that the primer is predicted to exist primarily in a random coil state.
4. Ensure that the region of the template, to which the primer binds, is accessible. In cases where no such region can be found, we place as much of the primer as possible in a random coil portion of the amplicon that we term the anchor region. This method as applied to probe design is described below; the application to primer design is analogous.
5. Eliminate primers that are capable of self-priming.
6. Eliminate amplicons that are capable of self-priming.
7. Primer-dimer check: Once primers for the single-plex assays are designed, we check all possible pairs of primers for their potential to form primer dimers and redesign where necessary.

The URP assay utilizes primer regions previously described in the literature⁷⁻⁸, which were then subjected to the review described and possible redesign discussed above. Primers for the MTB assay were either designed using Primer3⁹ or were designed manually before undergoing the review described above.

C. Probe Design

In the NAAT assay presented in the manuscript, three (3) distinct probe design methodologies have been used:

1. Quantification probes to monitor the depletion of the limiting primers during multiplex PCR. These probes were used in the URP assay.
2. Detection probes to examine presence or absence of the target. These probes were used mainly in URP assay.
3. SNP identification probe pairs to detect mutations within the ROIs. These probes were used in the MTB assay.

C.1. Quantification Probes

Each quantification probe for the URP assay is the reverse complement of, p_r , the limiting primer whose depletion it is designed to detect. The probe is labeled with FAM-TAM at its 3'-end, and its fluorescence is quenched when the BHQ2-labeled limiting primer binds. All simulations include the poly-T spacer at the 5'-end of the probe as described in manuscript and a 7-base poly-T stretch at the 3'-end as a stand in for FAM-TAM, which OMP is currently unable to simulate directly. Quantification probe sequences for the URP assay are given in **Table Supp. II**.

PRIMER	PRIMER SEQUENCE (5'->3')	SIMULATED PROBE SEQUENCE (5'->3')
FluA-1 Limiting	BHQ2-GTAAGGCTTGCATGAATGTTATTTGCTC	TTTTTTGAGCAAATAACATTCATGCAAGCCTTACTTTTTTT
FluA-2 Limiting	BHQ2-AGGGCATTYTGACAAAKCGTCTA	TTTTTTTAGACGCTTTGTCCACAATGCCCTTTTTTTT
FluB Limiting	BHQ2-CGGTGCTCTTGACCAAATTGG	TTTTTTCCAATTTGGTCAAGAGCACCGTTTTTTTT
RSV Limiting	BHQ2-TCTTTTTCTAGGACATTGTAYTGAACAG	TTTTTTCTGTTCACTACAATGTCTTAGAAAAAGATTTTTTT
Para-2 Limiting	BHQ2-ACCTCCTGGTATAGCAGTGACTGAAC	TTTTTTGTTTCAGTCACTGCTATAACCAGGAGTTTTTTTT
Adv-C Limiting	BHQ2-GCCACAGGTCCTCATATAGCAA	TTTTTTTTGCTATATGAGGACCTGTGGCTTTTTTTT
Adv-E Limiting	BHQ2-CCTGGCTGTTATTTTCCACCAAC	TTTTTTGTTGGTGAAAAATAACAGCCAGGTTTTTTTT

Table Supp. II: URP assay quantification probe sequences. A poly-T spacer is added to the 5'-end of the reverse complement of the corresponding limiting primer sequence, and a 7-base poly-T stretch is added to the 3'-end to represent FAM-TAM in simulations. Limiting primers are labeled with black hole quencher 2 (BHQ2) at the 5' end.

C.2. Detection Probes

The detection probes used in the URP assay are designed to produce a signal when a particular target is present, and are placed close to the excess primer in order to facilitate the “sticky-end probe design” described in manuscript and below. In certain cases, we instead used probes described in the literature⁶⁻⁷. All probes were simulated using OMP to ensure that the binding of the probe to the amplicon is thermodynamically favorable and that, whenever possible, the probes and their binding sites on the amplicon exist in a random coil state. Probes are simulated with the 5' poly-T spacer and a 7-base poly-T stretch at the 3'-end.

After these probes are designed, we convert them into probes that can capture the 5'-end of the primer region, i.e., the “sticky-end method”. This novel technique brings the quencher into close proximity of the fluorophore without the need for incorporation of quencher-modified nucleotides into the amplicon. To accomplish this, we attach a fluorophore to the 3'-end of the probe and a quencher to the 5'-end of the excess primer so that the single-stranded amplicons produced by asymmetric PCR are quencher-labeled at the 5' end. Then, in order to bring the 5' end of the amplicon in close proximity to the fluorophore-labeled probe, we add a small number of bases to the 3' end of the probe that are complementary to the 5' end of the excess primer. These “sticky end” probes then hybridize to both the 5'-end of the amplicon and to the region that is complementary to the original probe design. An example of this design is given in **Fig. Supp. 25**.

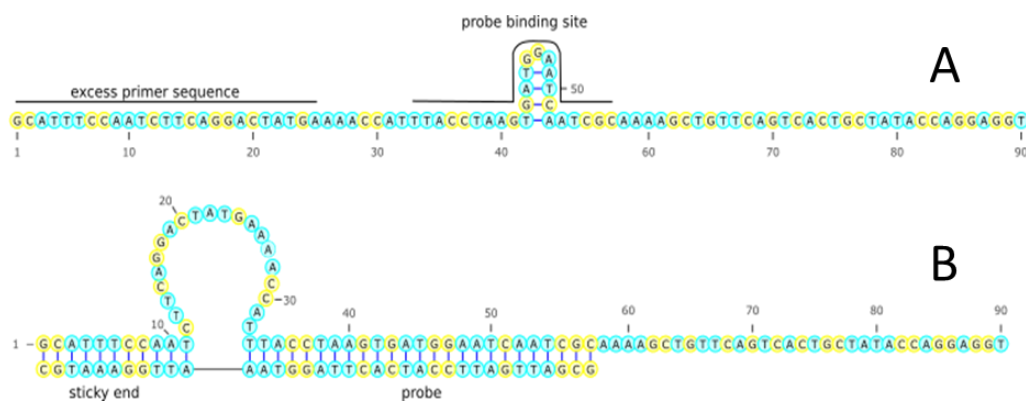


Figure Supp. 25: “Sticky-end probe design”. (A) OMP predicts that the binding site for the probe is largely located in a random coil region of the most thermodynamically favorable conformation of the Para-2 amplicon. (B) Binding of the probe brings the 5'-end of the amplicon into close proximity of the 3'-end of the probe, which allows for contact quenching of the amplicon's fluorophore.

The sticky end of the probe must be sufficiently long to capture the 5'-end of the amplicon at the hybridization temperature while minimizing background signal produced by binding to the excess primer itself (**Fig. Supp. 26**). To balance these two competing factors, we create a series of probes with 4-15 bases complementary to the 5'-end of the excess primers. We then run thermodynamic simulations of these candidates using OMP in the presence of either the amplicon or the excess primer and evaluate them for their ability to discriminate between these two species. For instance, in **Fig. Supp. 27**, adding 11 bases that are complementary to the Para-2 excess primer yields a probe with a large separation between the melt curves at the hybridization temperature for the excess primer versus the amplicon.

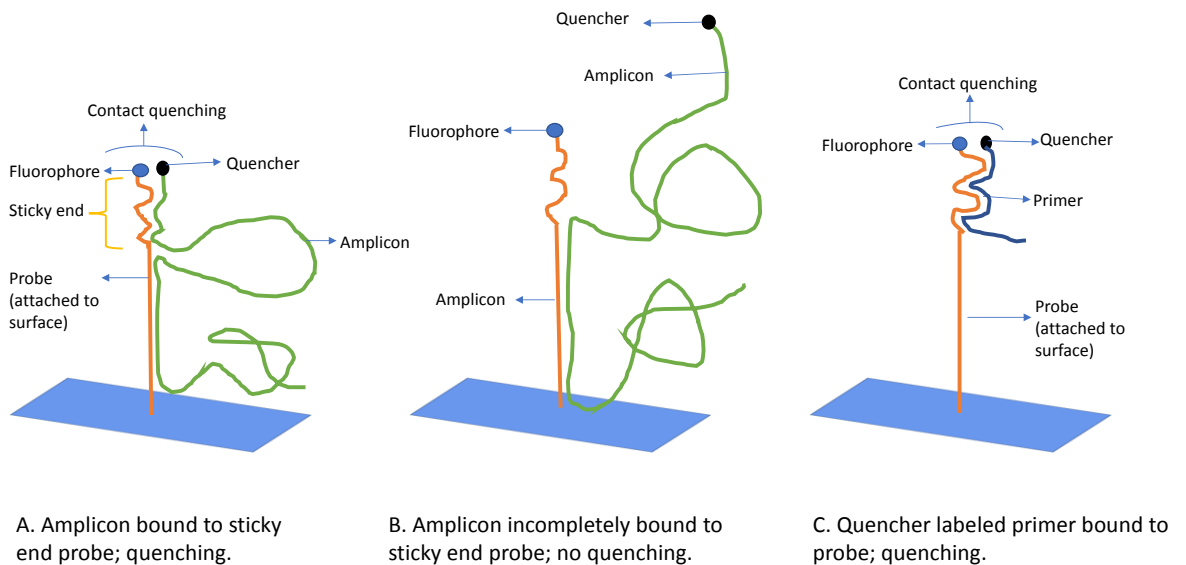


Figure Supp. 26: Sticky end probe design. (A) A short stretch of bases that are complementary to the excess primer (the primer section) is added to the probe in order to capture the 5' end of the amplicon and bring the quencher in close proximity to the probe's fluorophore. (B) If the primer section is too short, it will not capture the amplicon. (C) If it is too long, however, it will capture the excess primer and give rise to background signal. These competing effects determine the optimal length of the primer section.

C.3. SNP Identification Probe Pairs

The *M. Tuberculosis* (MTB) genotyping assay uses probe pairs that are designed to discriminate between the wildtype (WT) and mutant (MT) sequences. A flow chart of the probe design process is given in **Fig. Supp. 28**. For each mutation coordinate, we generate probe candidates by moving sliding windows of lengths 15 through 25 along the sequence such that the mutation is kept within the middle third of the probe. These specific lengths are selected to ensure that we create an exhaustive probe candidate list applicable to both CG-rich and AT-rich genomic regions. At each location for this window, we generate a pair of probes in which one probe is complementary to the wildtype target and the other probe is complementary to the target containing the mutation.

We next assess *in silico* each candidate probe pair's ability to discriminate between the wildtype and mutant sequences by simulating a melt curve at thermodynamic equilibrium using OMP. Clearly, sequence mismatches between the probe and its binding site on the amplicon will decrease the strength of the hybridization relative to a perfect match, and hence probes with more mismatches will begin to dissociate from the amplicon at lower temperatures than probes with fewer mismatches. This leads to a shift in the melt curve for the wildtype target bound to the mutant probe relative to the wildtype target bound to the wildtype probe, and similarly for the mutant target (**Fig. Supp. 29**). InSilixa's assay makes use of the shifts in these characteristic melt curves to determine whether the target contains the wildtype or mutant sequence.

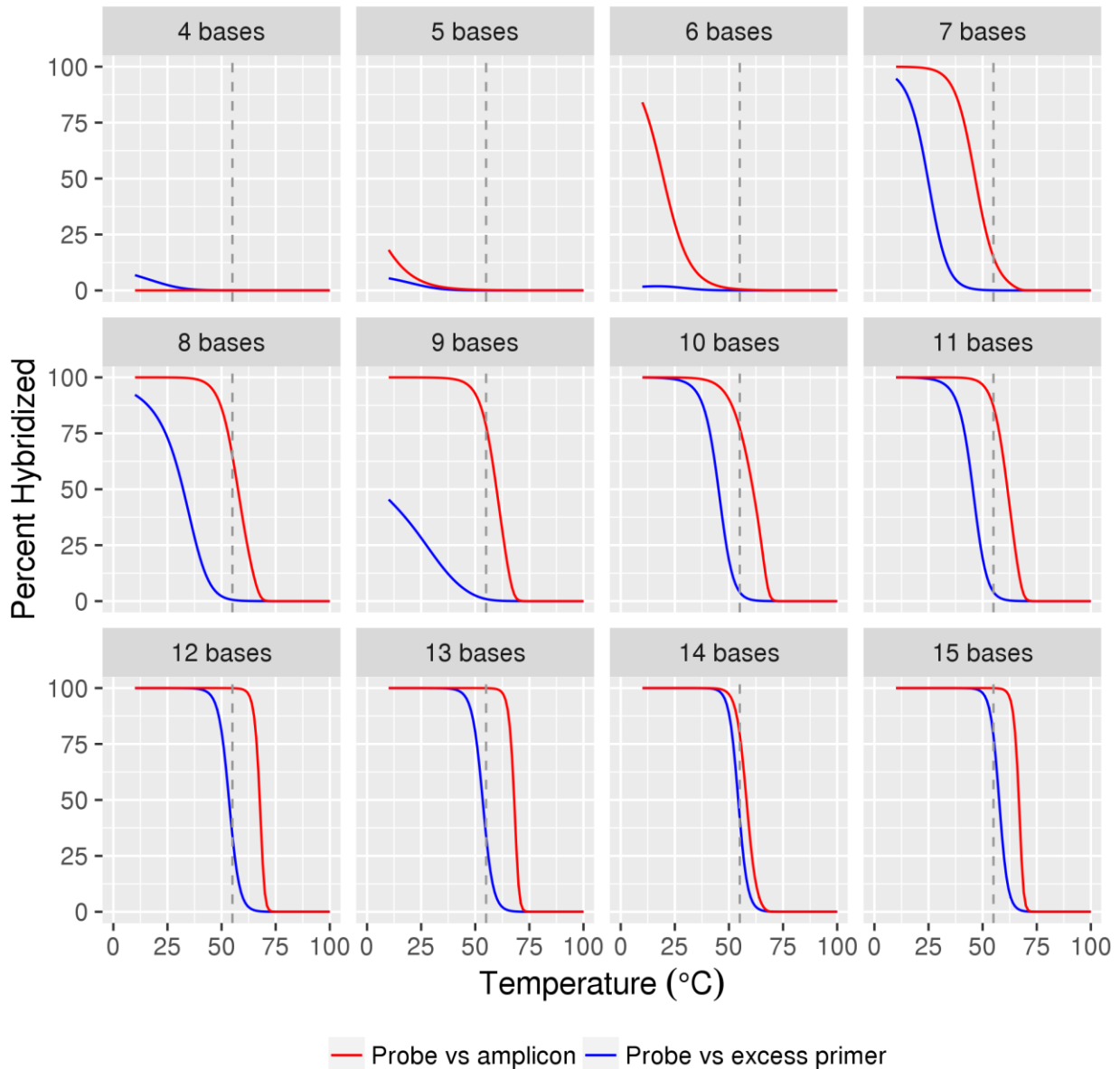


Figure Supp. 27: The sticky end must be sufficiently long to capture the 5' region of the amplicon to allow quenching to occur, but not so long that it captures the excess primer itself and gives rise to background signal. Melt curves for both cases simulated by OMP allow for selection of a sticky end probe length that balances these competing factors. In the case of the Para-2-pb1 probe from the URP panel, a sticky end length of 11 bases minimizes background signal from the primer (blue) and maximizes signal from the amplicon (red). The hybridization temperature of 55°C is indicated by a dashed line.

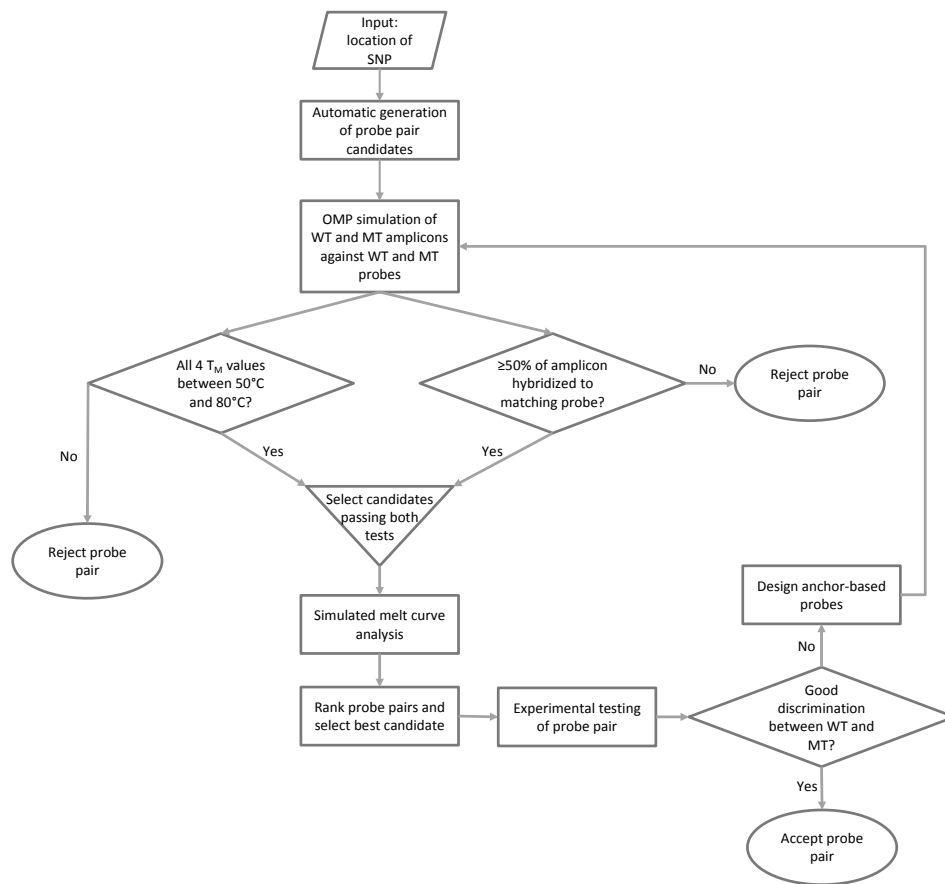


Figure Supp. 28: The design process for SNP detection probes.

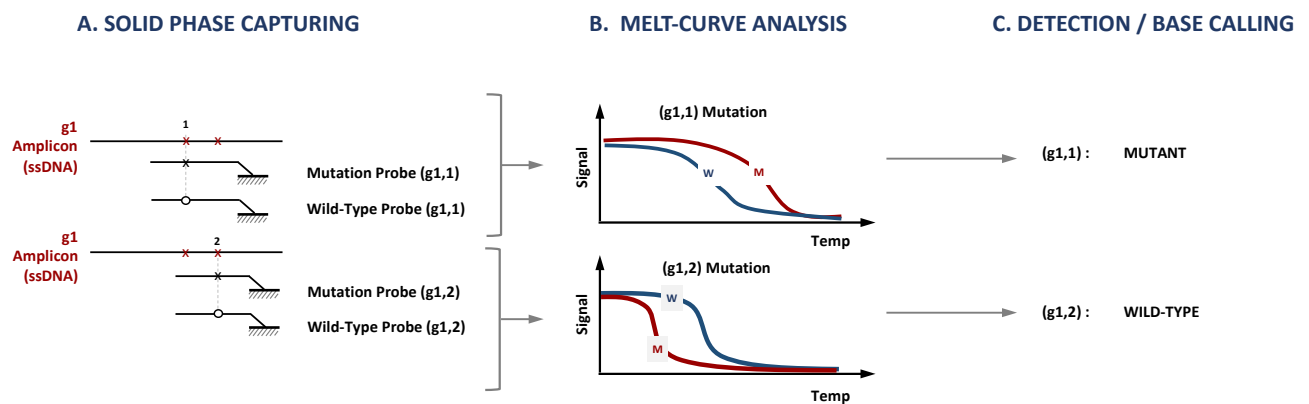


Figure Supp. 29: Differential melt curves for mutation detection. (A) Two mutations in close proximity are detected using two separate probe pairs. In this case, the amplicon contains the mutant base at position 1 (top) and a wildtype base at position 2 (bottom). (B) Each probe pair gives rise to a pair of melt curves in which the probe that more closely matches the amplicon's sequence gives rise to a melt curve that is shifted towards higher temperatures. (C) This separation between the melt curves allows us to determine whether the amplicon contains the wildtype or the mutant base at the position the probe pair assays.

We select the best wildtype/mutant probe pair by simulating melt curves for each probe's hybridization to both the wildtype and mutant amplicon and ranking them by a heuristic parameter that increases as the area between the two pairs of resulting melt curves increases. This parameter is given by

$$\frac{1}{N} \sqrt{\sum_{T_{\min}}^{T_{\max}} ((C_{WW} - C_{MW})^2 + (C_{MM} - C_{WM})^2)} \quad (1)$$

in which C_{WW} is the concentration of the wildtype probe bound to the wildtype target, C_{MW} is the concentration of the mutant probe bound to the wildtype target, C_{WM} is the concentration of the wildtype probe bound to the mutant target, C_{MM} is the concentration of the mutant probe bound to the mutant target, and N is the number of temperatures at which these concentrations were calculated. Furthermore, we reject probes that bind to their intended targets with a T_M of less than 50°C or greater than 80°C, or for which less than 50% of amplicons are expected to bind to probe at the hybridization temperature.

C.4. Anchor-based Probes

In some cases probes cannot be placed in random coil regions, typically because a mutation we wish to detect is buried within a hairpin structure and hence is not readily accessible for binding to a probe. For instance, the A74S and D94G *gyrA* mutations on the TB1 amplicon are located within hairpins with high melting temperatures (**Fig. Supp. 30a**). To overcome this problem, we examine the secondary structure of the amplicon under the hybridization conditions and pick the nearest 12 -15 bases that are more readily accessible and that therefore can act as an anchor for probe binding. Once the anchor region binds, the remainder of the probe is able to compete more effectively for the portion of the binding site that is located within secondary structure. For example, an anchor consisting of bases 38-51 is used to aid detection of the A74S mutation (GCC-74-TCC) located in the first hairpin of the TB1 amplicon.

In another example, bases 88-100 are selected to anchor the D94G mutation (GAC-94-GGC). However, the anchor region for the D94G probe is somewhat distant (18 bases) from the mutation site. In this case, the probe is designed to bind to two non-contiguous regions on the amplicon (positions 88-100 and 112-128 in **Fig. Supp. 30a**) to enable discrimination between WT and MT sequences; inclusion of the intervening bases 101-111 in the probe would give rise to melt curves too similar for discrimination of a one base mismatch between the wildtype probe and mutant amplicon sequence (or vice versa). Six probe bases between the two regions are added to reduce steric hindrance without base pairing with the amplicon. The structure of the D94G probe bound to the amplicon is shown in **Fig. Supp. 30b**; OMP predicts that over 99% of both the wildtype and mutant amplicons will bind to the probes with exact sequence matches at thermodynamic equilibrium, and experimental results confirm that binding occurs at a rate that is sufficient for detection.

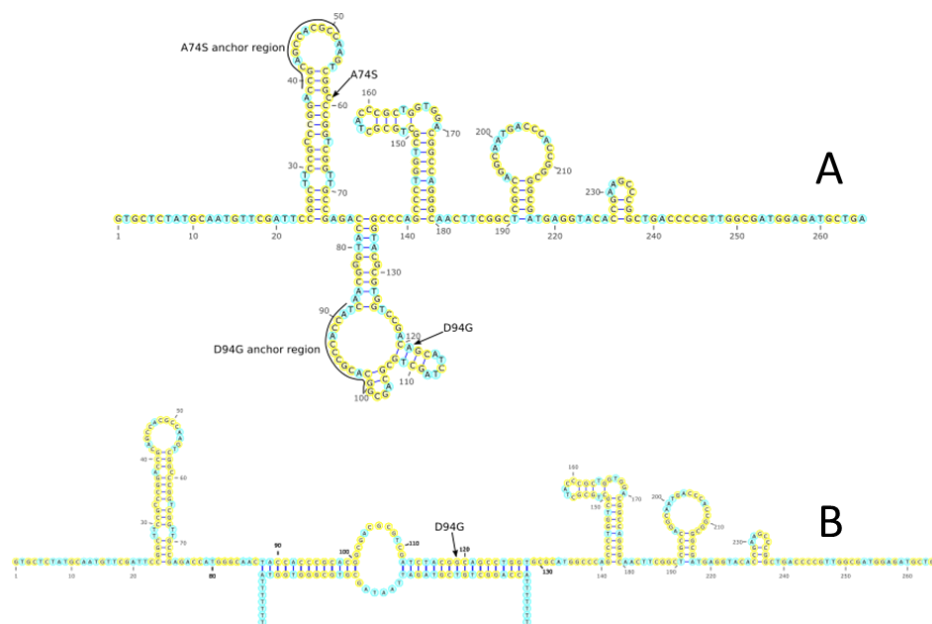


Figure Supp. 30: Anchor-based probe design. (A) The A74S and D94G mutations in the TB assay’s gyrase A TB1 amplicon are both located within hairpin structures. Anchor regions consisting of significant stretches of bases that are more readily accessible to the probe serve to drive the kinetics of binding. **(B)** The D94G probe binds to two discontinuous regions of the amplicon, which keeps the probe length short enough to allow for discrimination of the bases while still taking advantage of the availability of a somewhat distant anchor site.

Supplementary Note 11

Description: URP detection and quantification assay.

The multiplexed URP assay discussed in the manuscript was first designed and verified using conventional molecular biology and PCR techniques. Subsequently, the optimized primers and probes were transferred to the CMOS biochip platform. Furthermore, in certain cases, the results generated were verified after CMOS biochip experiments. In this supplementary, we describe the methods employed and provide additional results and analysis.

A. Materials and Methods

A.1. Samples and Nucleic Acid Templates

Synthetic nucleic acid templates for multiplex assay development and standard curve generation. Synthetic target DNA (ssDNA, dsDNA) was obtained from LGC BioSearch Technologies (Novato, CA) as PAGE purified material provided in Tris-HCl pH 8.5 at 1×10^6 copies/ μ l. Single stranded RNA (ssRNA) was produced via transcription from chemically synthesized double stranded DNA (dsDNA) containing an SP6 promoter, DNaseI digested, PAGE purified and provided in sodium citrate pH 6.4 at 1×10^6 copies/ μ l. All synthetic materials were separated into 10ul aliquots, stored at -80°C and used once as needed (to prevent freeze-thaw cycles). The sequences of the synthetic nucleic acids used to develop the assay and for standard curve generation along with the genome regions from which they originate and the viral genes they code for are listed in **Table Supp. III**.

Whole genome material used for multiplex NAAT. Total nucleic acid extracts from cultured viral material containing whole viral genomes was used for multiplex NAAT on chip (**Fig. 4**, and **Fig. Supp. 31**) experiments. Two sources for whole genome material were used:

- I. Inactivated, cultured viruses (NATrol[®] controls) purchased from Zeptomatrix Corporation (Buffalo, NY). For RNA viruses, RNA was extracted from this material using standard QIAamp[®] Viral RNA Mini Kit part number (p/n) 80204 (Qiagen, Hilden Germany) as per manufacturer's instructions and quantitated using qRT-PCR as described below. For DNA viruses, DNA was extracted from this material using QIAamp[®] DNA/RNA Mini Kit p/n 52904 (Qiagen) as per manufacturer's instructions and quantitated using qPCR as described below.
- II. Total nucleic acid extracts from viral culture material were obtained from American Type Culture Collection (ATCC, Manassas, VA) and quantitated using qPCR as described below.

Upon completion of nucleic acid extraction or receipt of total nucleic acid extracts, samples were split into 10 μ l aliquots and stored undiluted at -80°C and each aliquot used once as needed.

Table Supp. III: URP Assay Amplicons/Synthetic Nucleic Acid Sequences			
Amplicon Name	Viral Gene	Genome Region	Sequence
FluA-1	NS1	Segment 8 Bases 636-793	GGACCTCCACTTACTCCAAAACAGAAACGGAAAATGGCGAGAACAACTAGGTCAAAGTTC GAAGAGATAAGATGGCTGATTGAAGAAAGTGAGACACAGACTGAAAACAACTGAGAATAGT TTTGAGCAAATAACATTCATGCAAGCCTTAC
FluA-2	M	Segment 7 Bases 171-276	GACCAATCCTGTACCTCTGACTAAGGGGATTTAGGATTTGTGTTACGCTCACCGTGCCC AGTGAGCGAGGACTGCAGCGTAGACGCTTTGTCCAAAATGCCCT
FluB	NS1	Segment 8 Bases 720-822	TCCTCAACTCACTCTTCGAGCGTCTTAATGAAGGACATTCAAAGCCAATTCGAGCAGCTGAA ACTGCGGTGGGAGTCTTATCCCAATTTGGTCAAGAGCACCG
RSV	M	3179-3262	GGCAAATATGGAACATACGTGAACAACTTCACGAAGGCTCCACATACACAGCTGCTGT CAATACAATGTCCTAGAAAAAGA
Para-2	F	7451-7540	GCATTTCCAATCTTCAGGACTATGAAAACCATTACCTAAGTATGGAATCAATCGAAAAG CTGTTCACTACTGCTATACCAGGAGGT
Adv-C	E1A	919-1100	TCGATCTTACCTGCCACGAGGCTGGCTTTGCACCCAGTGACGACGAGGATGAAGAGGGTGA GGAGTTTGTGTAGATTATGTGGAGCAGCCCGGGCAGGTTGCAGGCTTGTCTATTACCC GGAGGAATACGGGGGACCCAGATATTATGTGTTCCGCTTTGCTATATGAGGACCTGTGGC
Adv-E	E4	34196-34349	TGCAATTTTGTGGTTTCGATAACGGCGGGGAGGGAAGAACAGGAAGAACCATGATTA ATTTTATCCAAACGGTCTCGGAACACTTCAAATGCAAGTCCCGGAGGTGGCACCTCTCGC CCCCACTGTGTTGGTGAAAATAACAGCCAGG
Pos. Cont.	N/A	N/A	ATGGAGCGAATCCAGCAACAGATAGATAATGAATCTCACTTTCACCGGATGGCCAATCCA ATTCGCTTTATGATAACAATCTGTGATTGTCACCATAAGCAGCCACAATAAAATAAAGGAA ACACGGACACCCAAAGTAGTCGGTCCGCCACGGACTTGCAGGTTACGACAGGCCAATCAC TGG

Data reported in **Fig. 4b** and **Fig. 4c** utilized a dilution series (10,000 copies/ μ l, 3,000 copies/ μ l, 1,000 copies/ μ l, 300 copies/ μ l, 100 copies/ μ l) of Influenza A total nucleic acid extracts obtained from ATCC: VR-1680D Influenza A RNA, strain A/Aichi/2/68 (H3N2) plus synthetic polio RNA positive control (8,000 copies/ μ l in each sample) performed in triplicate experiments.

Data reported in **Fig. Supp. 31a** utilized 10,000 copies/ μ l of Influenza A total nucleic acid extracts obtained from ATCC: VR-1680D Influenza A RNA, strain A/Aichi/2/68 (H3N2) plus synthetic polio RNA positive control (8,000 copies/ μ l)

Data reported in **Fig. Supp. 31b** utilized a mixture of total nucleic acid extracts from Influenza B (RNA virus) [NATtrol™ NATFLUB-ST Influenza B (B/Florida/02/06) Zeptomatrix] spiked at high concentration (11,600 copies/ μ l) and Adenovirus E (DNA virus) at low concentration (170 copies/ μ l) [NATtrol™ Adenovirus Type 4 Stock Zeptomatrix] plus positive control RNA (8,000 copies/ μ l).

Data reported in **Fig. Supp. 31c** utilized a mixture of total nucleic acid extracts from:

- FluA [Influenza A/H3N2/Brisbane/10/07 NATtrol™ Flu Verification Panel Zeptomatrix] at 1160 copies/ μ l
- FluB [Influenza B/Florida/02/06 NATtrol™ Flu Verification Panel Zeptomatrix] at 176 copies/ μ l
- RSV-A [RSV A NATtrol™ Flu Verification Panel Zeptomatrix] at 528 copies/ μ l
- Adenovirus C [AdvC ATCC VR-1: Adenovirus 1 strain Adenoid 71] at 232 copies/ μ l
- Adenovirus E [AdvE NATtrol™ Adenovirus Type 4 Stock Zeptomatrix] at 17 copies/ μ l

- Parainfluenza Virus 2 (PIV-2 NATtrol™ Respiratory Verification Panel Zeptomatrix) at 72 copies/μl
- Synthetic Poliovirus RNA (Positive Control) at 8,000 copies/μl

Patient Clinical Samples. Patient samples were collected with nasopharyngeal swabs, eluted into viral transport media and archived at -80°C. One or more 200μL portions of each thawed sample were processed with the Qiagen EZ1 Virus Mini Kit v2.0 (p/n 955134) and supporting EZ1 Advanced XL instrument (p/n 9001492) and Virus Card v2.0 (p/n 9018708) (Qiagen, Hilden Germany). Sixty microliter (60μL) elution volumes were divided into three equal 20μl aliquots, and stored at -80°C prior to use.

Note: Each patient sample was previously tested with a respiratory virus panel (GenMark eSensor XT-8, Carlsbad, USA) at the Stanford University Clinical Virology Lab according to the manufacturer instructions.

A.2. Assay Verification and Sample Qualification prior to CMOS Biochip Experiments

Assay Verification. The multiplex assay used for the experiments described in **Fig. 4** and **Fig. Supp. 31** utilized a combination of primer sequences derived from references. The primer sequences utilized are listed in **Table Supp. IV**.

Table Supp. IV: URP Assay Primer Sequences				
Primer Name	Reaction Concentration	Target Gene	Genome Region	Sequence
FluA-1 Excess	300nM	NS1	Segment 8 Bases 636-793	BHQ2-GGACCTCCACTTACTCCAAAACAGAAAC
FluA-1 Limiting	50nM			BHQ2-GTAAGGCTTGCATGAATGTTATTTGCTC
FluA-2 Excess	300nM	M	Segment 7 Bases 171-276	BHQ2-GACCRATCCTGTCACTCTGAC
FluA-2 Limiting	50nM			BHQ2-AGGGCATTYTGACAAAKCGTCTA
FluB Excess	300nM	NS1	Segment 8 Bases 720-822	BHQ2-TCCTCAACTCACTCTTCGAGCG
FluB Limiting	50nM			BHQ2-CGGTGCTCTTGACCAATTGG
RSV Excess	300nM	M	Bases 3179-3262	BHQ2-GGCAATATGGAACATACGTGAA
RSV Limiting	50nM			BHQ2-TCTTTTCTAGGACATTGTAYTGAACAG
Para-2 Excess	300nM	F	Bases 7451-7540	BHQ2-GCATTTCATCTACAGGACTATGA
Para-2 Limiting	50nM			BHQ2-ACCTCTGGTATAGCAGTGACTGAAC
Adv-C Excess	300nM	E1A	Bases 919-1100	BHQ2-TCGATCTTACCTGCCACGAG
Adv-C Limiting	50nM			BHQ2-GCCACAGTCCTCATATAGCAA
Adv-E Excess	300nM	E4	Bases 34196-34349	BHQ2-TGCAATTTTGTGGGTTTCGATAAC
Adv-E Limiting	50nM			BHQ2-CCTGGCTGTTATTTCCACCAAC
Pos. Cont. Excess	300nM	N/A	N/A	BHQ2-ATGGAGCGAATCCAGCAAAC
Pos. Cont. Limiting	50nM			BHQ2-CCAGTGATTGGCTGTCGTA

Iterative development of multiplex RT-PCR assay using off-chip RT-PCR and Luminex System. The assay was developed by iterative addition of primer sets together and tested using a mixture of synthetic templates and multiplex RT-PCR followed by hybridization to MagPix bead-conjugated probes and readout on a MagPix instrument (Millipore).

Synthetic templates for potential primer/probe sets included in reference⁷⁻⁸ were purchased as quantitated ssRNA (for RNA viruses targeted) or ssDNA (for dsDNA viruses targeted) synthetic nucleic acids as described. A mixture of all potential templates (including positive control template designed in house) was made at 1,000copies/μl and frozen in 10μl aliquots at -80°C until used. Each aliquot was used once to avoid freeze-thaw cycles. For each multiplex assay test initially conducted during the multiplex development phase, 1μl of this template mix was added per reaction.

Table Supp. V: URP Assay Probe Sequences		
Probe Name	Function	Sequence
FluA-1-Pb1	Detection	AminoC6-TTTTTTTGACCTAGTTGTTCTCGCCAGTGAGGTCC[T(FAM)]TTTTTT-TAMRA
FluA-1-Pb2	Detection	AminoC6-TTTTTTTGACCTAGTTGTTCTCGCCAGGAGGTCC[T(FAM)]TTTTTT-TAMRA
FluA-1-PDPb	Quantitation	AminoC6-TTTTTT[Spacer 3]GAGCAAATAACATTCATGCAAGCCTTAC[T(FAM)]TTTTTT-TAMRA
FluA-2-Pb1	Detection	AminoC6-TTTTTTCGGTGAGCGTGAACACAAATCCAGGATTGGTC[T(FAM)]TTTTTT-TAMRA
FluA-2-Pb2	Detection	AminoC6-TTTTTTCGGTGAGCGTGAACACAAATCCAGGATTGGTC[T(FAM)]TTTTTT-TAMRA
FluA-2-PDPb	Quantitation	AminoC6-TTTTTT[Spacer 3]TAGACGCTTTGTCCACAATGCCCT[T(FAM)]TTTTTT-TAMRA
FluB-Pb1	Detection	AminoC6-TTTTTCTCGAATTGGCTTGAATGTCTTCGAGTTGAGGA[T(FAM)]TTTTTT-TAMRA
FluB-Pb2	Detection	AminoC6-TTTTTCACCGCAGTTTCAGCTGCTCGAATTGGGAGTTGAGGA[T(FAM)]TTTTTT-TAMRA
FluB-PDPb	Quantitation	AminoC6-TTTTTT[Spacer 3]CCAATTTGGTCAAGAGCACCGT[T(FAM)]TTTTTT-TAMRA
RSV-Pb1	Detection	AminoC6-TTTTTTCAGCAGCTGTGTATGTGGAGCTCCATATTTGCC[T(FAM)]TTTTTT-TAMRA
RSV-Pb2	Detection	AminoC6-TTTTTCTGTGTATGTGGAGCTTCGTGAAGCTCCATATTTGCC[T(FAM)]TTTTTT-TAMRA
RSV-PDPb	Quantitation	AminoC6-TTTTTT[Spacer 3]CTGTCTACTACAATGCCTAGAAAAAGA[T(FAM)]TTTTTT-TAMRA
Para-2-Pb1	Detection	AminoC6-TTTTTGCGATTGATTCATCACTTAGGTAATTTGAAATGC[T(FAM)]TTTTTT-TAMRA
Para-2-Pb2	Detection	AminoC6-TTTTTGCGATTGATTCATCACTTAGGTAAGATTGAAATGC[T(FAM)]TTTTTT-TAMRA
Para-2-PDPb	Quantitation	AminoC6-TTTTTT[Spacer 3]GTTCACTCACTGCTATACCAGGAGGT[T(FAM)]TTTTTT-TAMRA
Adv-C-Pb1	Detection	AminoC6-TTTTTTGCTCCACATAATCTAACACAACTCCTCACCCAGGTAAGATCGA[T(FAM)]TTTTTT-TAMRA
Adv-C-Pb2	Detection	AminoC6-TTTTTTGCTCCACATAATCTAACACAACTCCTCACCCAGGTAAGATCGA[T(FAM)]TTTTTT-TAMRA
Adv-C-PDPb	Quantitation	AminoC6-TTTTTT[Spacer 3]TTGCTATATGAGGACCTGTGGC[T(FAM)]TTTTTT-TAMRA
Adv-E Pb	Detection	AminoC6-TTTTTTTAATCATGGTCTCTCTGTTCTCCCTCCCAAATTGCA[T(FAM)]TTTTTT-TAMRA
Adv-E-PDPb	Quantitation	AminoC6-TTTTTT[Spacer 3]GTTGGTGGAAAATAACAGCCAGGT[T(FAM)]TTTTTT-TAMRA
Pos. Control Pb	Detection	AminoC6-TTTTTTATCCGGTGAAAGTGAGATTCAATATCATTGCTCCAT[T(FAM)]TTTTTT-TAMRA
Pos. Control-PDPb	Quantitation	AminoC6-TTTTTT[Spacer 3]TACGACAGCCAATCACTGGT[T(FAM)]TTTTTT-TAMRA
Neg. Control Pb	Detection Baseline	AminoC6-TTTTTCAAAGTGGGAGACGTCGTTGT[T(FAM)]TTTTTT-TAMRA

The SuperScriptIII® (SSIII) One-step RT-PCR enzyme system (Thermo Fisher) was used to generate RT-PCR amplicons. Multiplex RT-PCR mix was composed of 2X SSIII Reverse Transcriptase + Platinum® Taq

Polymerase mix [1µl per 25µl reaction vs. the manufacturer recommended 0.5µl per 25µl], 1X SSIII RT-PCR Buffer, 5mM MgSO₄, plus primer mix to which was added the template mixture described above. The primer mix contained a 6:1 ratio of Excess vs. Limiting primers (300nM each excess primer and 50nM each limiting primer). Additionally, all primers were labelled with Black Hole Quencher 2 (BHQ2) (LGC BioSearch) at their 5' ends as shown in **Table Supp. IV**. Amplicons thus generated were then hybridized to a mixture of MagPix bead-conjugated fluorescent probes designed by InSilixa to detect the amplicons (**Table Supp. V**) and read on MagPix instrument. Sub-optimal primer/probe combinations were eliminated from the multiplex panel and the final panel configurations for both Luminex and On-Chip RT-PCR experiments are reported.

NOTE: Quantitation probes were used only for On-Chip RT-PCR and not during development phase.

Sample Qualification. Standard curves were generated using synthetic ssDNA templates or ssRNA templates ranging from 1 to 1,000,000 copies/µl in triplicate. qPCR was performed in 25µl volumes with 2U Platinum Taq DNA Polymerase (Thermo Fisher), 1X Platinum Taq PCR Buffer, 5mM MgSO₄, 200µM each dNTP, 400µM each primer, and 200µM TaqMan probe (LGC BioSearch). qRT-PCR was performed in 25µl volumes using 2X SuperScriptIII Reverse Transcriptase + Platinum Taq Polymerase mix [1µl per 25µl reaction], 1X SuperScriptIII RT-PCR buffer, 5mM MgSO₄, 400µM each primer, and 200µM TaqMan probe with FAM/BHQ1 pairs (**Table Supp. VI**). PCR reactions were performed in 96-well plates on a CFX1000 Touch with an initial denaturation at 95°C for 2 min, 45 cycles at 95°C for 15 s, 62°C for 30 s, and 68°C for 30 s, followed by a final extension at 68°C for 3 min. RT-PCR reactions were run in 96-well plates on a CFX1000 Touch with 55°C reverse transcription for 5 min., RT Kill and denaturation at 95°C for 2 min, 45 cycles at 95°C for 15 s, 62°C for 30 s, and 68°C for 30 s, followed by a final extension at 68°C for 3 min. Data was analyzed and standard curves were generated using the CFX Manager Software.

Table Supp. VI: URP Assay TaqMan Primer/Probe Sequences			
Target	F Primer	R Primer	Probe
FluA-1	GGACCTCCACTTACTCCAAAACAGAAAC	GTAAGGCTTGCATGAATGTTATTTGCTC	FAM-TTGACCTAGTTGTTCTCGCCA-BHQ1
FluA-2	GACCRATCCTGTACCTCTGAC	AGGGCATTYTGACAAKCGTCTA	FAM-TGCAGTCCTCGCTCACTGGGCACG-BHQ1
FluB	TCCTCAACTCACTCTTCGAGCG	CGGTGCTCTTGACCAAATTGG	FAM-CCAATTCGAGCAGCTGAAACTGCGGTG-BHQ1
RSV	GGCAAATATGGAAACATACGTGAA	TCTTTTCTAGGACATTGTAYTGAACAG	FAM-CTGTGTATGTGGAGCCTTCGTGAAGCT-BHQ1
Para-2	GCATTTCCAATCTACAGGACTATGA	ACCTCCTGGTATAGCAGTGAAC	FAM-CCATTTACCTAAGTGATGGAATCAATCGCAA-BHQ1
Adv-C	TCGATCTTACCTGCCACGAG	GCCACAGGTCCTCATATAGCAA	FAM-TGCTCCACATAATCTAACACAAACTCCTACCC-BHQ1
Adv-E	TGCAATTTTGTGGGTTTCGATAAC	CCTGGCTGTATTTCCACCAAC	FAM-TTAATCATGGTTCTTCTGTTCTTCCCTCCC-BHQ1
Pos. Cont.	ATGGAGCGAATCCAGCAAAC	CCAGTGATTGGCCTGTCGTA	FAM-CGACTACTTTGGGTGTCGGT-BHQ1

Templates used for on-chip RT-PCR (prior to on-chip RT-PCR for commercial samples, after completion of on-chip RT-PCR for clinical samples) were quantitated via qRT-PCR in 25µl volumes using 2X SSIII Reverse Transcriptase + Platinum Taq Polymerase mix [1µl per 25µl reaction], 1X SSIII RT-PCR buffer, 5mM MgSO₄, 400µM each primer, and 200µM TaqMan probe utilizing FAM/BHQ1 pairs. Templates were diluted prior to qRT-PCR (typically 1:10³ to 1:10⁵ dilutions were used) and tested in triplicate reactions.

RT-PCR reactions were performed using 96-well plates on a CFX1000 Touch with 55°C reverse transcription for 5 min., RT Kill and denaturation at 95°C for 2 min, 45 cycles at 95°C for 15 s, and 62°C for 30 s, followed by a final extension at 68°C for 3 min. Data was analyzed against standard curves using the CFX Manager Software. Fluorescence measurements were taken at each annealing step.

A.3. CMOS Biochip Layout and Probes

URP Array Layout (Table Supp. VII). See key below for probe content. Probes not referenced in this study are labeled as Test Probes (T). B=Blank and denote areas where no probes were spotted; CP=Control Probe; PM=Process Monitor.

The blank spots (B) are used to estimate the background optical signal. These spots are used to accurately perform background subtraction operation to obtain the signal values from the individual spots. 15 locations are spotted with the control probe (CP). These spots are used to obtain the characteristics of FAM-TAM fluorophore construct and enables the correction and calibration for the temperature dependence and bleaching of surface-bound fluorophores. 13 locations are spotted with the process monitor probe (PM). These spots are used to verify the quality of surface functionalization and spotting process. These probes are designed to be universal across the different panels.

Identifier	Probe Content	Identifier	Probe Content	Identifier	Probe Content	Identifier	Probe Content
001	FluA-1-Pb1	012	RSV-PDPb	023	Neg. Control Pb	T08	Test_Probe_08
002	FluA-1-Pb2	013	Para-2-Pb1	B	Blank (No Probe)	T09	Test_Probe_09
003	FluA-1-PDPb	014	Para-2-Pb2	CP	Control Probe	T10	Test_Probe_10
004	FluA-2-Pb1	015	Para-2-PDPb	PM	Process Monitor	T11	Test_Probe_11
005	FluA-2-Pb2	016	Adv-C-Pb1	T01	Test_Probe_01	T12	Test_Probe_12
006	FluA-2-PDPb	017	Adv-C-Pb2	T02	Test_Probe_02	T13	Test_Probe_13
007	FluB-Pb1	018	Adv-C-PDPb	T03	Test_Probe_03	T14	Test_Probe_14
008	FluB-Pb2	019	Adv-E Pb	T04	Test_Probe_04	T15	Test_Probe_15
009	FluB-PDPb	020	Adv-E-PDPb	T05	Test_Probe_05	T16	Test_Probe_16
010	RSV-Pb1	021	Pos. Control Pb	T06	Test_Probe_06		
011	RSV-Pb2	022	Pos. Control-PDPb	T07	Test_Probe_07		

+	1	2	3	4	5	6	7	8	9	10	11	12	13	14	15	16	17	18	19	20	21	22	23	24	25	26	27	28	29	30	31	32	
1	PM	B	T07	B	T08	B	016	B	017	B	019	B	T09	B	021	B	PM	B	023	B	T10	B	T11	B	T12	B	T13	B	004	B	B	PM	
2	B	B	B	B	B	B	B	B	B	B	B	B	B	B	B	B	B	B	B	B	B	B	B	B	B	B	B	B	B	B	B	B	B
3	005	B	007	B	008	B	013	B	014	B	010	B	011	B	T14	B	CP	B	T15	B	022	B	006	B	009	B	015	B	012	B	003	B	
4	B	B	B	B	B	B	B	B	B	B	B	B	B	B	B	B	B	B	B	B	B	B	B	B	B	B	B	B	B	B	B	B	
5	T16	B	018	B	020	B	001	B	002	B	T01	B	T02	B	T03	B	T04	B	T05	B	T06	B	CP	B	T08	B	016	B	017	B	B		
6	B	B	B	B	B	B	B	B	B	B	B	B	B	B	B	B	B	B	B	B	B	B	B	B	B	B	B	B	B	B	B	B	
7	019	B	T09	B	021	B	023	B	B	B	CP	B	T10	B	T11	B	T12	B	T13	B	CP	B	004	B	B	B	005	B	CP	B	007	B	
8	B	B	B	B	B	B	B	B	PM	B	B	B	B	B	B	B	B	B	B	B	B	B	B	B	B	PM	B	B	B	B	B	B	
9	008	B	013	B	014	B	010	B	B	B	011	B	T14	B	T15	B	022	B	006	B	009	B	015	B	B	B	012	B	003	B	T16	B	
10	B	B	B	B	B	B	B	B	B	B	B	B	B	B	B	B	B	B	B	B	B	B	B	B	B	B	B	B	B	B	B	B	
11	018	B	020	B	001	B	CP	B	001	B	002	B	T01	B	T02	B	T03	B	T04	B	T05	B	T06	B	T07	B	T08	B	002	B	T01	B	
12	B	B	B	B	B	B	B	B	B	B	B	B	B	B	B	B	B	B	B	B	B	B	B	B	B	B	B	B	B	B	B	B	
13	T02	B	T03	B	T04	B	016	B	017	B	019	B	T09	B	021	B	023	B	CP	B	T10	B	T11	B	T12	B	T13	B	T05	B	T06	B	
14	B	B	B	B	B	B	B	B	B	B	B	B	B	B	B	B	B	B	B	B	B	B	B	B	B	B	B	B	B	B	B	B	
15	B	B	CP	B	T07	B	004	B	005	B	007	B	008	B	013	B	B	B	014	B	010	B	011	B	T14	B	T15	B	T08	B	B	B	
16	PM	B	B	B	B	B	B	B	B	B	B	B	B	B	B	B	PM	B	B	B	B	B	B	B	B	B	B	B	B	B	B	PM	
17	B	B	016	B	017	B	022	B	006	B	009	B	015	B	CP	B	B	B	012	B	003	B	CP	B	T16	B	018	B	019	B	B	B	
18	B	B	B	B	B	B	B	B	B	B	B	B	B	B	B	B	B	B	B	B	B	B	B	B	B	B	B	B	B	B	B	B	
19	T09	B	021	B	023	B	CP	B	020	B	001	B	002	B	T01	B	T02	B	T03	B	T04	B	T05	B	T06	B	T07	B	T10	B	T11	B	
20	B	B	B	B	B	B	B	B	B	B	B	B	B	B	B	B	B	B	B	B	B	B	B	B	B	B	B	B	B	B	B	B	
21	T12	B	T13	B	004	B	T08	B	016	B	017	B	019	B	T09	B	021	B	023	B	T10	B	T11	B	T12	B	T13	B	005	B	007	B	
22	B	B	B	B	B	B	B	B	B	B	B	B	B	B	B	B	B	B	B	B	B	B	B	B	B	B	B	B	B	B	B	B	
23	008	B	013	B	014	B	004	B	B	B	005	B	007	B	008	B	CP	B	013	B	014	B	010	B	B	B	CP	B	010	B	011	B	
24	B	B	B	B	B	B	B	B	PM	B	B	B	B	B	B	B	B	B	B	B	B	B	B	B	PM	B	B	B	B	B	B	B	
25	T14	B	T15	B	CP	B	011	B	B	B	T14	B	T15	B	022	B	006	B	009	B	015	B	012	B	B	B	003	B	022	B	006	B	
26	B	B	B	B	B	B	B	B	B	B	B	B	B	B	B	B	B	B	B	B	B	B	B	B	B	B	B	B	B	B	B	B	
27	009	B	015	B	012	B	T16	B	018	B	020	B	001	B	002	B	T01	B	T02	B	T03	B	T04	B	T05	B	T06	B	003	B	T16	B	
28	B	B	B	B	B	B	B	B	B	B	B	B	B	B	B	B	B	B	B	B	B	B	B	B	B	B	B	B	B	B	B	B	
29	018	B	020	B	001	B	002	B	T01	B	T02	B	T03	B	T04	B	T05	B	T06	B	CP	B	T07	B	T08	B	016	B	017	B	019	B	
30	B	B	B	B	B	B	B	B	B	B	B	B	B	B	B	B	B	B	B	B	B	B	B	B	B	B	B	B	B	B	B	B	
31	B	B	T09	B	021	B	023	B	T10	B	T11	B	T12	B	T13	B	B	B	004	B	005	B	007	B	008	B	013	B	014	B	B	B	
32	PM	B	B	B	B	B	B	B	B	B	B	B	B	B	B	B	PM	B	B	B	B	B	B	B	B	B	B	B	B	B	B	PM	

The signal probes are classified as two types. One is the “PbX” type, which is used to obtain the melt curve signatures. These probes employ the IFT technique for detection as shown in **Fig. 2b**. The second

is the “PDPb” type, which are used for quantification during qPCR reaction. These probes monitor the depletion of limiting primer during the PCR cycling as explained before. At least 5 replicates of each signal probe is printed on the CMOS biochip as shown in the array layout.

A.4. CMOS Biochip Experiments

Three sets of experiments were conducted on the CMOS biochip to demonstrate the capabilities of our system. Qualified and quantitated templates, as described above, were used for generation of data reported in **Fig. 4** and **Fig. Supp. 31** and **32**.

The first set of experiments reported in **Fig. 4**, were to demonstrate on-chip detection and quantitation of Influenza A. We performed a total of 15 experiments utilizing 15 separate biochips to demonstrate the quantitation capability of our system. Dilutions of total nucleic acid extract obtained from ATCC [VR-1680D Influenza A RNA, strain A/Aichi/2/68 (H3N2)] containing FluA were generated. These samples were then each mixed with positive control RNA and RT-PCR reaction mixtures (see below) to final concentrations of 10,000 copies/ μ l to 100 copies/ μ l of FluA as described above and 8,000 copies/ μ l of positive control and tested in triplicate.

The second set of experiments reported in **Fig. Supp 31** and **32**, was to demonstrate detection and differentiation of one or multiple targets via melt curve analysis. Mixtures of templates obtained from commercial sources or a single template and quantitated as described above were used for three separate on-chip RT-PCR experiments. Post RT-PCR melt curves which differentiate between the various generated amplicons.

The third set of experiments reported in **Fig. 4**, was to demonstrate the ability of the CMOS biochip to detect pathogens in clinical nasopharyngeal swab samples. Each patient sample was previously tested with a respiratory virus panel (GenMark eSensor XT-8, Carlsbad, USA) at the Stanford University Clinical Virology Lab according to the manufacturer instructions. One of the three aliquots of each clinical sample extract was used for on-chip RT-PCR as described in “*on-chip inverse fluorescence RT-PCR of clinical samples*” described below. A separate aliquot of each clinical sample was used for quantitation of the pathogen nucleic acid detected in the clinical sample. The summarized results of the CMOS biochip, GenMark tests, and qRT-PCR of those samples are presented in the manuscript.

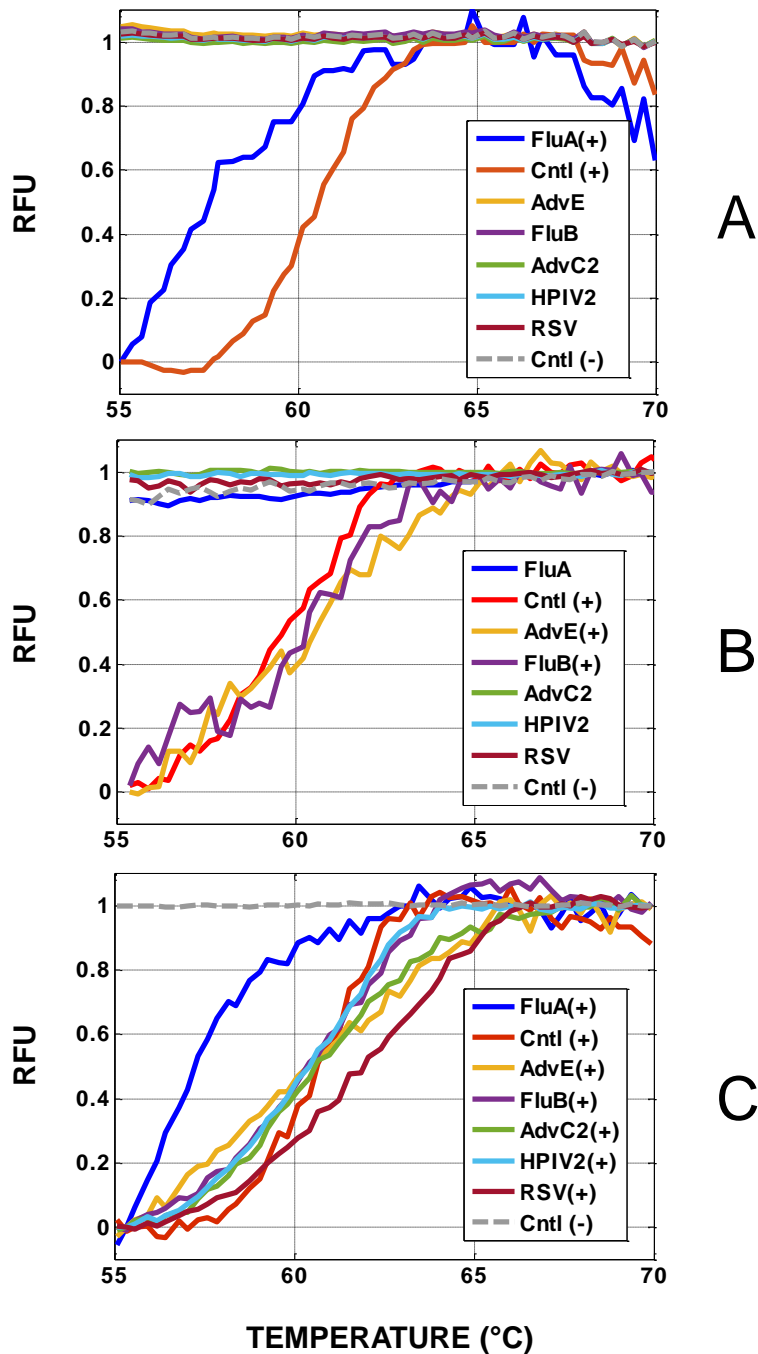


Figure Supp. 31: Identification of one or multiplex pathogens in a sample via melt curve analysis post on-chip RT-PCR using CMOS biochip. (A) melt curves generated on FluA and positive control probes after CMOS biochip was spiked with a mixture containing total nucleic acid extracts from FluA at 10,000 copies/ μ l and positive control RNA at 8,000 copies/ μ l. (B) Shows melt curves generated on FluB, Adenovirus E (AdvE), and positive control probes after CMOS biochip was spiked with a mixture of FluB at 11,600 copies/ μ l, AdvE at 170 copies/ μ l, and positive control RNA at 8,000 copies/ μ l. (C) Shows melt curves generated on all amplicon-targeted probes after CMOS biochip was spiked with a mixture of FluA at 1160 copies/ μ l, FluB at 176 copies/ μ l, RSV-A at 528 copies/ μ l, AdvC at 232 copies/ μ l, AdvE at 17 copies/ μ l, PIV-2 at 72 copies/ μ l and positive control RNA at 8,000 copies/ μ l. In all the reported curves, the data points are the mean of 5 replicate probes on the same CMOS biochip.

On-Chip inverse-fluorescence NAAT qRT-PCR for commercial samples. SuperScriptIII® (SSIII) One-step RT-PCR reagent (Thermo Fisher) was used to generate RT-PCR amplicons. Multiplex RT-PCR mix consisted of 2X SSIII Reverse Transcriptase + Platinum® Taq Polymerase mix [1µl per 25µl reaction], 1X SSIII RT-PCR Buffer, 5mM MgSO₄, plus primer mix and synthetic positive control RNA and various targets as reported. The primer mix contained a 6:1 ratio of excess:limiting primers (300nM:50nM, respectively). All primers were BHQ2 labelled (LGC BioSearch) at the 5' terminus. For each experiment, a total volume of 100µl of this mix was generated. The mix was staged on ice prior to loading.

On-chip cycling conditions for commercial samples. Chips were pre-treated by loading 60µl of a mix containing 2X SSIII Enzyme mix, 1X SSIII buffer and 5mM MgSO₄ (no templates or primers) and the following heating protocol: 55°C for 5 min, 95°C for 3 min, 5 cycles at 95°C for 30 s, 60°C for 1 min, and one cycle of 68°C for 3min. After pre-treatment, the liquid was replaced with 60µl of the RT-PCR mix and thermal cycled as follows: 55°C for 5 min, 95°C for 3 min, 45 cycles at 95°C for 30 s, 60°C for 1 min, followed by a final extension at 68°C for 3 min. A 50µl aliquot of the same mix was loaded on to a 200µl well of a PCR plate and cycled using the same thermal profile on a CFX Touch instrument (BioRad, Hercules, CA) as a control to enable comparison of on-chip vs. off-chip RT-PCR efficiency.

On-Chip inverse-fluorescence RT-PCR of clinical samples. To three ZipScript (Enzymatics/Qiagen, Beverly, MA) one-step RT-PCR dried reagent beads was added an 8-plex mix of Excess and Limiting primers plus water and positive control synthetic poliovirus RNA diluted in water to a final volume of 110µl. To this mix was added 15µl of a 20µl total nucleic acid extract from a clinical sample for a final volume of 125µl containing 300nM of each Excess primer, 50nM of each limiting primer, 8,000 copies/µl of positive control synthetic RNA, and 1X enzyme plus buffer mix. Sixty microliters (60µl) of this mix was drawn into a pipette and loaded by negative pressure on to one chip per clinical sample and cycled as follows: 55°C for 5 min, 95°C for 3 min, 45 cycles at 95°C for 30 s, 60°C for 1 min, followed by a final extension at 68°C for 3 min. Another 50µl of the same mix was loaded on to a 200µl well of a PCR plate and cycled using the same thermal cycling parameters on a BioRad CFX Touch instrument as an off-chip RT-PCR control to enable comparison of on-chip vs. off-chip RT-PCR efficiency.

Imaging and quantitation via primer depletion. For all samples (clinical and commercial) beginning at PCR cycle 15, and at each subsequent cycle through the end of PCR, two images were collected at the end of each annealing/extension step. Fluorescent signals corresponding to FAM-TAM-labeled primer depletion probes (PDPr) were collected to produce a cycle to cycle comparison of signal. Measurements were compiled, normalized and reported (**Fig. 4**).

On-chip hybridization and melt. After completion of on-chip RT-PCR, the chip was heated at 55°C for 30min and fluorescence measurements taken at 2min intervals. This was followed by a 20min melt from 55-95°C using high frequency imaging. Again, measurements were compiled, normalized and reported (**Fig. 4** and **Fig. Supp. 31**).

A.5. Post CMOS Biochip Verification

qPCR. 62°C for 30 s, and 68°C for 30 s, followed by a final extension at 68°C for 3 min. Fluorescence measurements were taken at each annealing step.

TaqMan quantitation of on-chip and off-chip amplicon generated. After on-chip and off-chip amplification, amplicon was removed from chips/tubes and log-diluted in nucleic acid dilution buffer (10mM Tris-HCl pH8.2, 0.01% Tween 20) from 1:10 to 1:10⁷. Typically, 1:10⁴, 1:10⁵, and 1:10⁶ dilutions were used. Each dilution was tested in triplicate qPCR reactions. Each 25µl qPCR reaction contained 2U Platinum Taq DNA Polymerase, 1X Platinum Taq PCR Buffer, 5mM MgSO₄, 200µM each dNTP, 400µM each primer, 200µM TaqMan probe, and 5ul of amplicon to be quantitated. PCR reactions were performed using 96-well plates on a CFX1000 Touch with an initial denaturation at 95°C for 2 min, 45 cycles at 95°C for 15 s, Results for FluA detection/quantitation experiments are detailed in **Table Supp. VIII**. The amplification of the FluA template is marginally more efficient in tubes vs. on chip.

Table Supp. VIII: URP Assay post-RT-PCR Quantitation Results		
Initial FluA Concentration	On-Chip RT-PCR Amplicon Concentration (µ±σ)*	Off-Chip RT-PCR Amplicon Concentration (µ±σ)
100,000 copies/ul	57nM±5nM	119nM±7nM
10,000 copies/ul	48nM±6nM	89nM±7nM
3,000 copies/ul	55nM±10nM	96nM±16nM
1,000 copies/ul	34nM±8nM	71nM±12nM
300 copies/ul	30nM±2nM	66nM±6nM
100 copies/ul	33nM±4nM	49nM±6nM

* Average + standard deviation (SD)

B. URP Assay Melt Signatures

CMOS chip melt curves and URP signatures. **Fig. Supp. 32** shows the melt curve signatures for the different probes and targets obtained using the CMOS biochip. The biochip experiment was performed by spiking the biochip with a mixture of FluA at 1160 copies/µl, FluB at 176 copies/µl, RSV-A at 528 copies/µl, AdvC at 232 copies/µl, AdvE at 17 copies/µl, PIV-2 at 72 copies/µl and positive control RNA at 8,000 copies/µl. Melt curve signatures are observed on Pb1 probe sequences for the six different pathogens.

Fig. Supp. 32 shows the comparison between the obtained melt curve signatures and the simulated melt curve results obtained for probe/target interactions using VISUALOMP software. These simulation require special considerations as the probe sequences employ the IFT technique, as depicted in **Fig. 2b**. Each probes has two regions – the “sticky-end” region which is complementary to the 5’ end of the excess primer labelled with the quencher and the “anchor” region which is complementary to specific sequence on the target. Because of this structure, not all possible heterodimer duplexes between the probe and the target contribute to the quenching. Maximum quenching is obtained in those cases where the “sticky-end” region is bound to the target along with the “anchor”, bringing the fluorophore near 3’ end of the probe and quencher near the 5’ end of the target amplicon in close proximity.

The simulated melt curve results are obtained by combining the results of two simulations explained below. The first simulation is done using only the target (*T*) and the “anchor” region of the probe (*A*) to estimate the [*T* + *A*] heterodimer concentration. Both the target and anchor regions are simulated with the same 10nM concentration. The second simulation is done using the target (*T*) and the “sticky-end” region of the probe (*SE*) to estimate the [*T* + *SE*] heterodimer concentration. In this case the effective concentration of the target is set to a significantly higher value of 3mM, to simulate the effect of target

enrichment near the surface due to the attachment of the “anchor” region. The value of 3mM is chosen as it corresponds to average loop distance of 15bp between the sticky end and anchor section on the target amplicon. The total effective heterodimer concentration is given by the product to the two heterodimer concentrations,

$$[T + P] = [T + A][T + SE] \quad (K1)$$

The effective quenching signal is given by

$$Q = 1 - [T + P] = 1 - [T + A][T + SE] \quad (K2)$$

The simulated melt curves obtained using the above method closely predicted the experimental data as shown in **Fig. Sup. 32**.

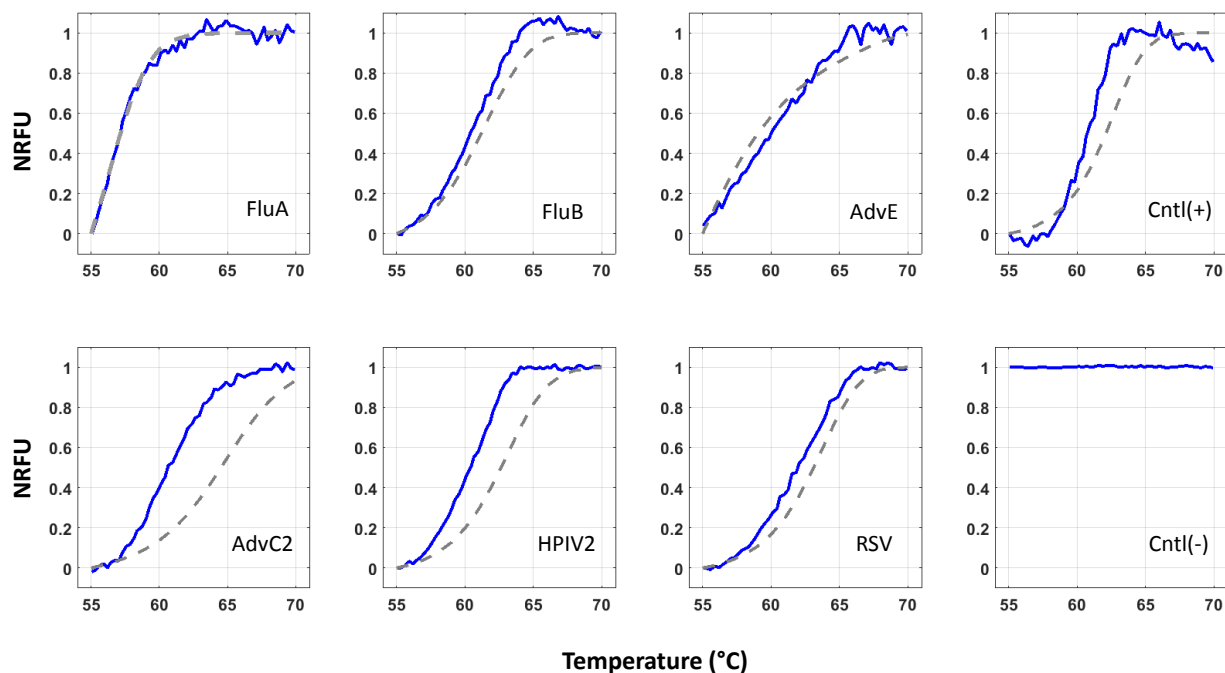


Figure Sup. 32: Signature melt curve plots obtained for each of the six different pathogen targets FluA, AdvE, FluB, AdvC2, HPIV2, and RSV and the Cntl (+) with their corresponding Pb1 probes (Table K4). The experimental melt curve plot is in blue and the simulated result in dashed grey. The measured signals are the average of 5 probe replicated from a single CMOS biochip experiment.

Supplementary Note 12

Description: M. tuberculosis (MTB) drug resistance mutation detection assay.

The multiplexed MTB assay discussed in the manuscript was first designed and verified using conventional molecular biology and PCR techniques. The multiplex assay was then transferred to the CMOS biochip platform for NAAT. In select cases, the results generated in the CMOS biochip experiments were validated using conventional qPCR. We describe the methods used and also provide additional information and analysis in the section below.

A. Materials and Methods

A.1. Samples and Nucleic Acid Templates

Synthetic nucleic acid templates for multiplex standard curve generation. Synthetic single-stranded target DNAs of each amplicon sequence listed in **Table Supp. IX** were obtained from Integrated DNA Technologies (Redwood City, CA) as PAGE-purified Ultramers and were re-suspended in 10mM Tris-HCl, 0.1mM EDTA, pH 8.0. The templates were quantified on a Beckman DU800 UV spectrophotometer and stored as aliquots at 10 μ M and 10nM concentrations in the -80 $^{\circ}$ C freezer. Standard curves for qPCR quantifications were generated with serial dilutions generated from single-use 10nM aliquots.

Wild-type MTB genomic DNA: Wild-type H37Rv MTB genomic DNA (**Table Supp. IX**) was purchased from the American Type Culture Collection (Cat. No. 25618D-2) and quantified on a Beckman DU800 UV Spectrophotometer. For all initial assay development testing, we used wild-type H37Rv to generate wild-type amplicons, which were then quantified via qPCR or directly hybridized to glass microarrays spotted with MTB capture probes.

Clinical mutant MTB genomic DNA: Clinical mutant MTB genomic DNA thermolysates (**Table Supp. IX**) were obtained from the BCCM/ITM Mycobacteria collection (<http://bccm.belspo.be/about-us/bccm-itm>), Institute of Tropical Medicine, Antwerp, Belgium) as 0.5ml to 1ml bacterial suspensions cultured from single-colony isolates and heat inactivated in TE buffer.

A.2. Sample Qualification and Assay Verification prior to CMOS Biochip Experiments

Qualification of thermolysates using quantitative Real-Time quantitative PCR (qPCR). For each mutant strain, 200 μ l of the thermolysate was purified and concentrated using spin-columns (Qiagen, Cat.No.28104), according to the manufacturer's protocol, and eluted in 30 μ l Qiagen Buffer EB (10mM Tris-Cl, pH 8.5). Purified thermolysates were then diluted 1000-fold and pre-amplified as described previously [L1]. Briefly, each 30 μ l pre-amplification PCR reaction consisted of 1x Advantage 2 Buffer (Clontech, Cat.No. 639202), 0.6 μ l of 10mM dNTP mix (Thermofisher, Cat. No. R0191), 0.6 μ l Advantage 2 polymerase, 20.8 μ l of 100 μ M pre-amplification primers mix (equal volumes of forward and reverse primers for each of 743 genes, Biosearch), and 2 μ l of purified thermolysate. PCR was performed on an ABI 9800 Fast Thermocycler for 15 cycles at 95 $^{\circ}$ C for 30 s, 60 $^{\circ}$ C for 20 s, and 68 $^{\circ}$ C for 1 min. H37Rv genomic DNA from 10⁴ to 10⁶ copies was included as a standard curve reference. Pre-amplified material

was quantified using qPCR of 24 randomly selected genes from the 743-MTB gene primer mix. Each qPCR reaction consisted of 0.1µl pre-amplified DNA, 1x SensiFast Probe No-Rox PCR mix (Bioline, Cat. No. BIO-86005), 300nM each primer, and 100nM FAM/BHQ-labeled probe in a 10µl reaction volume. Reactions were performed in a 384-well plate on a LightCycler 480 (Roche) using the Mono Color Hydrolysis Probe detection format for FAM. Reactions were denaturated at 95°C for 5 min, followed by 40 cycles at 95°C for 30 s and 60°C for 30 s, and a final cool down at 40°C for 30 s. Data was obtained using the Second Derivative High Confidence algorithm in Roche's LightCycler 480 software. Concentrations for purified thermolysates were calculated based on a standard curve using the median of Cts for all 24 individual genes in H37Rv from 10⁴ to 10⁶ copies. Single-use aliquots were prepared at 10⁵ copies/2µl and stored at -40°C.

Source	Strain ID	TDR-TB Strain ID	Drug Resistance	Gene	Mutation 1		Mutation 2		
					Amino Acid Change	Codon Change	Gene	Amino Acid Change	Codon Change
ATCC	H37Rv	wild-type	none						
BCCM/ITM	960854	TDR0005	FQ	<i>gyrA</i>	Ala 384 Val	GCA 384 <u>G</u> TA			
BCCM/ITM	970472	TDR0009	INH	<i>katG</i>	Ser 315 Ile	AGC 315 <u>A</u> TC			
BCCM/ITM	991451	TDR0021	RIF, INH	<i>rpoB</i>	Asp 516 Tyr	GAC 516 <u>I</u> AC	<i>katG</i>	Ser 315 Thr	AGC 315 <u>A</u> CC
BCCM/ITM	000930	TDR0036	RIF, INH	<i>rpoB</i>	His 526 Asp	CAC 526 <u>G</u> AC	<i>katG</i>	Ser 315 Thr	AGC 315 <u>A</u> CC
BCCM/ITM	041244	TDR0117	RIF, INH	<i>rpoB</i>	His 526 Tyr	CAC 526 <u>I</u> AC	<i>katG</i>	Ser 315 Thr	AGC 315 <u>A</u> CC
BCCM/ITM	041291	TDR0133	FQ	<i>gyrA</i>	Gly 247 Ser	GGC 247 <u>A</u> GC			
BCCM/ITM	042603	TDR0160	RIF	<i>rpoB</i>	Ile 572 Phe	ATC 572 <u>T</u> TC			
BCCM/ITM	042611	TDR0168	RIF, INH	<i>rpoB</i>	His 526 Arg	CAC 526 <u>C</u> GC	<i>katG</i>	Ser 315 Asn	AGC 315 <u>A</u> AC
BCCM/ITM	042924	TDR0191	RIF, INH	<i>rpoB</i>	Asp 516 Val	GAC 516 <u>G</u> TC	<i>katG</i>	Ser 315 Asn	AGC 315 <u>A</u> AC
BCCM/ITM	052785	TDR0226	FQ	<i>gyrA</i>	Asp 94 Gly	GAC 94 <u>G</u> GC			
BCCM/ITM	092045	TDR0231	FQ	<i>gyrA</i>	Ala 90 Val	GCG 90 <u>G</u> TG			

Table Supp. IX: Bacterial strains and their associated drug resistance mutations. RIF: Rifampin, FQ: Fluoroquinolone, INH: Isoniazid.

Multiplex PCR development using qPCR. For multiplex assay development, the initial focus was on product generation for the 5 primer sets (5-plex) covering the most challenging gene, *rpoB*, using wild-type H37Rv as the DNA template. Once the polymerase, buffer conditions, concentrations of BHQ10-modified dCTP and of unlabeled dCTP, and the PCR thermoprofile were established, assay optimization was performed using all 16 primer sets (**Table Supp. X**) in asymmetric multiplex PCR. Determination of primer concentrations was obtained systematically, as excess primer concentrations ranging from 100nM to 500nM were tested along with excess to limiting primer ratios at 5:1, 10:1, 15:1, and 20:1. Amplicon quantification was performed using real-time quantitative PCR (Roche LightCycler480) as described in below. Iterative primer concentration adjustments were made to specific individual primer sets until optimal amplicon yields were generated.

Probe pair verification. The probe pairs specified in **Table Supp. XI** were designed for SNP identification. Fifty-four probe pairs were designed targeting 54 different mutations in *gyrA*, *katG*, *aphC*, *inhA* and *rpoB* genes, located in 16 different amplicons. The probes are named as <gene>_<amplicon>_<mutation>_wild/mutant. The probes were printed on a 1"x3" silicon slide and qualified by hybridization to a unique synthetic target (300nM concentration) for each mutation in a 50µl flow-through chamber. Hybridization was done at 45°C for 60 min and was followed by a 45-95°C melt over 25 min, during which the slides were imaged every 10 s using a Leica DMI8 inverted microscope. The probe pairs were qualified by verifying that the expected melting curve signatures were obtained for the wild-type and mutant targets for each individual probe pair.

Probe Pair	Wild-type Probe Sequence (5'-3')	Mutant Probe Sequence (5'-3')
<i>gyrA</i> _TB1_A74S	AACCGACCGGGCCGACTTGGCGAAATGGCTGT	AACCGACCGGGACGACTTGGCGAAATGGCTGT
<i>gyrA</i> _TB1_TB80A	TGCGGGTGGTAGTTGCCCATGGCTCGGCCAA	TGCGGGTGGTAGTTGCCCATGGCTCGGCCAA
<i>gyrA</i> _TB1_G88C	ACGCGTCGCGCTGCGGGT	ACGCGTCGCACTGCGGGT
<i>gyrA</i> _TB1_D89N	GACGCGTTCGCGTGC	GACGCGTTCGCGTGC
<i>gyrA</i> _TB1_A90G	AGGCTTTATCGACGCGTCGCCGTGCGGGTGGTA	AGGCTTTATCGACCCGTCGCCGTGCGGGTGGTA
<i>gyrA</i> _TB1_A90V	AGGCTTTATCGACGCGTCGCCGTGCGGGTGGTA	AGGCTTTATCGACACGTCGCCGTGCGGGTGGTA
<i>gyrA</i> _TB1_D94G	ACCAGGCTGTCGTAGATTAATAGCGTTCGCGGGTGGTA	ACCAGGCTGCGGTAGATTAATAGCGTTCGCGGGTGGTA
<i>gyrA</i> _TB1_D94H	ACCAGGCTGTCGTAGATGCGGTGCGGGTGGTA	ACCAGGCTGTCGTAGATGCGGTGCGGGTGGTA
<i>gyrA</i> _TB1_D94N	ACCAGGCTGTCGTAGATGCGGTGCGGGTGGTA	ACCAGGCTGTCGTAGATGCGGTGCGGGTGGTA
<i>gyrA</i> _TB1_D94Y	ACCAGGCTGTCGTAGATGCGGTGCGGGTGGTA	ACCAGGCTGTCGTAGATGCGGTGCGGGTGGTA
<i>gyrA</i> _TB2_G247S	CCGCGGCTAGTTTTGTAGGT	CCGCGGCTAGTTTTGTAGGT
<i>gyrA</i> _TB3_A384V	ACGCTCGTTTGCCTTGC	ACGCTCGTTTACCTTGC
<i>gyrB</i> _TB4_D500N	GGCCGAGTACCTTCTACGA	GGCCGAGTTACCTTCTACGA
<i>gyrB</i> _TB5_N538K1	ACTTCGGTGTCTTTAGCAC	ACTTCGGTGTCTTTAGCAC
<i>gyrB</i> _TB5_N538K2	ACTTCGGTGTCTTTAGCA	ACTTCGGTTTTCTTTAGCA
<i>ahpC</i> _TB6_P2S	AGGTTAGCAGTGGCATGACT	AGGTTAGCAGTGACATGACT
<i>ahpC</i> _TB6_L3K	CAATGGTTAGCAGTGGCATGT	CAATGGTTAGCTTTGGCATGT
<i>ahpC</i> _TB7_L191R	CGAAGCCTTGAGGAGTTC	CGAAGCCTTGCGGAGTTC
<i>inhA</i> _TB8_C-15T	CGACAACCTATCGTCTCGCCGC	CGACAACCTATCATCTCGCCGC
<i>inhA</i> _TB8_T-8C	GTCACCCCGACAACTATCGTC	GTCACCCCGACAGCCTATCGTC
<i>katG</i> _TB9_G273S	CATGGGTCTTACCGAAAGTGT	CATGGGTCTTACTGAAAGTGT
<i>katG</i> _TB10_S315I	ACGATGCCGCTGGTGATCCTTACCGGTTCC	ACGATGCCGATGGTGATCCTTACCGGTTCC
<i>katG</i> _TB10_S315N	ACGATGCCGCTGGTGATCCTTACCGGTTCC	ACGATGCCGTTGGTGATCCTTACCGGTTCC
<i>katG</i> _TB10_S315T1	ACGATGCCGCTGGTGATCCTTACCGGTTCC	ACGATGCCGCTGGTGATCCTTACCGGTTCC
<i>katG</i> _TB10_S315T2	ACGATGCCGCTGGTGATCCTTACCGGTTCC	ACGATGCCGCTGGTGATCCTTACCGGTTCC
<i>katG</i> _TB10_I335V	GTACAGGATCTCGAGGT	GTACAGGACCTCGAGGT
<i>katG</i> _TB11_R463L	ATCCCGATGCCAGGATCTGT	ATCCCGATGCCAGGATCTGT
<i>rpoB</i> _TB12_P126L	ACAAGGAGTCCCAGAACCTCAAGT	ACAAGGAGTCTAGAACCTCAAGT
<i>rpoB</i> _TB13_V251F	CAGCTGGCTGAACACCACA	CAGCTGGCTGAACACCACA
<i>rpoB</i> _TB14_Q490R	TGTTGATCAACGTCGCGGTGA	TGTTGATCAACGTCGCGGTGA
<i>rpoB</i> _TB15_L511P	AGAATTGGCTCAGCTGGCT	AGAATTGGCTCAGCTGGCT
<i>rpoB</i> _TB15_Q513K	GTCCATGAATTTGCTCAGC	GTCCATGAATTTGCTCAGC
<i>rpoB</i> _TB15_Q513L	TCCATGAATGGCTCAGC	TCCATGAATAGGCTCAGC
<i>rpoB</i> _TB15_Q513P	GGTCCATGAATGGCTCAGT	GGTCCATGAATGGGCTCAGT
<i>rpoB</i> _TB15_D516F	CGGGTTGTTCTGGTCCATGAATTTGT	CGGGTTGTTCTGGTAAATGAATTTGT
<i>rpoB</i> _TB15_D516G	GCGGGTTGTTCTGGTCCATGAAT	GCGGGTTGTTCTGGTCCATGAAT
<i>rpoB</i> _TB15_D516V	GGGTTGTTCTGGTCCATGAAT	GGGTTGTTCTGGACCATGAAT
<i>rpoB</i> _TB15_D516Y	GGGTTGTTCTGGTCCATGAATTTGT	GGGTTGTTCTGGTACATGAATTTGT
<i>rpoB</i> _TB15_S522L	GGTCAACCCCGACAGCGGT	GGTCAACCCCGACAGCGGT
<i>rpoB</i> _TB15_S522Q	GGGTCAACCCCGACAGCGGGT	GGGTCAACCCCGACAGCGGGT
<i>rpoB</i> _TB15_S522T	GGTCAACCCCGACAGCGGT	GGGTCAACCCCGTACAGCGGGT
<i>rpoB</i> _TB15_H526C	AGTCGGCGCTTGTGGGTCAACCCC	AGTCGGCGCTTGCAGGTCACCC
<i>rpoB</i> _TB15_H526D	GTCCGGCGCTTGTGGGTCAACCCC	GTCCGGCGCTTGTGGGTCAACCCC
<i>rpoB</i> _TB15_H526L	AGTCGGCGCTTGTGGGTCAAC	AGTCGGCGCTTGTGGGTCAAC
<i>rpoB</i> _TB15_H526N	GTCCGGCGCTTGTGGGTCAACCCC	GTCCGGCGCTTGTGGGTCAACCCC
<i>rpoB</i> _TB15_H526R	AGTCGGCGCTTGTGGGTCAAC	AGTCGGCGCTTGTGGGTCAAC
<i>rpoB</i> _TB15_H526Y	AGTCGGCGCTTGTGGGTCAACCCC	AGTCGGCGCTTGTAGGTCAACCCC
<i>rpoB</i> _TB15_S531C	CCCAGCGCCGACAGTCGGAAATGTGGGTCAAC	CCCAGCGCACACAGTCGGAAATGTGGGTCAAC
<i>rpoB</i> _TB15_S531F	CCCAGCGCCGACAGTCGGGTGGGTCAAC	CCCAGCGCACACAGTCGGGTGGGTCAAC
<i>rpoB</i> _TB15_S531L	CCCAGCGCCGACAGTCGGGTGGGTCAAC	CCCAGCGCACACAGTCGGGTGGGTCAAC
<i>rpoB</i> _TB15_S531W	CCCAGCGCCGACAGTCGGGTGGGTCAAC	CCCAGCGCACACAGTCGGGTGGGTCAAC
<i>rpoB</i> _TB15_L533P	TCACGTGACAGACGGGCCCGCCGACAGTGTGGGT	TCACGTGACAGACGGGCCCGCCGACAGTGTGGGT
<i>rpoB</i> _TB16_I572F	CGAGCCGATCAGACCGATGT	CGAGCCGATCAGACCGATGT
<i>rpoB</i> _TB16_F586V	CGTTTTCGATGAACCCGAACT	CGTTTTCGATGACCCGAACT

Table Supp. XI: Wild-type and mutant probe pairs used to capture MTB amplicons during on-chip hybridization

A.3. CMOS Biochip Layout and Probes

MTB Array Layout and Key (Table Supp. XII). The probe pairs for 54 different mutations were spotted on the biochip. In some cases, the wild type probes were shared across mutations in the same region such as in D94H, D94N and D94Y in *gyrA*. At least 5 replicates of each probe were spotted in the array, as shown in the array map. See key below for probe content. Probes not referenced in this study are labeled as Test Probes (T). B=Blank and denote areas where no probes were spotted; CP=Control Probe; PM=Process Monitor.

Table Supp. XII: MTB Array Layout Key

Identifier	Probe Content	Identifier	Probe Content	Identifier	Probe Content	Identifier	Probe Content
001	<i>gyrA_TB1_A74S_Mt</i>	031	<i>ahpC_TB6_P2S_Wt</i>	061	<i>rpoB_TB15_D516Y_Mt</i>	094	<i>rpoB_TB15_S531L_Mt</i>
002	<i>gyrA_TB1_A74S_Wt</i>	032	<i>ahpC_TB7_L191R_Mt</i>	062	<i>rpoB_TB15_D516Y_Wt</i>	095	<i>rpoB_TB15_S531W_Mt</i>
003	<i>gyrA_TB1_A90G_Mt</i>	033	<i>ahpC_TB7_L191R_Wt</i>	063	<i>rpoB_TB15_H526C_Mt</i>		<i>rpoB_TB15_S531W_Wt</i>
	<i>gyrA_TB1_A90G_Wt</i>	034	<i>inhA_TB8_C-15T_Mt</i>	064	<i>rpoB_TB15_H526C_Wt</i>	096	<i>rpoB_TB15_S531L_Wt</i>
004	<i>gyrA_TB1_A90V_Mt</i>	035	<i>inhA_TB8_C-15T_Wt</i>	065	<i>rpoB_TB15_H526D_Mt</i>		<i>rpoB_TB15_S531F_Wt</i>
005	<i>gyrA_TB1_A90V_Wt</i>	036	<i>inhA_TB8_T-8C_Mt</i>	066	<i>rpoB_TB15_H526D_Wt</i>	097	<i>rpoB_TB16_F586V_Mt</i>
006	<i>gyrA_TB1_D89N_Mt</i>	037	<i>inhA_TB8_T-8C_Wt</i>	067	<i>rpoB_TB15_H526L_Mt</i>	098	<i>rpoB_TB16_F586V_Wt</i>
007	<i>gyrA_TB1_D89N_Wt</i>	038	<i>katG_TB9_G273S_Mt</i>	068	<i>rpoB_TB15_H526L_Wt</i>	099	<i>rpoB_TB16_I572F_Mt</i>
008	<i>gyrA_TB1_D94G_Mt</i>	039	<i>katG_TB9_G273S_Wt</i>	069	<i>rpoB_TB15_H526N_Mt</i>	100	<i>rpoB_TB16_I572F_Wt</i>
009	<i>gyrA_TB1_D94G_Wt</i>	040	<i>katG_TB10_I335V_Mt</i>	070	<i>rpoB_TB15_H526N_Wt</i>	B	Blank (No Probe)
010	<i>gyrA_TB1_D94H_Mt</i>	041	<i>katG_TB10_I335V_Wt</i>	071	<i>rpoB_TB15_H526R_Mt</i>	CP	Control Probe
	<i>gyrA_TB1_D94H_Wt</i>	042	<i>katG_TB10_S315I_Mt</i>	072	<i>rpoB_TB15_H526R_Wt</i>	PM	Process Monitor
011	<i>gyrA_TB1_D94N_Mt</i>	043	<i>katG_TB10_S315N_Mt</i>	073	<i>rpoB_TB15_H526Y_Mt</i>	T01	Test_Probe_1
	<i>gyrA_TB1_D94Y_Mt</i>	044	<i>katG_TB10_S315T1_Mt</i>	074	<i>rpoB_TB15_H526Y_Wt</i>	T02	Test_Probe_2
012	<i>gyrA_TB1_D94N_Wt</i>	045	<i>katG_TB10_S315T2_Mt</i>	075	<i>rpoB_TB15_L511P_Mt</i>	T03	Test_Probe_3
013	<i>gyrA_TB1_D94Y_Wt</i>		<i>katG_TB10_S315T2_Wt</i>	076	<i>rpoB_TB15_L511P_Wt</i>	T04	Test_Probe_4
014	<i>gyrA_TB1_G88C_Mt</i>		<i>katG_TB10_S315T1_Wt</i>	077	<i>rpoB_TB15_L533P_Mt</i>	T05	Test_Probe_5
015	<i>gyrA_TB1_G88C_Wt</i>	046	<i>katG_TB10_S315N_Wt</i>	078	<i>rpoB_TB15_L533P_Wt</i>	T06	Test_Probe_6
016	<i>gyrA_TB1_T80A_Mt</i>		<i>katG_TB10_S315I_Wt</i>	079	<i>rpoB_TB15_Q513K_Mt</i>	T07	Test_Probe_7
017	<i>gyrA_TB1_T80A_Wt</i>	047	<i>katG_TB11_R463L_Mt</i>	080	<i>rpoB_TB15_Q513K_Wt</i>	T08	Test_Probe_8
018	<i>gyrA_TB2_G247S_Mt</i>	048	<i>katG_TB11_R463L_Wt</i>	081	<i>rpoB_TB15_Q513L_Mt</i>	T09	Test_Probe_9
019	<i>gyrA_TB2_G247S_Wt</i>	049	<i>rpoB_TB12_P126L_Mt</i>	082	<i>rpoB_TB15_Q513L_Wt</i>	T10	Test_Probe_10
020	<i>gyrA_TB3_A384V_Mt</i>	050	<i>rpoB_TB12_P126L_Wt</i>	083	<i>rpoB_TB15_Q513P_Mt</i>	T11	Test_Probe_11
021	<i>gyrA_TB3_A384V_Wt</i>	051	<i>rpoB_TB13_V251F_Mt</i>	084	<i>rpoB_TB15_Q513P_Wt</i>	T12	Test_Probe_12
022	<i>gyrB_TB4_D500N_Mt</i>	052	<i>rpoB_TB13_V251F_Wt</i>	085	<i>rpoB_TB15_S522L_Mt</i>	T13	Test_Probe_13
023	<i>gyrB_TB4_D500N_Wt</i>	053	<i>rpoB_TB14_Q490R_Mt</i>	086	<i>rpoB_TB15_S522L_Wt</i>	T14	Test_Probe_14
024	<i>gyrB_TB5_N538K1_Mt</i>	054	<i>rpoB_TB14_Q490R_Wt</i>	087	<i>rpoB_TB15_S522Q_Mt</i>	T15	Test_Probe_15
025	<i>gyrB_TB5_N538K1_Wt</i>	055	<i>rpoB_TB15_D516F_Mt</i>	088	<i>rpoB_TB15_S522Q_Wt</i>	T16	Test_Probe_16
026	<i>gyrB_TB5_N538K2_Mt</i>	056	<i>rpoB_TB15_D516F_Wt</i>	089	<i>rpoB_TB15_S522T_Mt</i>	T17	Test_Probe_17
027	<i>gyrB_TB5_N538K2_Wt</i>	057	<i>rpoB_TB15_D516G_Mt</i>	090	<i>rpoB_TB15_S522T_Wt</i>	T18	Test_Probe_18
028	<i>ahpC_TB6_L3K_Mt</i>	058	<i>rpoB_TB15_D516G_Wt</i>	091	<i>rpoB_TB15_S531C_Mt</i>	T19	Test_Probe_19
029	<i>ahpC_TB6_L3K_Wt</i>	059	<i>rpoB_TB15_D516V_Mt</i>	092	<i>rpoB_TB15_S531C_Wt</i>	T20	Test_Probe_20
030	<i>ahpC_TB6_P2S_Mt</i>	060	<i>rpoB_TB15_D516V_Wt</i>	093	<i>rpoB_TB15_S531F_Mt</i>		

+	1	2	3	4	5	6	7	8	9	10	11	12	13	14	15	16	17	18	19	20	21	22	23	24	25	26	27	28	29	30	31	32	
1	PM	B	B	B	B	B	B	B	B	B	B	B	B	B	B	B	PM	B	B	B	B	B	B	B	B	B	B	B	B	B	B	B	PM
2	T11	T12	CP	077	078	079	080	081	082	083	084	085	086	087	088	CP	089	090	091	092	093	096	095	096	097	098	CP	099	100	T13	T14	T15	
3	001	002	003	004	006	007	008	009	010	011	T17	011	013	011	014	015	T01	T02	T03	T04	016	017	018	019	020	021	T05	T06	022	023	T07	T08	
4	B	B	B	B	B	B	B	B	B	B	B	B	B	B	B	B	B	B	B	B	B	B	B	B	B	B	B	B	B	B	B	B	B
5	026	027	028	029	CP	030	031	032	033	034	035	CP	043	046	038	039	040	041	042	046	CP	T13	044	046	094	096	047	048	061	062	051	052	
6	053	054	055	056	001	002	003	004	006	007	093	096	010	011	012	011	014	015	T01	T02	034	035	016	017	018	019	057	058	059	060	061	062	
7	B	B	B	B	B	B	B	B	B	B	B	B	B	B	B	B	B	B	B	B	B	B	B	B	B	B	B	B	B	B	B	B	B
8	063	064	065	066	018	019	020	021	PM	T17	T18	022	023	T07	T08	024	025	026	027	T19	T20	030	031	CP	PM	T19	T20	T13	067	068	069	070	
9	071	072	073	074	075	076	043	046	094	096	040	041	042	046	043	046	045	046	CP	047	048	049	050	T19	T20	CP	053	054	T11	T12	079	080	
10	B	B	B	B	B	B	B	B	B	B	B	B	B	B	B	B	B	B	B	B	B	B	B	B	B	B	B	B	B	B	B	B	B
11	081	082	083	084	CP	T09	T10	055	056	057	058	059	060	061	062	063	064	065	066	067	068	069	070	071	072	073	074	085	086	T14	087	088	
12	091	092	093	096	073	074	075	076	077	078	T16	T11	T12	079	080	081	082	083	084	T16	085	086	087	088	089	090	T14	095	096	097	098	CP	
13	B	B	B	B	B	B	B	B	B	B	B	B	B	B	B	B	B	B	B	B	B	B	B	B	B	B	B	B	B	B	B	B	B
14	099	100	T13	013	011	091	092	094	096	097	098	099	100	013	011	T15	001	002	005	004	006	007	008	009	013	011	005	004	003	004	005	004	
15	006	007	008	009	010	011	012	011	T17	T18	T01	T02	T03	T04	016	017	018	019	020	021	T05	T06	022	023	044	046	024	025	012	011	014	015	
16	PM	B	B	B	B	B	B	B	B	B	B	B	B	B	B	B	PM	B	B	B	B	B	B	B	B	B	B	B	B	B	B	B	PM
17	T17	T18	CP	T03	T04	024	025	026	027	028	029	030	031	032	033	034	035	036	037	038	039	CP	040	041	042	046	043	046	044	046	045	046	
18	T05	T06	T19	T20	045	046	047	048	049	050	051	052	T09	T10	053	054	055	056	T17	T18	059	060	061	062	063	064	065	066	T07	T08	024	025	
19	B	B	B	B	B	B	B	B	B	B	B	B	B	B	B	B	B	B	B	B	B	B	B	B	B	B	B	B	B	B	B	B	B
20	028	029	030	031	065	066	067	068	069	070	071	072	073	074	075	076	T11	T12	077	078	079	080	081	082	083	084	085	086	032	033	034	035	
21	036	037	038	039	CP	087	088	089	090	091	092	CP	093	096	095	096	097	098	099	100	095	096	094	096	CP	001	002	094	096	043	046	CP	
22	B	B	B	B	B	B	B	B	B	B	B	B	B	B	B	B	B	B	B	B	B	B	B	B	B	B	B	B	B	B	B	B	B
23	045	046	047	048	003	004	005	004	006	007	008	009	010	011	012	011	014	015	T01	T02	T03	T04	016	017	089	090	T15	049	050	T19	T20	CP	
24	053	054	055	056	020	021	T05	T06	PM	022	023	T07	T08	077	078	026	027	028	029	030	031	032	033	T14	PM	036	037	057	058	059	060	T15	
25	B	B	B	B	B	B	B	B	B	B	B	B	B	B	B	B	B	B	B	B	B	B	B	B	B	B	B	B	B	B	B	B	B
26	063	064	065	066	036	037	038	039	040	041	042	046	044	046	045	046	049	050	051	052	T09	T10	053	054	055	056	067	068	069	070	075	076	
27	071	072	T16	073	074	057	058	059	060	CP	061	062	063	064	065	066	067	068	069	070	T16	071	072	073	074	075	076	T13	T11	T12	077	078	
28	B	B	B	B	B	B	B	B	B	B	B	B	B	B	B	B	B	B	B	B	B	B	B	B	B	B	B	B	B	B	B	B	B
29	079	080	081	082	083	084	085	086	087	088	089	090	091	092	093	096	095	096	097	098	099	100	T14	013	011	001	002	003	004	005	004	T15	
30	008	009	010	011	012	011	014	015	T01	T02	T16	T03	T04	016	017	018	019	020	021	T05	T06	022	023	T09	T10	024	025	026	027	028	029	CP	
31	B	B	B	B	B	B	B	B	B	B	B	B	B	B	B	B	B	B	B	B	B	B	B	B	B	B	B	B	B	B	B	B	B
32	PM	032	033	034	035	036	037	038	039	040	041	042	046	044	046	CP	PM	047	048	049	050	051	052	T09	T10	T07	T08	055	056	057	058	PM	

A.4. CMOS Biochip Experiments

We conducted 12 experiments on 12 separate CMOS biochips to demonstrate the SNP detection capabilities of our system. In **Fig. 5** and **Table I**, we demonstrate differential solid-phase melting curve identification of 13 SNP mutations that confer drug resistance in *M. tuberculosis*¹⁰. Melting curves for a probe pair designed in an easily accessible region, as in the case of I572F in the *rpoB* gene, and for a probe pair designed in a complex and thermodynamically stable secondary structure, as in the case of D94G mutation in *gyrA*, are shown in **Fig. 5**. The results from screening one drug-sensitive wild-type strain (H37RV) and 11 drug-resistant mutant strains, which harbor 13 SNPs conferring antibiotic resistance are reported in **Table I**. The detailed methods of these biochip experiments can be found below.

Multiplex Asymmetric PCR Amplification and Quencher Incorporation. Sixteen-plex asymmetric PCR was performed in the presence of BHQ10-modified dCTP for the purpose of generating single-stranded quencher-labeled PCR amplicons complementary to fluorophore-labeled capture probes (**Fig. 2c**). The ratio of excess to limiting primer (BioSearch Technologies & Integrated DNA Technologies) was 10:1 (500nM excess primer, 50nM limiting primer), except TB1 and TB9 primers where used at 30:1 and 20:1 ratios, respectively (1.5 μ M TB1 excess primer and 1.0 μ M TB9 excess primer, 50nM each limiting primer). PCR was performed in 25 μ l volumes using a modified PCR buffer generated in-house (20mM Tris-HCl, pH8.9, 50mM KCl, 30mM NH₄Cl, 3.2mM MgCl₂, 4mM CHAPS, and 1mg/ml BSA), 400 μ M each dNTP (400 μ M dATP, dTTP, and dGTP, 200 μ M dCTP [Thermo-Fisher Scientific], and 200 μ M BHQ10-dCTP [Biosearch Technologies]), 0.5U/ μ l Taq polymerase (New England Biolabs, Inc.), and 5000 copies of genomic DNA template/25 μ l reaction. PCR was carried out in a C1000 Touch (BioRad Laboratories, Inc.) as follows: 1) reactions were heat denatured at 95°C for 3 min, followed by 2) five cycles of initial amplification at 95°C for 30 s, 62°C for 40 s, and 68°C for 40 s, then 3) an additional 50 cycles of 95°C for 30 s, 58°C for 40 s, and 68°C for 40 s, and 4) a final extension step for 3 min extension at 68°C. For each biochip experiment, four individual 25 μ l reactions were run and pooled post-PCR.

Purification of PCR Product. Desalting and removal of unincorporated BHQ10-dCTPs from amplified PCR product was performed using a Microcon YM-30 filter (EMD Millipore) according to the manufacturer's recommendations. Briefly, 80 μ l of PCR product was brought up to 200 μ l volume in 10mM Tris-HCl pH 8.5, applied to the Microcon filter device, and centrifuged at 5000 xg for 12 min, until 20-30 μ l of concentrate remained. A second wash step was performed by bringing the volume of concentrate up to 200 μ l with 10mM Tris-HCl pH 8.5 and centrifuging at 5000 xg for 12 min. The concentrate was collected into a new microfuge tube by inverting the column and spinning at 1000 xg for 1 min. Concentrate volume was brought up to 40 μ l with 10mM Tris-HCl pH 8.5 and diluted 1:1 in 2X Hybridization Buffer (50mM Tris, 110mM NaCl, 7mM MgCl₂).

Hybridization and Melt of PCR Products on CMOS Biochip. Purified PCR mix was heat denatured at 95°C for 5 min, cooled in an ice water bath, and centrifuged at 10,000 xg for 1 min. Sixty-two μ l was then loaded into the chamber of the CMOS biochip. The remaining volume was saved for amplicon quantification via qPCR. A two-temperature hybridization for probe capture of amplicons was performed on-chip for 90 min at 55°C and 30 min at 45°C, followed by a melt from 45°C to 95°C over 25 min.

A.5. Post-CMOS Biochip Verification

qPCR Confirmation of 16-Plex Asymmetric PCR Products. Quantification of the 16-plex asymmetric PCR products loaded on the biochip was conducted to confirm depletion of limiting primers and the generation of single-stranded PCR product (**Table Supp. XIII**). Purified 16-Plex PCR products for each *M. tuberculosis* strain tested (**Fig 5.** and **Table I**) were diluted either 10³-fold or 10⁴-fold and added to a 10 μ l final volume reaction mix containing 1X SensiFast Probe No-Rox PCR mix (Bioline), 0.3 μ M each primer, and 0.1 μ M TaqMan probe (BioSearch Technologies & Integrated DNA Technologies). The qPCR reactions were carried out in a 384-well plate on a LightCycler 480 (Roche), with an initial denaturation step at 95°C for 5 min, followed by 40 cycles at 95°C for 30 s and 60°C for 30 s, and a final cool down at 40°C for 30 s. Amplicon yields were calculated based on standard curves generated using synthetic ssDNA templates ranging from 0.05 to 10pM (n=6 replicates). Because it takes one cycle to generate dsDNA from ssDNA template, one Cq was subtracted from each threshold value obtained with the single-stranded template to generate a double-stranded template calibration curve. Amplicon yields over 50nM, the concentration of each limiting primer, indicated that the limiting primer was depleted and that single-stranded product was generated in the original asymmetric PCR.

		Strain											
		H37Rv	TDR0005	TDR0009	TDR0021	TDR0036	TDR0117	TDR0133	TDR0160	TDR0168	TDR0191	TDR0226	TDR0231
Concentration (nM)	TB1	67/66	95/124	77/82	73/60	127/122	109/101	94/96	114/112	89/85	123/120	103/74	51/52
	TB2	455/604	510/507	538/522	573/593	570/563	476/499	463/410	447/429	519/465	535/507	493/487	434/419
	TB3	158/155	189/189	192/194	199/167	170/199	171/182	191/198	173/155	151/165	192/195	140/151	111/136
	TB4	185/182	212/232	240/228	237/202	242/232	225/248	149/220	216/199	206/194	257/260	187/182	132/137
	TB5	201/183	252/252	261/268	297/252	285/231	281/264	259/259	249/218	202/226	261/270	188/224	192/178
	TB6	337/349	363/346	337/337	380/370	406/425	358/393	289/307	316/291	218/191	372/393	213/244	264/225
	TB7	377/379	431/381	416/390	450/447	429/442	527/497	281/377	320/341	379/364	458/429	395/362	395/311
	TB8	224/221	265/258	239/226	296/265	311/307	241/244	146/136	256/220	236/235	283/277	215/259	173/191
	TB9	93/101	117/107	107/107	124/119	126/116	103/112	96/109	125/108	109/111	125/129	109/84	62/77
	TB10	190/179	220/218	226/226	194/226	235/235	206/221	206/240	207/202	191/189	208/211	233/203	196/182
	TB11	735/644	339/499	408/408	772/897	967/853	370/534	657/717	682/609	730/772	726/699	739/758	230/228
	TB12	129/137	157/164	150/152	170/133	178/145	130/156	135/149	185/165	148/104	173/166	157/127	109/97
	TB13	277/258	332/343	277/315	399/407	374/410	306/319	364/347	371/379	343/350	371/394	336/310	167/142
	TB14	370/325	481/429	258/286	457/512	570/542	394/441	512/494	795/859	470/445	586/603	558/695	108/108
	TB15	330/320	378/365	352/446	357/418	431/431	373/337	443/421	456/389	327/286	480/450	395/440	224/278
	TB16	114/113	158/143	141/130	162/162	172/173	141/137	72/69	161/160	157/162	200/186	158/162	82/80

Table Supp. XIII: Measured final product concentrations, conducted by qPCR for all MTB amplicons and strains (2 replicates separated by “/”).

B. Amplicon Structure, Mutation Coordinates, and Probe Sequences

Shown below are the optimal monomer structures of each individual amplicon simulated using the OMP software, along with the location of each individual mutation (**Fig. Supp. 33-48**). Each structure was simulated using 87mM monovalent salt and 3.56mM divalent salt at 55°C. The table shows the mutation name, probe name for identifying the mutation, the probe pair sequences, and the probe type. Random coil probes are the simplest probes and are directly complementary to a continuous region on the amplicon surrounding the mutation. This is used when the mutation lies in the random coil region of the amplicon, see I572F mutation in *rpoB* gene of TB16 amplicon (**Fig. 5a**). Anchor probes are designed for mutations, which lie in the hairpin structure and are not readily accessible to probe binding. In this case, the probes have an “anchor” section, which binds to a nearby more readily accessible region, for example the D94G mutation in *gyrA* of the TB1 amplicon (**Fig. 5b**).

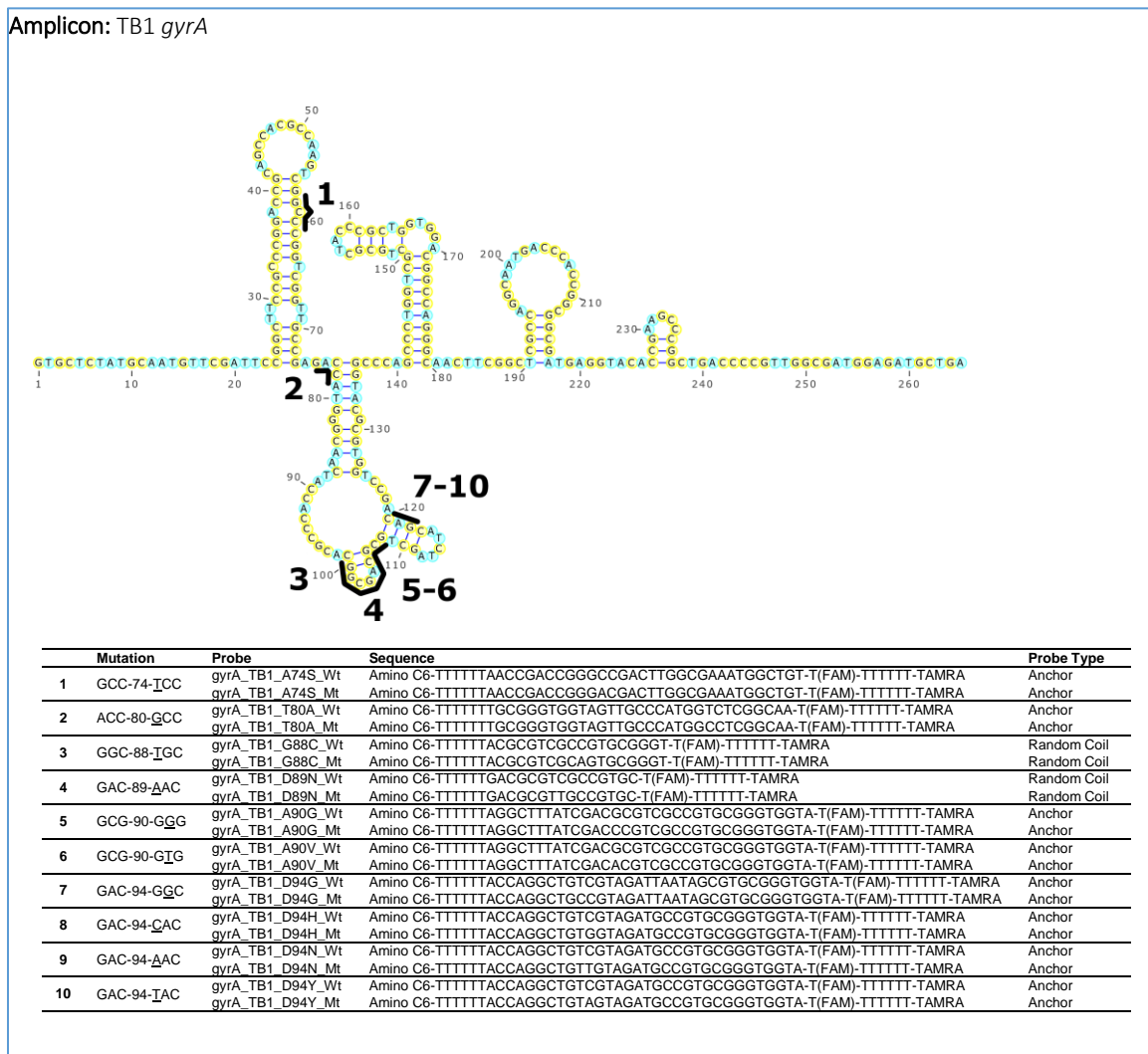


Figure Supp. 33: Secondary structure of TB1 amplicon at 55°C, location of the mutations and IFT probes sequences.

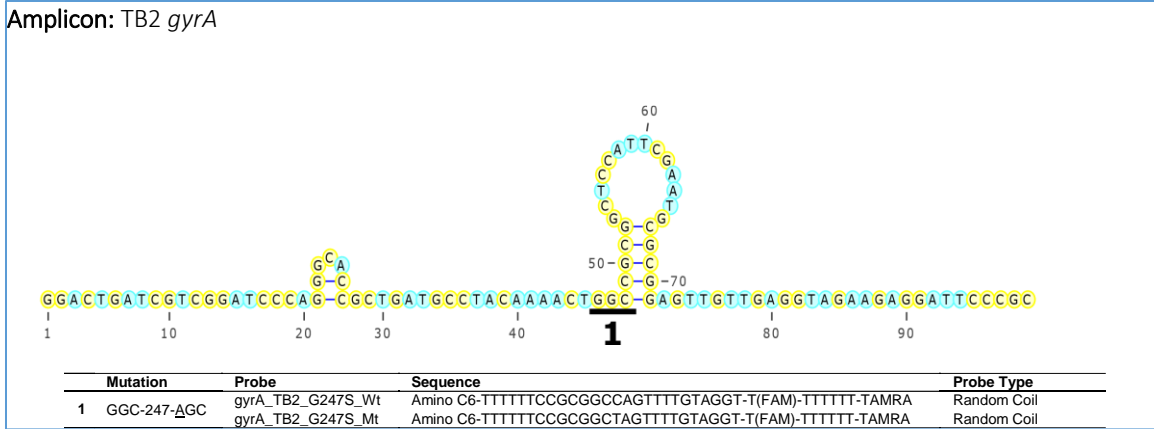


Figure Supp. 34: Secondary structure of TB2 amplicon at 55°C, location of the mutations and IFT probes sequences.

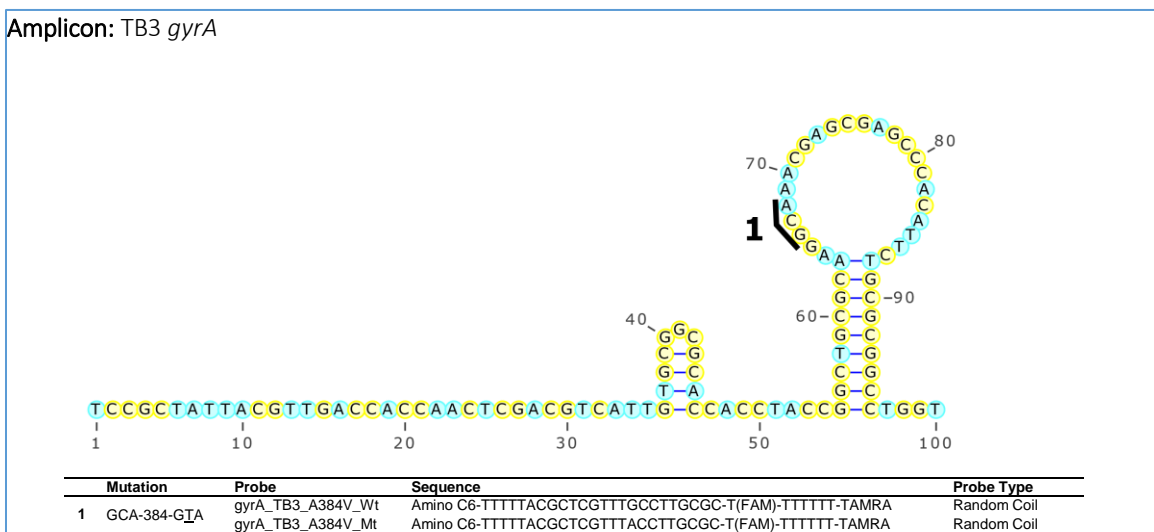


Figure Supp. 35: Secondary structure of TB3 amplicon at 55°C, location of the mutations and IFT probes sequences.

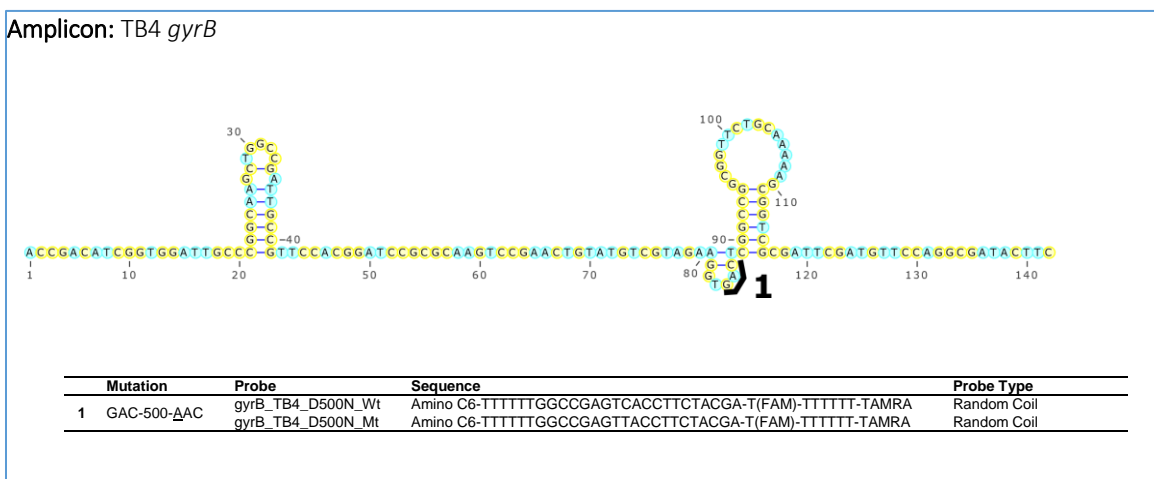


Figure Supp. 36: Secondary structure of TB4 amplicon at 55°C, location of the mutations and IFT probes sequences.

Amplicon: TB5 *gyrB*

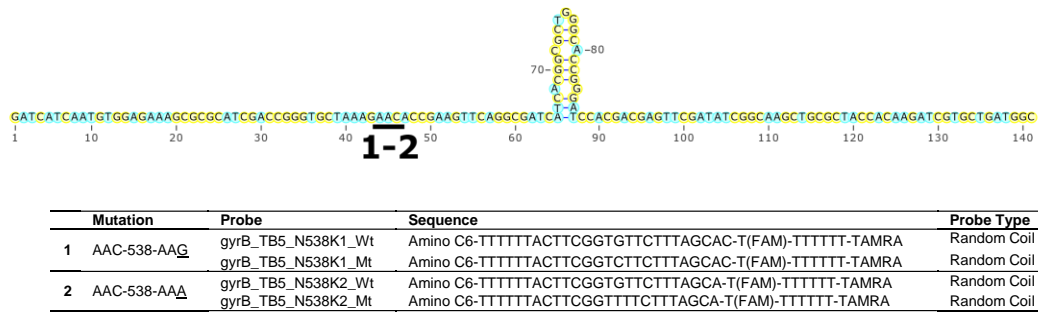


Figure Supp. 37: Secondary structure of TB5 amplicon at 55°C, location of the mutations and IFT probes sequences.

Amplicon: TB6 *ahpC*

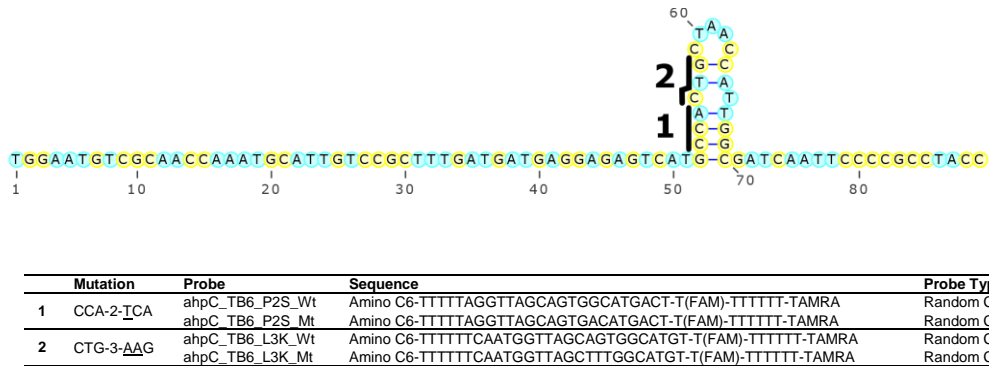


Figure Supp. 38: Secondary structure of TB6 amplicon at 55°C, location of the mutations and IFT probes sequences.

Amplicon: TB7 *ahpC*

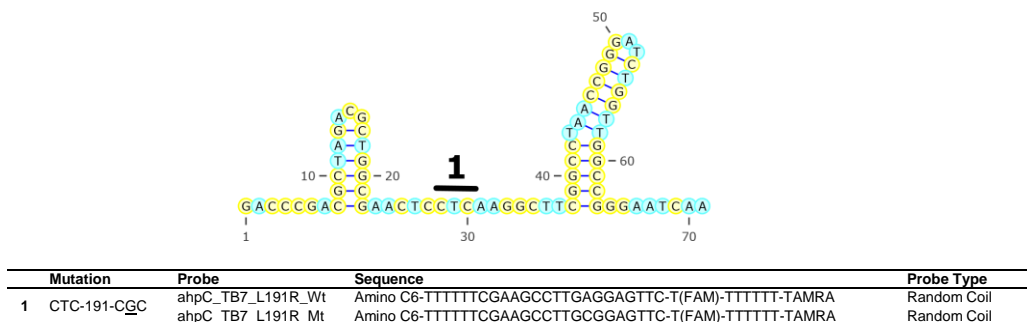
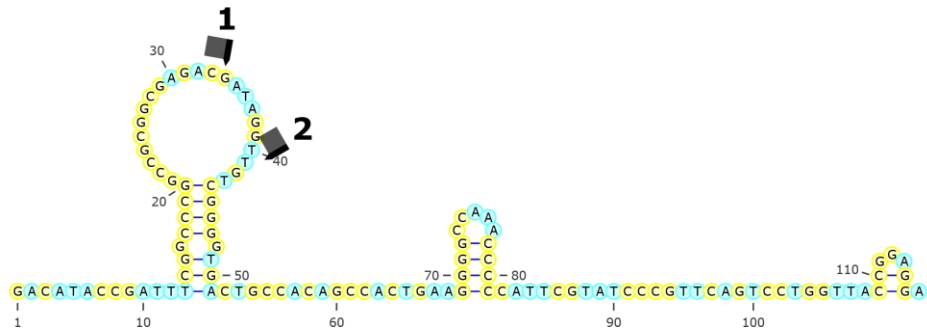


Figure Supp. 39: Secondary structure of TB7 amplicon at 55°C, location of the mutations and IFT probes sequences.

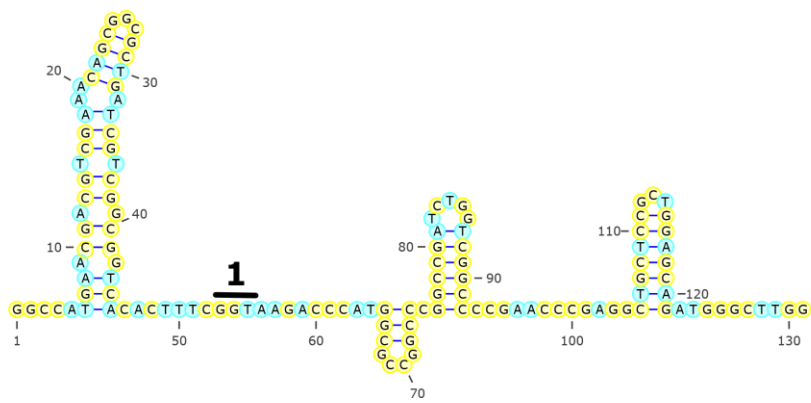
Amplicon: TB8 *fabG1-inhA*



Mutation	Probe	Sequence	Probe Type
1 T(-)C	inhA_TB8_C-15T_Wt	Amino C6-TTTTTTCGACAACCTATCGTCTCGCCGC-T(FAM)-TTTTTT-TAMRA	Random Coil
	inhA_TB8_C-15T_Mt	Amino C6-TTTTTTCGACAACCTATCATCTCGCCGC-T(FAM)-TTTTTT-TAMRA	Random Coil
2 C(-)T	inhA_TB8_T-8C_Wt	Amino C6-TTTTTTGTCACCCCGACAACCTATCGTC-T(FAM)-TTTTTT-TAMRA	Random Coil
	inhA_TB8_T-8C_Mt	Amino C6-TTTTTTGTCACCCCGACAGCCTATCGTC-T(FAM)-TTTTTT-TAMRA	Random Coil

Figure Supp. 40: Secondary structure of TB8 amplicon at 55°C, location of the mutations and IFT probes sequences.

Amplicon: TB9 *katG*



Mutation	Probe	Sequence	Probe Type
1 GGT-273-AGT	katG_TB9_G273S_Wt	Amino C6-TTTTTTCATGGGTCTTACCGAAAGTGT-T(FAM)-TTTTTT-TAMRA	Random Coil
	katG_TB9_G273S_Mt	Amino C6-TTTTTTCATGGGTCTTACTGAAAGTGT-T(FAM)-TTTTTT-TAMRA	Random Coil

Figure Supp. 41: Secondary structure of TB9 amplicon at 55°C, location of the mutations and IFT probes sequences.

Amplicon: TB10 *katG*

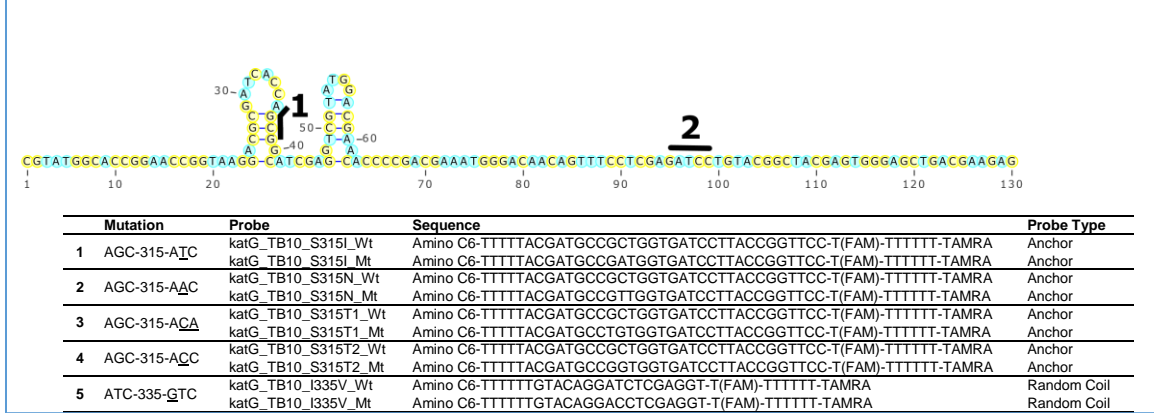


Figure Supp. 42: Secondary structure of TB10 amplicon at 55°C, location of the mutations and IFT probes sequences.

Amplicon: TB11 *katG*

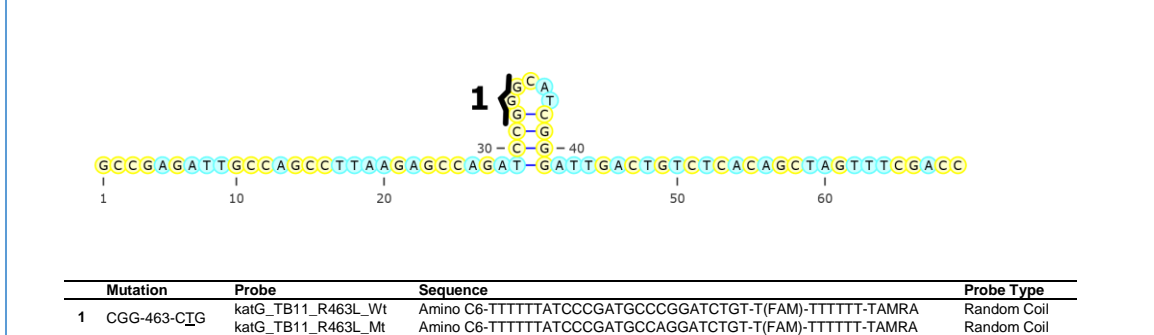


Figure Supp. 43: Secondary structure of TB11 amplicon at 55°C, location of the mutations and IFT probes sequences.

Amplicon: TB12 *rpoB*

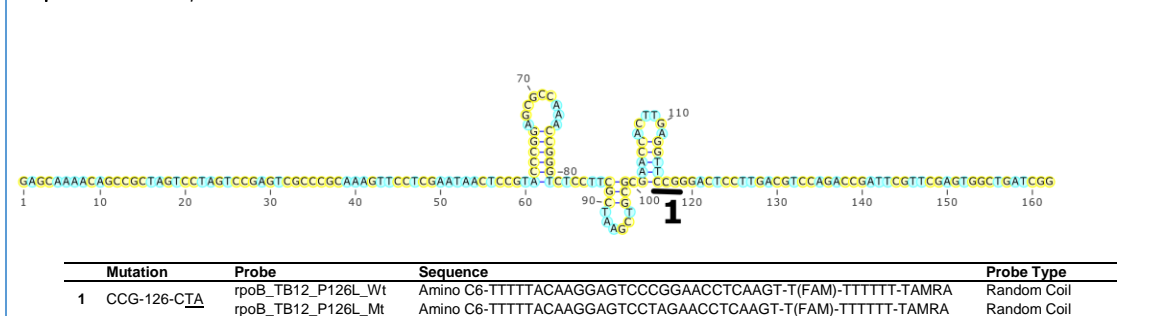
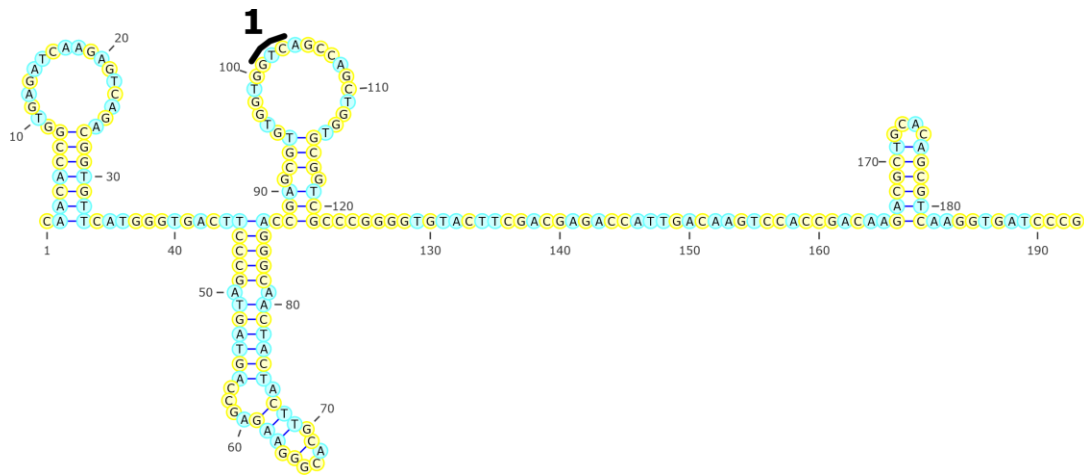


Figure Supp. 44: Secondary structure of TB12 amplicon at 55°C, location of the mutations and IFT probes sequences.

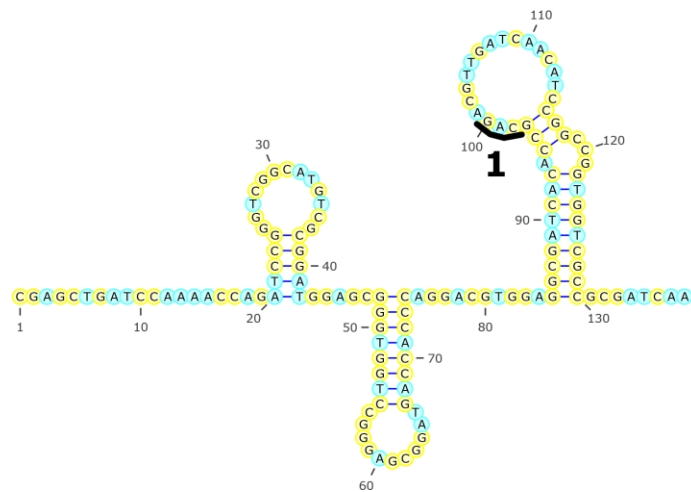
Amplicon: TB13 *rpoB*



Mutation	Probe	Sequence	Probe Type
1 GTC-251-ITC	rpoB_TB13_V251F_Wt rpoB_TB13_V251F_Mt	Amino C6-TTTTTTCAGCTGGCTGACCACCACA-T(FAM)-TTTTTT-TAMRA Amino C6-TTTTTTCAGCTGGCTGAACACCACA-T(FAM)-TTTTTT-TAMRA	Random Coil Random Coil

Figure Supp. 45: Secondary structure of TB13 amplicon at 55°C, location of the mutations and IFT probes sequences.

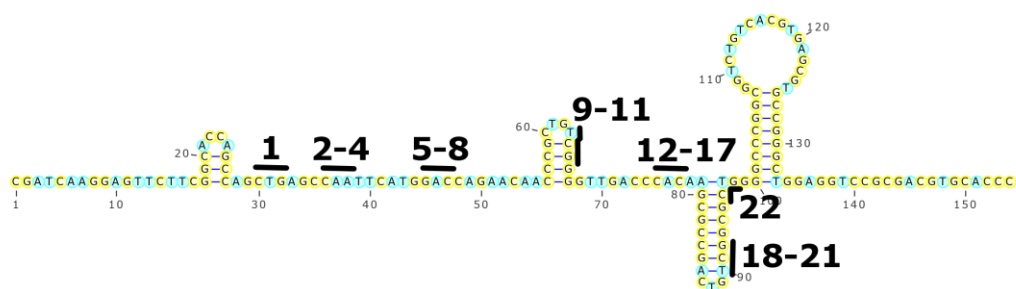
Amplicon: TB14 *rpoB*



Mutation	Probe	Sequence	Probe Type
1 CAG-490-CGG	rpoB_TB14_Q490R_Wt rpoB_TB14_Q490R_Mt	Amino C6-TTTTTTTGTTGATCAACGTCTGCGGTGA-T(FAM)-TTTTTT-TAMRA Amino C6-TTTTTTTGTTGATCAACGTCCGCGGTGA-T(FAM)-TTTTTT-TAMRA	Random Coil Random Coil

Figure Supp. 46: Secondary structure of TB14 amplicon at 55°C, location of the mutations and IFT probes sequences.

Amplicon: TB15 *rpoB*



Mutation	Probe	Sequence	Probe Type
1 CTG-511- CCG	rpoB_TB15_L511P_Wt rpoB_TB15_L511P_Mt	Amino C6-TTTTTAGAATTGGCTCAGCTGGCT-T(FAM)-TTTTTT-TAMRA Amino C6-TTTTTAGAATTGGCTCGGCTGGCT-T(FAM)-TTTTTT-TAMRA	Random Coil Random Coil
2 CAA-513- AAA	rpoB_TB15_Q513K_Wt rpoB_TB15_Q513K_Mt	Amino C6-TTTTTGTCCATGAATTGGCTCAGC-T(FAM)-TTTTTT-TAMRA Amino C6-TTTTTGTCCATGAATTGCTCAGC-T(FAM)-TTTTTT-TAMRA	Random Coil Random Coil
3 CAA-513- CTA	rpoB_TB15_Q513L_Wt rpoB_TB15_Q513L_Mt	Amino C6-TTTTTTCCATGAATTGGCTCAGC-T(FAM)-TTTTTT-TAMRA Amino C6-TTTTTTCCATGAATAGCTCAGC-T(FAM)-TTTTTT-TAMRA	Random Coil Random Coil
4 CAA-513- CCA	rpoB_TB15_Q513P_Wt rpoB_TB15_Q513P_Mt	Amino C6-TTTTTGGTCCATGAATTGGCTCAGT-T(FAM)-TTTTTT-TAMRA Amino C6-TTTTTGGTCCATGAATGGGCTCAGT-T(FAM)-TTTTTT-TAMRA	Random Coil Random Coil
5 GAC-516- TTC	rpoB_TB15_D516F_Wt rpoB_TB15_D516F_Mt	Amino C6-TTTTTCGGGTTGTTCTGGTCCATGAATTGT-T(FAM)-TTTTTT-TAMRA Amino C6-TTTTTCGGGTTGTTCTGGAACATGAATTGT-T(FAM)-TTTTTT-TAMRA	Random Coil Random Coil
6 GAC-516- GGA	rpoB_TB15_D516G_Wt rpoB_TB15_D516G_Mt	Amino C6-TTTTTGCGGGTTGTTCTGGTCCATGAATT-T(FAM)-TTTTTT-TAMRA Amino C6-TTTTTGCGGGTTGTTCTGTCCATGAATT-T(FAM)-TTTTTT-TAMRA	Random Coil Random Coil
7 GAC-516- GIC	rpoB_TB15_D516V_Wt rpoB_TB15_D516V_Mt	Amino C6-TTTTTGGGTTGTTCTGGTCCATGAAT-T(FAM)-TTTTTT-TAMRA Amino C6-TTTTTGGGTTGTTCTGGACCATGAAT-T(FAM)-TTTTTT-TAMRA	Random Coil Random Coil
8 GAC-516- IAC	rpoB_TB15_D516Y_Wt rpoB_TB15_D516Y_Mt	Amino C6-TTTTTGGGTTGTTCTGGTCCATGAATTGT-T(FAM)-TTTTTT-TAMRA Amino C6-TTTTTGGGTTGTTCTGGTACATGAATTGT-T(FAM)-TTTTTT-TAMRA	Random Coil Random Coil
9 TCG-522- TIG	rpoB_TB15_S522L_Wt rpoB_TB15_S522L_Mt	Amino C6-TTTTTGGTCAACCCCGACAGCGGT-T(FAM)-TTTTTT-TAMRA Amino C6-TTTTTGGTCAACCCCAACAGCGGT-T(FAM)-TTTTTT-TAMRA	Random Coil Random Coil
10 TCG-522- CAG	rpoB_TB15_S522Q_Wt rpoB_TB15_S522Q_Mt	Amino C6-TTTTTGGGTCAACCCCGACAGCGGGT-T(FAM)-TTTTTT-TAMRA Amino C6-TTTTTGGGTCAACCCCTGCAGCGGGT-T(FAM)-TTTTTT-TAMRA	Random Coil Random Coil
11 TCG-522- ACG	rpoB_TB15_S522T_Wt rpoB_TB15_S522T_Mt	Amino C6-TTTTTGGTCAACCCCGACAGCGGT-T(FAM)-TTTTTT-TAMRA Amino C6-TTTTTGGGTCAACCCCTCAGCGGGT-T(FAM)-TTTTTT-TAMRA	Random Coil Random Coil
12 CAC-526- IGC	rpoB_TB15_H526C_Wt rpoB_TB15_H526C_Mt	Amino C6-TTTTTAGTCGGCGCTTGTGGGTCAACCCCT-T(FAM)-TTTTTT-TAMRA Amino C6-TTTTTAGTCGGCGCTTGCAGGTCAACCCCT-T(FAM)-TTTTTT-TAMRA	Random Coil Random Coil
13 CAC-526- GAC	rpoB_TB15_H526D_Wt rpoB_TB15_H526D_Mt	Amino C6-TTTTTGTCGGCGCTTGTGGGTCAACCCCT-T(FAM)-TTTTTT-TAMRA Amino C6-TTTTTGTCGGCGCTTGTCCGTCAACCCCT-T(FAM)-TTTTTT-TAMRA	Random Coil Random Coil
14 CAC-526- CIC	rpoB_TB15_H526L_Wt rpoB_TB15_H526L_Mt	Amino C6-TTTTTAGTCGGCGCTTGTGGGTCAAC-T(FAM)-TTTTTT-TAMRA Amino C6-TTTTTAGTCGGCGCTTGTGGGTCAAC-T(FAM)-TTTTTT-TAMRA	Random Coil Random Coil
15 CAC-526- AAC	rpoB_TB15_H526N_Wt rpoB_TB15_H526N_Mt	Amino C6-TTTTTGTCGGCGCTTGTGGGTCAACCCCT-T(FAM)-TTTTTT-TAMRA Amino C6-TTTTTGTCGGCGCTTGTGGGTCAACCCCT-T(FAM)-TTTTTT-TAMRA	Random Coil Random Coil
16 CAC-526- CGC	rpoB_TB15_H526R_Wt rpoB_TB15_H526R_Mt	Amino C6-TTTTTAGTCGGCGCTTGTGGGTCAAC-T(FAM)-TTTTTT-TAMRA Amino C6-TTTTTAGTCGGCGCTTGTGGGTCAAC-T(FAM)-TTTTTT-TAMRA	Random Coil Random Coil
17 CAC-526- IAC	rpoB_TB15_H526Y_Wt rpoB_TB15_H526Y_Mt	Amino C6-TTTTTAGTCGGCGCTTGTGGGTCAACCC-T(FAM)-TTTTTT-TAMRA Amino C6-TTTTTAGTCGGCGCTTGTAGGTCAACCC-T(FAM)-TTTTTT-TAMRA	Random Coil Random Coil
18 TCG-531- TGT	rpoB_TB15_S531C_Wt rpoB_TB15_S531C_Mt	Amino C6-TTTTTCCCAGCGCCGACAGTCGGAAAATGTGGGTCAAC-T(FAM)-TTTTTT-TAMRA Amino C6-TTTTTCCCAGCGCACAGTCGGAAAATGTGGGTCAAC-T(FAM)-TTTTTT-TAMRA	Anchor Anchor
19 TCG-531- TIC	rpoB_TB15_S531F_Wt rpoB_TB15_S531F_Mt	Amino C6-TTTTTCCCAGCGCCGACAGTCGGTGTGGGTCAAC-T(FAM)-TTTTTT-TAMRA Amino C6-TTTTTCCCAGCGCAACAGTCGGTGTGGGTCAAC-T(FAM)-TTTTTT-TAMRA	Anchor Anchor
20 TCG-531- TIG	rpoB_TB15_S531L_Wt rpoB_TB15_S531L_Mt	Amino C6-TTTTTCCCAGCGCCGACAGTCGGTGTGGGTCAAC-T(FAM)-TTTTTT-TAMRA Amino C6-TTTTTCCCAGCGCAACAGTCGGTGTGGGTCAAC-T(FAM)-TTTTTT-TAMRA	Anchor Anchor
21 TCG-531- TGG	rpoB_TB15_S531W_Wt rpoB_TB15_S531W_Mt	Amino C6-TTTTTCCCAGCGCCGACAGTCGGTGTGGGTCAAC-T(FAM)-TTTTTT-TAMRA Amino C6-TTTTTCCCAGCGCCACAGTCGGTGTGGGTCAAC-T(FAM)-TTTTTT-TAMRA	Anchor Anchor
22 CTG-533- CCG	rpoB_TB15_L533P_Wt rpoB_TB15_L533P_Mt	Amino C6-TTTTTTTCACGTGACAGACGGGCCCGCCGCGCCGACAGTGTGGGT-T(FAM)-TTTTTT-TAMRA Amino C6-TTTTTTTCACGTGACAGACGGGCCCGCCGCGCCGACAGTGTGGGT-T(FAM)-TTTTTT-TAMRA	Anchor Anchor

Figure Supp. 47: Secondary structure of TB15 amplicon at 55°C, location of the mutations and IFT probes sequences.

Amplicon: TB16 *rpoB*

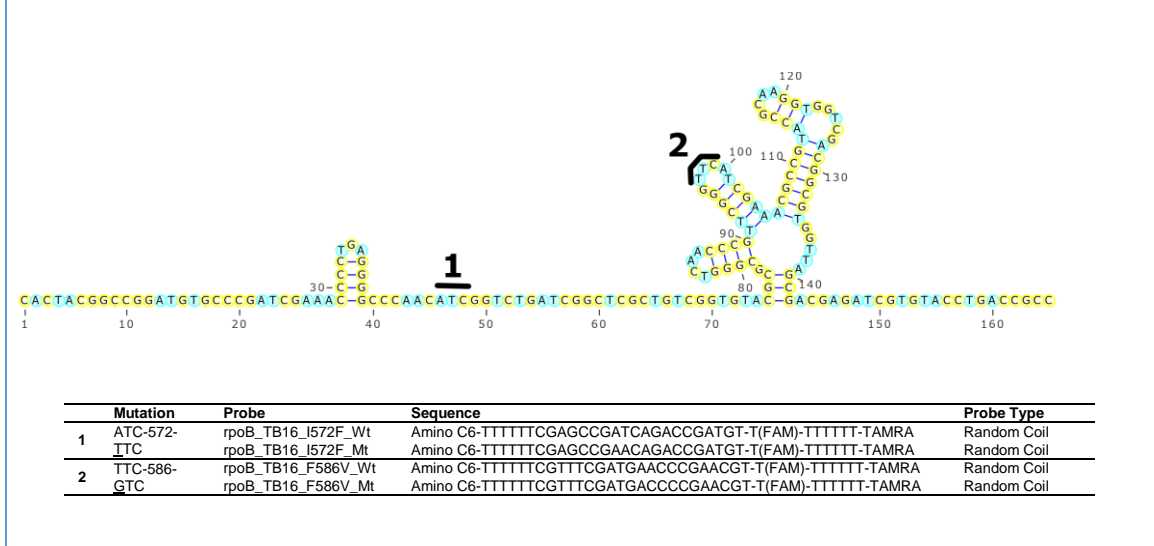


Figure Supp. 48: Secondary structure of TB16 amplicon at 55°C, location of the mutations and IFT probes sequences.

C. Example Result for Detecting the Exact Base Change

Single base specificity. One of the major concerns with hybridization-based solid-phase arrays is the ability to identify the specific mutation of interest, at the individual base level, in cases where several mutations are located in the same codon. In this section, we focus on the H526 codon region in *rpoB* (TB15 amplicon) where detecting one of seven different amino acid configurations (C, D, L, N, R and Y) is necessary in order to correctly classify a mutant strain (Table Supp. XIV).

Mutation name	Codon change	Base change
H526C	CAC-526- <u>T</u> G C	CA/TG
H526D	CAC-526- <u>G</u> A C	C/G
H526L	CAC-526- <u>C</u> T C	A/T
H526N	CAC-526- <u>A</u> A C	C/A
H526R	CAC-526- <u>C</u> G C	A/G
H526Y	CAC-526- <u>T</u> A C	C/T

Table Supp. XIV: Multiple mutations in the same codon (H526_ *rpoB*) region

CMOS biochip experiments were performed with three clinical mutant genomic DNA thermolysates, strains TDR0036, TDR0168 and TDR0117 (that have H526D, H526R and H526Y mutations, respectively) and one wild-type H37Rv *M. tuberculosis* genomic DNA, using the protocol described before. The generated experimental data was compared with the simulated melting curve data obtained using the OMP software. In Fig. Supp. 49, the simulated graphs for heterodimer % vs. temperature for four different targets (3 mutant + 1 wild-type) on each of the seven different probe pairs are shown. ΔT_m

between the wild-type and mutant-type probe (**Table Supp. XV**) clearly show different values for each amplicon-probe pair interaction, with the most negative ΔT_m observed for the most specific cases (H526D, H526R and H526Y detection probe pairs).

The results from the four CMOS biochip experiments are shown for the seven probe pairs in **Fig. Supp. 50**, along with the integral metric shown in **Table XVI**. As expected, the integral metric shows the most negative value for the specific SNP; thus, it is possible to identify the correct mutation. By collectively looking at the data from all the probe pairs, not only can we identify the region where the mutation is present, but we can also identify the specific mutation to a single-base accuracy.

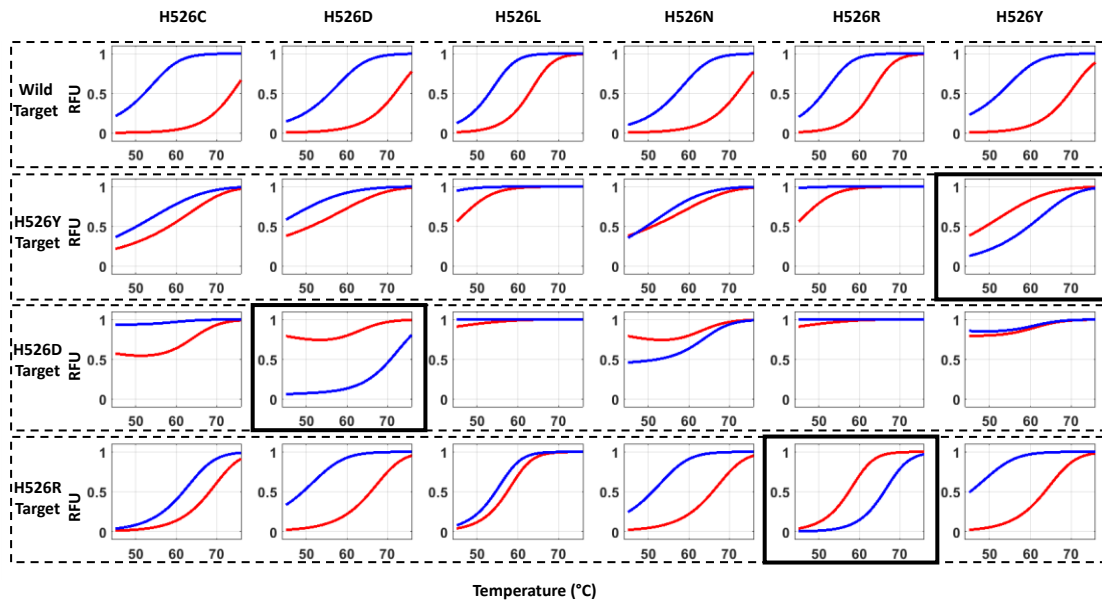


Figure Supp. 49: Simulation results for 7 probe pairs in H526 region with four different target strains. The signal from WT probe is in red and signal from MT probe is in blue for all cases.

Target	ΔT_m (WT-MT) (°C)					
	H526C	H526D	H526L	H526N	H526R	H526Y
Wild	9.6	6.68	5.39	6.72	5.91	6.79
H526Y	1.71	2.38	3.28	1.56	4.35	-2.01
H526D	4.34	-5.24	6.04	-0.8	5.36	0.43
H526R	2.98	6.26	1.56	6.26	-5.08	6.35

Table Supp. XV: Predicted ΔT_m through VISUALOMP tool for the 7 probe pairs in H526 region with four different target strains.

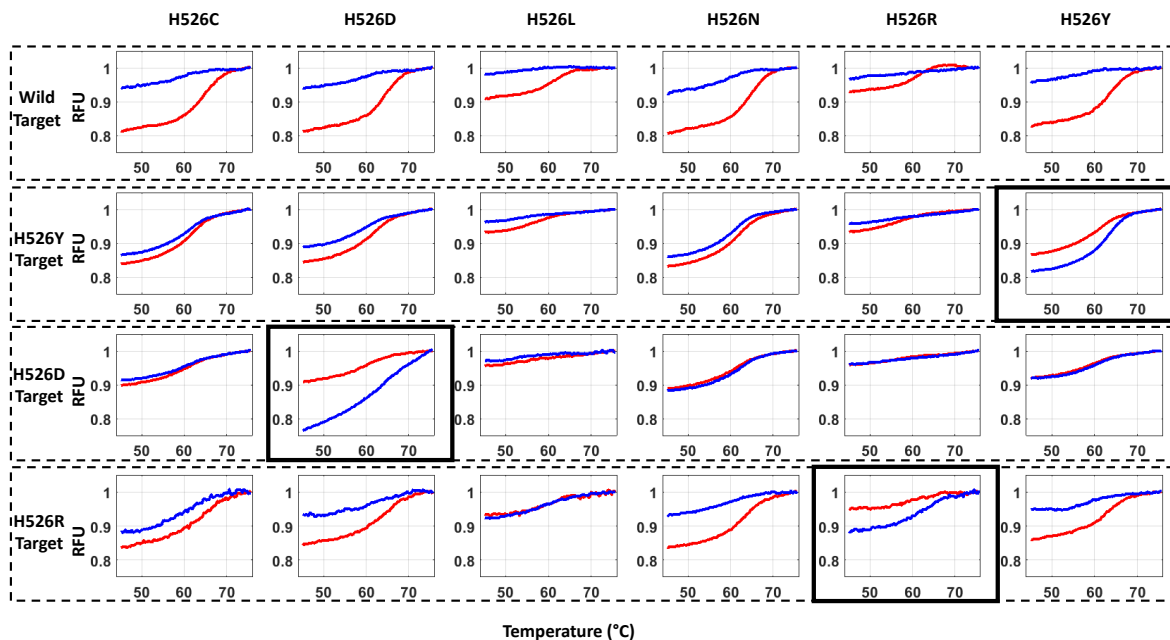


Figure Sup. 50: Experimental data from the 7 probe pairs in the H526 region from four different targets (three with mutations in H526 regions and one wild type). Each target was tested once. The curves are the average of 5 replicate probes.

Target	Integral Metric					
	H526C	H526D	H526L	H526N	H526R	H526Y
Wild	6.46	7.69	3.64	5.61	3.41	6.17
H526Y	1.44	4.06	1.51	0.84	0.93	-3.48
H526D	1.51	-4.23	0.53	-0.8	0.82	-0.15
H526R	5.48	9.23	-0.33	4.75	-1.49	5.63

Table Sup. XVI: Integral metric calculated from experimental data for the 7 probe pairs in H526 region with four different targets.

Supplementary References:

1. <https://www.thermofisher.com/us/en/home/references/molecular-probes-the-handbook/>
2. Grimm, J.B., English, B.P., Chen, J., Slaughter, J.P., Zhang, Z., Revyakin, A., Patel, R., Macklin, J.J., Normanno, D., Singer, R.H. and Lionnet, T., 2015. A general method to improve fluorophores for live-cell and single-molecule microscopy. *Nature methods*, 12(3), pp.244-250.
3. Schuler, B., Lipman, E.A., Steinbach, P.J., Kumke, M. and Eaton, W.A., 2005. Polyproline and the "spectroscopic ruler" revisited with single-molecule fluorescence. *Proceedings of the National Academy of Sciences of the United States of America*, 102(8), pp.2754-2759.
4. Preus, S., Kilså, K., Miannay, F.A., Albinsson, B. and Wilhelmsson, L.M., 2012. FRETmatrix: a general methodology for the simulation and analysis of FRET in nucleic acids. *Nucleic acids research*, 41(1), pp.e18-e18.
5. Claudio, G.C. and Bittner, E.R., 2003. Excitation transfer in aggregated and linearly confined poly (p-phenylene vinylene) chains. *The Journal of Physical Chemistry A*, 107(37), pp.7092-7100.
6. SantaLucia, J., 2007. Physical principles and visual-OMP software for optimal PCR design. *PCR Primer Design*, pp.3-33.
7. Létant, S.E., Ortiz, J.I., Tammero, L.F.B., Birch, J.M., Derlet, R.W., Cohen, S., Manning, D. and McBride, M.T., 2007. Multiplexed reverse transcriptase PCR assay for identification of viral respiratory pathogens at the point of care. *Journal of clinical microbiology*, 45(11), pp.3498-3505.
8. Weinberg, G.A., Schnabel, K.C., Erdman, D.D., Prill, M.M., Iwane, M.K., Shelley, L.M., Whitaker, B.L., Szilagyi, P.G. and Hall, C.B., 2013. Field evaluation of TaqMan Array Card (TAC) for the simultaneous detection of multiple respiratory viruses in children with acute respiratory infection. *Journal of Clinical Virology*, 57(3), pp.254-260.
9. Koressaar, T. and Remm, M., 2007. Enhancements and modifications of primer design program Primer3. *Bioinformatics*, 23(10), pp.1289-1291.
10. Galagan, J. and Schoolnik, G., 2013. The Mycobacterium Tuberculosis regulatory network and hypoxia. *Nature*, 499 (7457), pp. 178-183.